RADC-TR-80-217
Final Technical Report
July 1980

DEVELOPMENT OF LIQUID CRYSTAL AND MAGNETIC STRIPE DOMAIN MULTIMODE OPTICAL SWITCHES

Sperry Research Center

R. A. Soref
M. Kestigian

ROME AIR DEVELOPMENT CENTER
Air Force Systems Command
Griffiss Air Force Base, New York 13441

This report has been reviewed by the RADC Public Affairs Office (PA) and is releasable to the National Technical Information Service (NTIS). At NTIS it will be releasable to the general public, including foreign nations.

RADC-TR-80-217 has been reviewed and is approved for publication.

APPROVED: Kenneth P. Quinlan

KENNETH P. QUINLAN
Project Engineer

APPROVED: Clarence D. Turner

CLARENCE D. TURNER
Acting Director, Solid State Sciences Division

FOR THE COMMANDER: John P. Huss

JOHN P. HUSS
Acting Chief, Plans Office

SUBJECT TO EXPORT CONTROL LAWS

This document contains information for manufacturing or using munitions of war. Export of the information contained herein, or release to foreign nationals within the United States, without first obtaining an export license, is a violation of the International Traffic in Arms Regulations. Such violation is subject to a penalty of up to 2 years imprisonment and a fine of $100,000 under 22 U.S.C 2778.

Include this notice with any reproduced portion of this document.

If your address has changed or if you wish to be removed from the RADC mailing list, or if the addressee is no longer employed by your organization, please notify RADC (ESM) Hanscom AFB MA 01731. This will assist us in maintaining a current mailing list.

Do not return this copy. Retain or destroy.

UNCLASSIFIED

SECURITY CLASSIFICATION OF THIS PAGE (When Data Entered)

REPORT DOCUMENTATION PAGE	READ INSTRUCTIONS BEFORE COMPLETING FORM
1. REPORT NUMBER: RADC-TR-80-217	2. GOVT ACCESSION NO.: AD-A090 134
	3. RECIPIENT'S CATALOG NUMBER
4. TITLE (and Subtitle): DEVELOPMENT OF LIQUID CRYSTAL AND MAGNETIC STRIPE DOMAIN MULTIMODE OPTICAL SWITCHES.	5. TYPE OF REPORT & PERIOD COVERED: Final Technical Report 29 Mar 79 — 28 Mar 80
	6. PERFORMING ORG. REPORT NUMBER: SRC-CR-80-25
7. AUTHOR(s): R. A. Soref, M. Kestigian	8. CONTRACT OR GRANT NUMBER(s): F19628-79-C-0086
9. PERFORMING ORGANIZATION NAME AND ADDRESS: Sperry Research Center, 100 North Road, Sudbury MA 01776	10. PROGRAM ELEMENT, PROJECT, TASK AREA & WORK UNIT NUMBERS: 62702F, 46001740
11. CONTROLLING OFFICE NAME AND ADDRESS: Deputy for Electronic Technology (RADC/ESM), Hanscom AFB MA 01731	12. REPORT DATE: July 1980
	13. NUMBER OF PAGES: 126
14. MONITORING AGENCY NAME & ADDRESS (if different from Controlling Office): Same	15. SECURITY CLASS. (of this report): UNCLASSIFIED
	15a. DECLASSIFICATION/DOWNGRADING SCHEDULE: N/A

16. DISTRIBUTION STATEMENT (of this Report)

Approved for public release; distribution unlimited.

17. DISTRIBUTION STATEMENT (of the abstract entered in Block 20, if different from Report)

Same

18. SUPPLEMENTARY NOTES

RADC Project Engineer: Kenneth P. Quinlan (RADC/ESM)

19. KEY WORDS (Continue on reverse side if necessary and identify by block number)

fiber optics, liquid crystals, electro-optical devices, optical switching, optical communications, magnetic stripe domains, magneto-optical devices, rare-earth iron garnet films, liquid-phase epitaxy

20. ABSTRACT (Continue on reverse side if necessary and identify by block number)

Fiber-optical switching devices based on liquid crystals have been devleoped and tested over the 0.6 to 0.9 μm communications wavelength range. Prototype models of electrically controlled 2x2 optical switches have been tested. Four strands of multimode fiber are coupled to each switch by means of 2-mmD quarter-pitch Selfoc microlenses. Lenses with 0.255 pitch gave low loss in large switches. These 2x2 active couplers make use of voltage-controlled partial or total reflection of light

DD FORM 1 JAN 73 1473 EDITION OF 1 NOV 65 IS OBSOLETE (Cont'd)

UNCLASSIFIED

SECURITY CLASSIFICATION OF THIS PAGE (When Data Entered)

Item 20 (Cont'd)

obliquely incident on a thin, homogeneous layer of nematic liquid crystal such as Merck ZLI-1132 or BDH-E7. Optimum combinations of liquid crystal material and high-index glass (n ~ 1.7) have been identified. Switching performance was measured with 85-μmD-core, 0.17 NA step index fibers and with 63-μmD-core, 0.21 NA graded index fibers. Optical insertion loss was 1.0 dB for polarization independent switches in the voltage-off and voltage-on stages and was 4.0 dB in the voltage-on state of a single-polarization switch whose loss was 1.0 dB with voltage-off. Complete switching required 25 to 40 V rms at a frequency of approximately 2000Hz, depending upon the liquid crystal layer thickness that ranged from 4 to 6 μm. Control currents were less than 10μA. Optical crosstalk in the V = 0 state was -45 dB for the one-polarization switch while, with 30 V rms applied, the crosstalk was 13 dB below the optical signal output. A ten-fold improvement in switching speed has been obtained with a new technique. The fall time or natural relaxation time of the switch was reduced from 40 ms to 4 ms by increasing the optical incidence angle on the planar liquid crystal from 67° to 73°, and 1-ms on/off cycling times at room temperature are predicted.

Magnetic stripe domain research included the preparation, characterization, evaluation and device testing of magneto-optical garnet films.

Liquid-phase epitaxial films of bismuth substituted rare-earth iron garnet were deposited on non-magnetic garnet polished substrates. The optimumbismuth garnet composition film was deposited on commercially available gadolinium gallium garnet and its magneto-optic behavior was determined. These results revealed that higher figure of merit material would have to be developed if useful devices were to be achieved. The preparation of higher figure of merit films was investigated using two simultaneous approaches. Higher Faraday rotation materials and lower loss compositions were emphasized in this research. The former was accomplished by the incorporation of increased concentrations of bismuth in the LPE magneto-optic garnet film. This necessitated the use of garnet substrate material whose lattice parameter was much larger than that of 3G. Gadolinium scandium gallium garnet substrates were formulated, grown from the direct melt by the Czochralski technique and fabricated into polished substrate wafers. The x-ray lattice parameter of this substrate material is approximately 12.59 . LPE garnet films were grown on these substrates and their properties evaluated. In addition to refractive index and absorption curves, Faraday rotation values of over 60,000 degrees/centimeter were recorded for representative LPE films deposited on gadolinium scandium gallium garnet substrates. The refractive index and absorption values were determined as a function of wavelength and the results presented in tabular form. Optical diffraction values of 36 and 41.6% were determined for two gadolinium bismuth iron garnet magneto-optic thin films of 7.3 and 5.9 micrometers thickness, respectively.

Although the basic mechanisms and ultimate properties of bismuth substitued rare-earth iron garnet films were not determined completely during this twelve month contract, significant and original technical progress was achieved which merits further investigations and support.

TABLE OF CONTENTS

LIST OF ILLUSTRATIONS

LIST OF ILLUSTRATIONS (Cont.)

LIST OF TABLES

EVALUATION

Two fiber optical switching devices have been investigated: A device using liquid crystals and one with magnetic stripe-domain structures. The device based on liquid crystals has been developed to the point where prototypes are now available. This work has extremely successful and will be of great importance to the future optical fiber communications of the Air Force. The study of the magnetic stripe-domain structures was not completed but significant and original technical progress was achieved which merits future investigations.

Kenneth P. Quinlan

KENNETH P. QUINLAN
Project Engineer

SECTION I

INTRODUCTION

This is the Final Report under Contract No. F19628-79-C-0086.

The goals of this contract are to optimize liquid-crystal and magnetic stripe-domain structures for multimode fiber-optical switches, and to evaluate the performance of such structures in terms of fiber-optic communication-system applications. Expected structures will establish the feasibility of optical switching for light in the 0.8 to 1.1 micron wavelength range and will be demonstrated by self-contained prototype models.

This Final Report is divided into two self-contained parts: liquid crystal research, which comprises Sections II through IX, and magnetic stripe domain research, which is covered in Sections X through XVI.

SECTION II

APPLICATIONS

The liquid crystal (LC) switching structures covered in this contract are primarily 2 × 2 components with two fiber inputs and two fiber outputs. Functional diagrams are presented here to illustrate how such structures would be incorporated into fiber optic communication systems. The function of an individual 2 × 2 LC fiber optical switch is shown in Fig. 1. This binary-state device operates as a four-port optical reversing switch. In some situations, the second state is a partial-switching condition wherein some light travels from 1 to 3 and from 2 to 4.

Fiber optic networks with a loop architecture are now under development. Here, a series of terminals known as "stations" or "subscribers" is arranged along a fiber optic data bus. In the simplest case, unidirectional or simplex communication, there is one fiber strand between stations. The LC switches can function in such networks as active couplers that tap-off or feed-in optical information locally, or as optical bypass switches in a repeatered loop that send optical signals "around" a repeater-station if desired. These applications are shown in Fig. 2. In these examples, terminal #1 is "talking" to terminal #4 (Fig. 2a), while in Fig. 2b, repeaters #2 and #4 have been bypassed. (The repeatered link can also be connected as in Fig. 2a for optical fail-safe operation). This figure shows some of the possible end-uses of the components investigated in this contract. Further details are given in the Proceedings of the S. P. I. E., Vol. 176, April 1979.

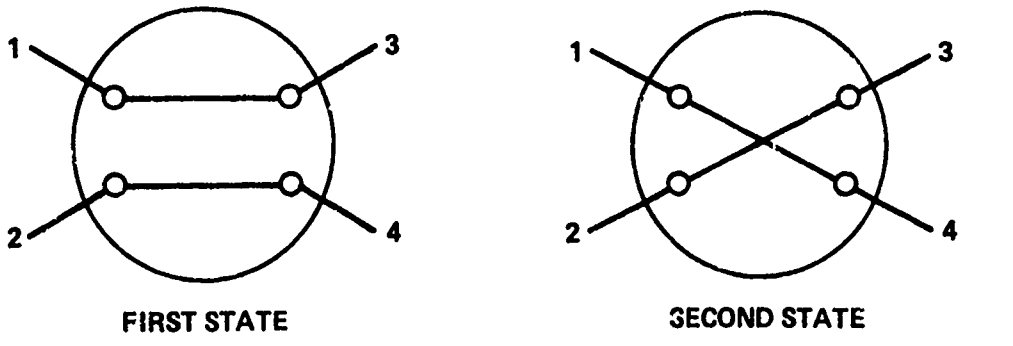

FIG. 1 Function of 2 x 2 switch.

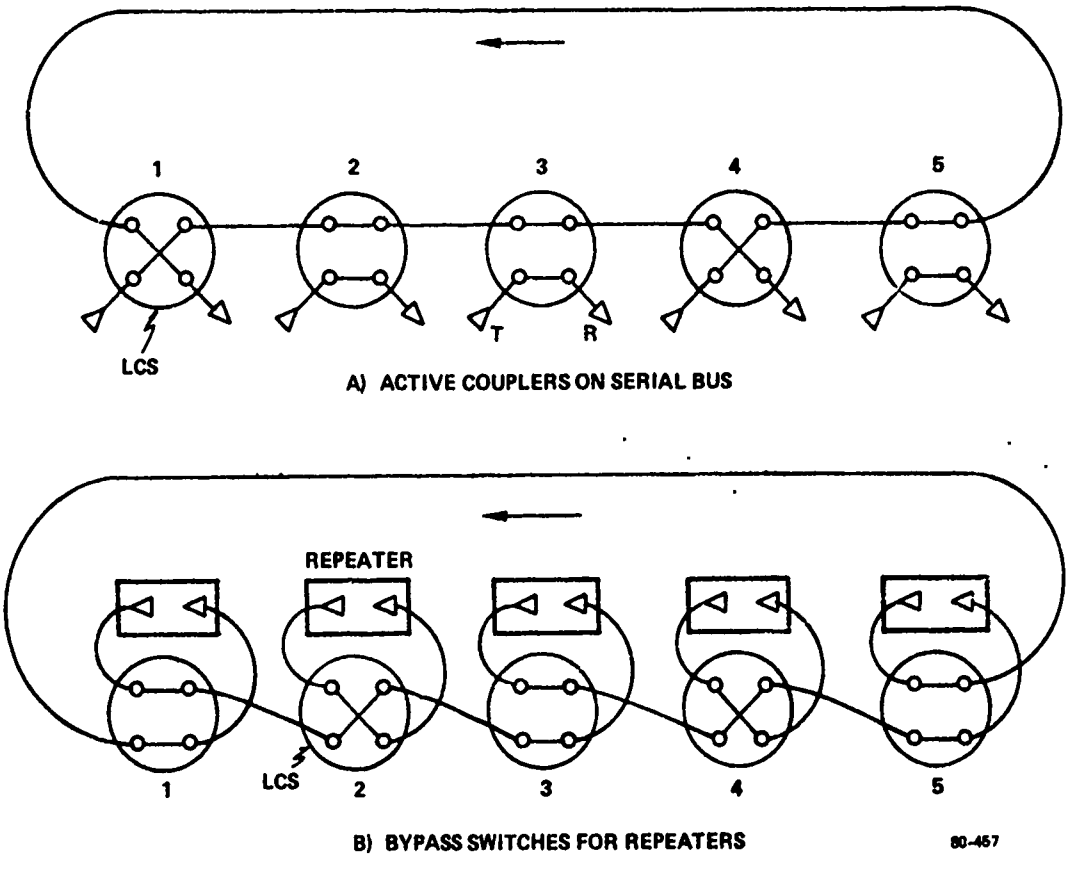

FIG. 2 Two fiber-optic system applications of LC switches.

SECTION III

PRINCIPLES OF OPERATION

The reorientation of a nematic LC by electric torques was noted many years ago by Freedericksz, and this effect has now been put to use in our switch. Each switching device uses a transparent layer of field-effect LC sandwiched between plane-parallel glass pieces. Both glass surfaces are covered with transparent conductive films for applying electric fields normal to the layer, and the layer is only 3 to 6 microns thick so that optical scattering losses will be less than 0.1 dB when light traverses the LC film. The birefringent LC has an extraordianry refractive index n_e and an ordinary index n_o, with the optical anisotropy $n_e - n_o$ ranging typically from +0.13 to +0.25. For switching, the glass material is chosen to have a relatively high refractive index n_g, such that the following two relations hold:

$$n_g > n_o$$

$$n_g \backsim n_e$$

Light is obliquely incident on the LC film so that one or both of the optical polarizations present in the multimode input beam is totally internally reflected at the glass/LC dielectric interface, that is, for at least one polarization, the optical incidence angle θ is greater than the critical angle θ_c defined by: $\theta_c = \arcsin (n_{\backsim}/n_g)$.

In the OFF state (no applied voltage), the LC has a uniaxial ordering determined by surface alignment films on the glass walls, such as angle-deposited SIO films. With an audio-frequency voltage applied (above a threshold voltage), the molecular ensemble is transformed, and at a sufficiently high voltage, about 30 to 50 V rms, the LC reaches a new, quasi-uniform ordering called the ON state. In the ON state, the critcal angles for one

or both polarizations have changed relative to the OFF state, so the optical reflection and transmission properties change. That is how our switch operates.

The LC responds to either dc or ac, although dc usually produces unwanted electro-chemical reactions in the LC; thus, ac is preferred for long life. If the frequency f of the applied voltage is lower than a critical space-charge-relaxation frequency, $f_c \sim 500$ Hz, then the LC will respond to the instantaneous voltage and the switch will modulate light at a frequency 2f. On the other hand, if $f > f_c$, the LC will respond to the rms value of the ac waveform. This is the preferred condition because it gives steady response; a time-independent ON-state level.

Figures 3, 4, and 5 present the LC orderings (the ON and OFF states for each initial order) employed in our switching devices. Optical ray paths are shown for light polarized in the plane of incidence ($E_{||}$) and polarized normal to the optical plane ($E_{\perp}$). (An incoming unpolarized beam can be decomposed into those orthogonal components). Considering first Fig. 3, the homogeneous planar order of Fig. 3a is initially parallel to the walls and parallel to the light plane. Because the LC has a positive dielectric anisotropy ($\varepsilon_{||} - \varepsilon_{\perp} > 0$), molecules align along the field, giving homeotropic order in the ON state. The order goes from homeotropic to planar in Fig. 3b where the molecules have negative dielectric anisotropy ($\varepsilon_{||} - \varepsilon_{\perp} < 0$). Because of the negative anisotropy, molecules align at right angles to the field as determined by microgrooves on the walls (parallel to the incidence plane in this case). In each case, the ON state is uniaxial, apart from two "sticky" layers at the walls (indicated by certain molecules in the figures) whose orientation does not change with voltage The local symmetry axis at any point in the nematic film is called the "director", a vector that coincides with the LC optic axis in the uniaxial condition. Whether light is reflected at the glass/LC interface depends on the LC's effective refractive index, an index that is voltage-dependent because the angle between the LC optic-axis and optical E-vector changes with voltage according to Figures 3-5.

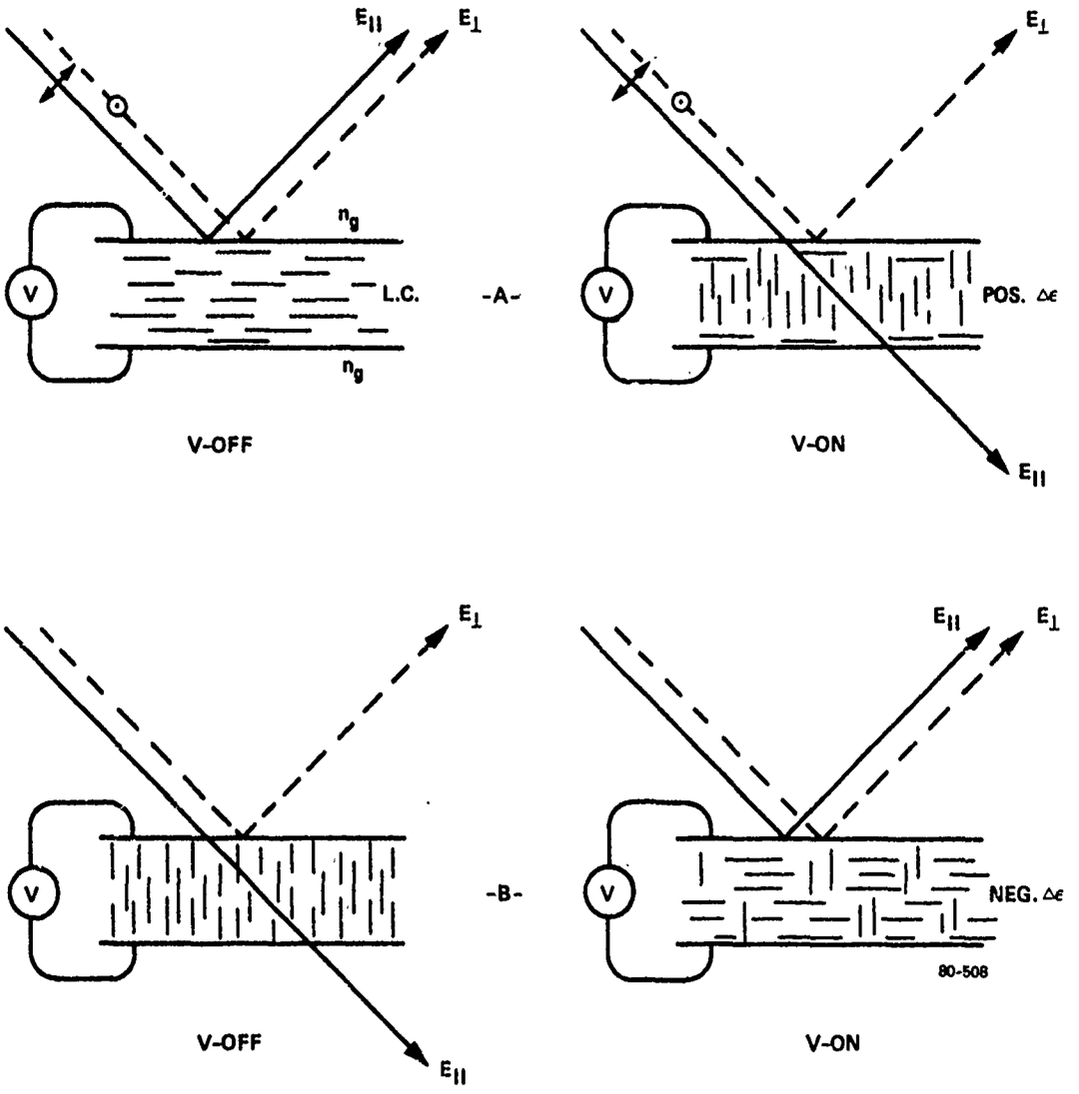

FIG. 3 Ordering of electro-optic nematic LC that offers low optical crosstalk in the TIR state: A) positive LC, B) negative LC.

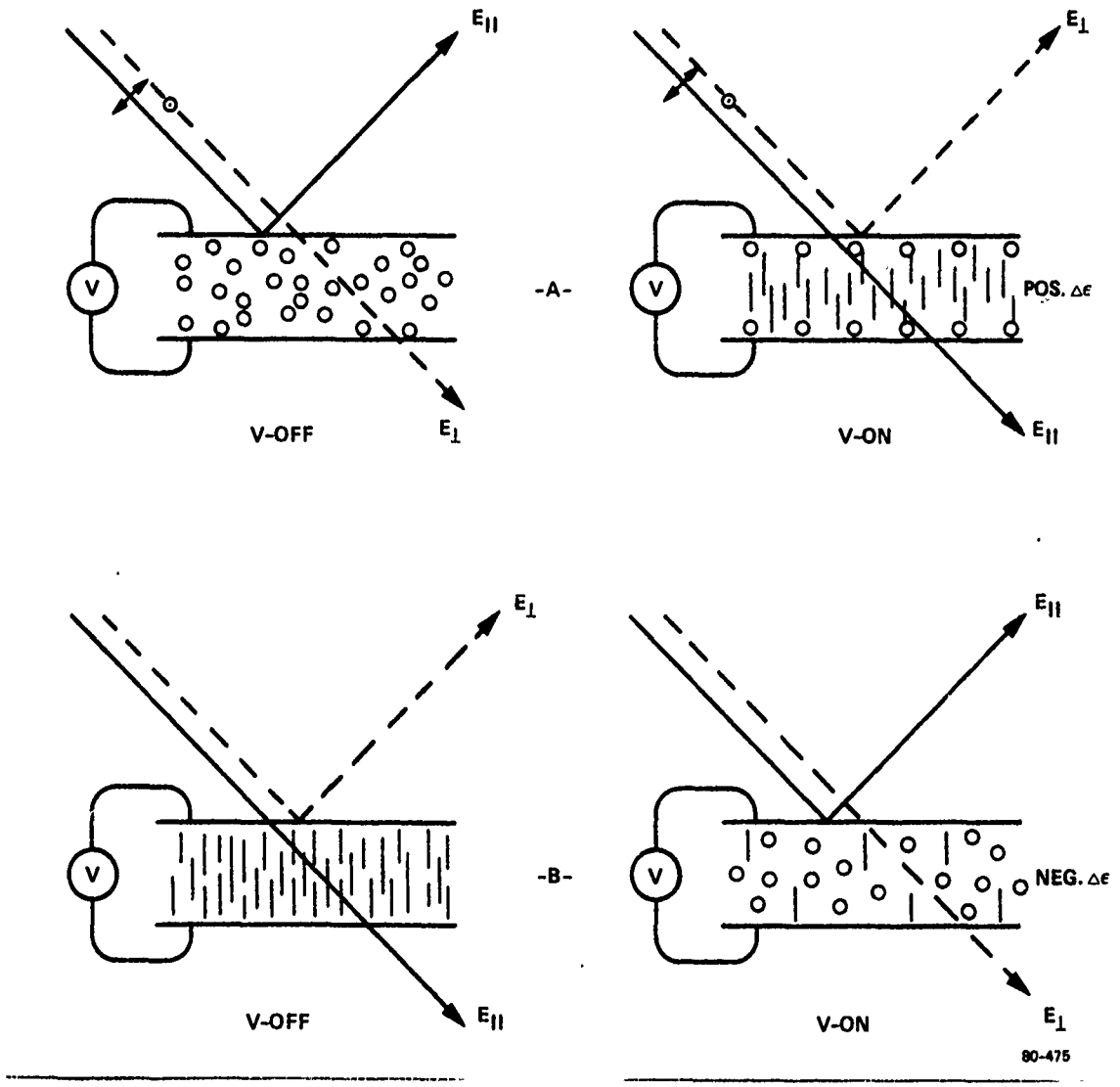

FIG. 4 Ordering of electro-optic nematic LC used primarily in double-pass switch: A) positive LC, B) negative LC.

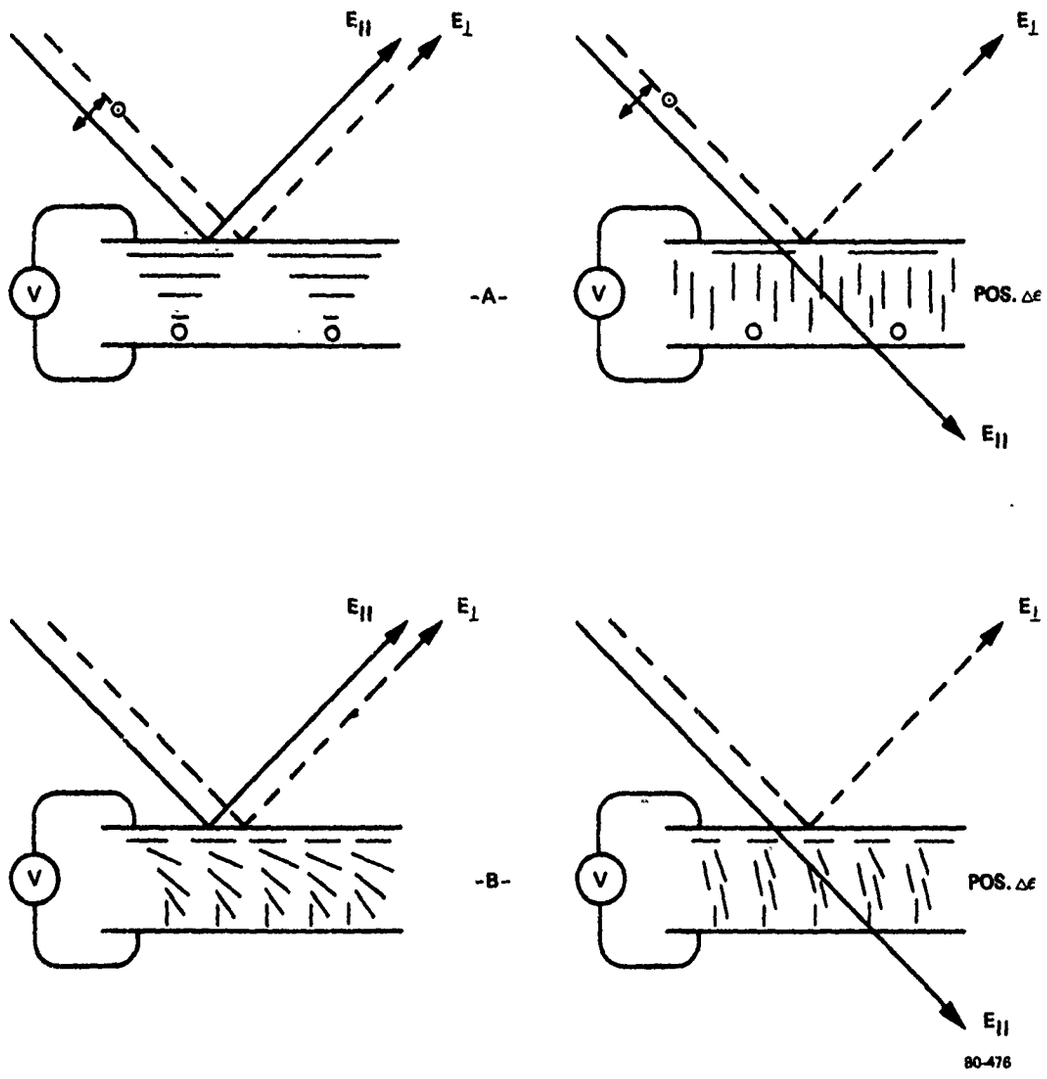

FIG. 5 90° twisted ordering (A), and hybrid ordering (B) of electro-optic LC offering low crosstalk in OFF state.

Figure 3a is probably the most important LC arrangmenet. Here, both polarizations are totally reflected in the V = 0 condition, and we find that leakage through the LC is extremely low because TIR is a "nearly perfect" process. When voltage is ON, $n_g \sim n(LC)$, for $E_{\parallel}$, and the liquid acts as a "leaky cladding" for the glass. Only the $E_{\parallel}$ component is switched (transmitted through the LC), the amount of transmission being voltage-tunable. The reversed sequence of Fig. 3b includes $E_{\parallel}$ transmission in the OFF state and TIR of both components in the ON state. Because of small discrepancies between n_g and n_e, the transmission process is "imperfect" compared to TIR, thus crosstalk is usually higher in the transmission case (the ON state in Fig. 3a or the OFF state in Fig. 3b). Also, the reflection process in the Fig. 3b ON state may not be perfect because of misoriented regions near the walls as indicated.

Figure 4 shows the order used in a double-pass switch (Optics Letters, Vol. 5, 147, (1980)). For positive LCs, the initial planar order is normal to the light plane (OFF state in Fig. 4a) as is the final order for the negative LC (ON state in Fig. 4b). This produces transmission of $E_{\perp}$ rather than of $E_{\parallel}$ as in the homeotropic ON state of Fig. 4a (or the Fig. 4b OFF state). Due to weak spurious reflections, the crosstalk is again higher in each state of Fig. 4 than it is in the Fig. 3 TIR condition. The selective reflection properties of Fig. 4 are used to split an unpolarized beam and to recombine beam components.

Turning now to Fig. 5, we consider the familiar 90°-twisted alignment used in wristwatch LCDs (Fig. 5a), as well as the "hybrid" alignment which is vertical at one wall and horizontal at the other (Fig. 5b). In each case, the ON state is mostly homeotropic (perpendicular to the walls) while the OFF state has either a twist or a bend.

An optical analysis reveals that the OFF-state properties for these positive liquids are identical to those in Fig. 3a; namely, both polarizations are totally internally reflected. With voltage ON, one component is switched as in Fig. 3.

Figure 6a illustrates the single-pass structure investigated on this contract. The OFF and ON conditions are shown, and the LC order is that of Fig. 3 or of Fig. 5. This structure will switch up to 50% of an unpolarized input or nearly 100% of a polarized input (see Optics Letters; Vol. 4, 155, (1979)). Under Sperry-sponsored programs, we also developed double-pass structures that are illustrated here for reference purposes.

In the original double-pass switch (Optics Letters, Vol. 5, 147, (1980)), light interacts twice with one LC layer and essentially all the multimode light is switched. In Fig. 6b, the Fig. 4 LC order is altered by voltage at only one LC location as indicated. Crosstalk is higher in Fig. 6b than in Fig. 6a. To remedy this, we designed an improved double-pass structure, shown in Fig. 6c, which is discussed in the Proceedings of a recent conference (Physics of Fiber Optics, Chicago, April 28-30, 1980). Crosstalk is very low in the Fig. 6c OFF state due to TIR. Here, there are two $\lambda/2$-retardation plates that rotate the optical plane of polarization by 90°, transforming $E_{\parallel}$ into $E_{\perp}$, and vice versa. When voltage is applied simultaneously to both interaction regions, the two polarizations are separated and then combined at the second output port as indicated, giving total switching. All of the structures shown in Fig. 6 operate as 2×2 components.

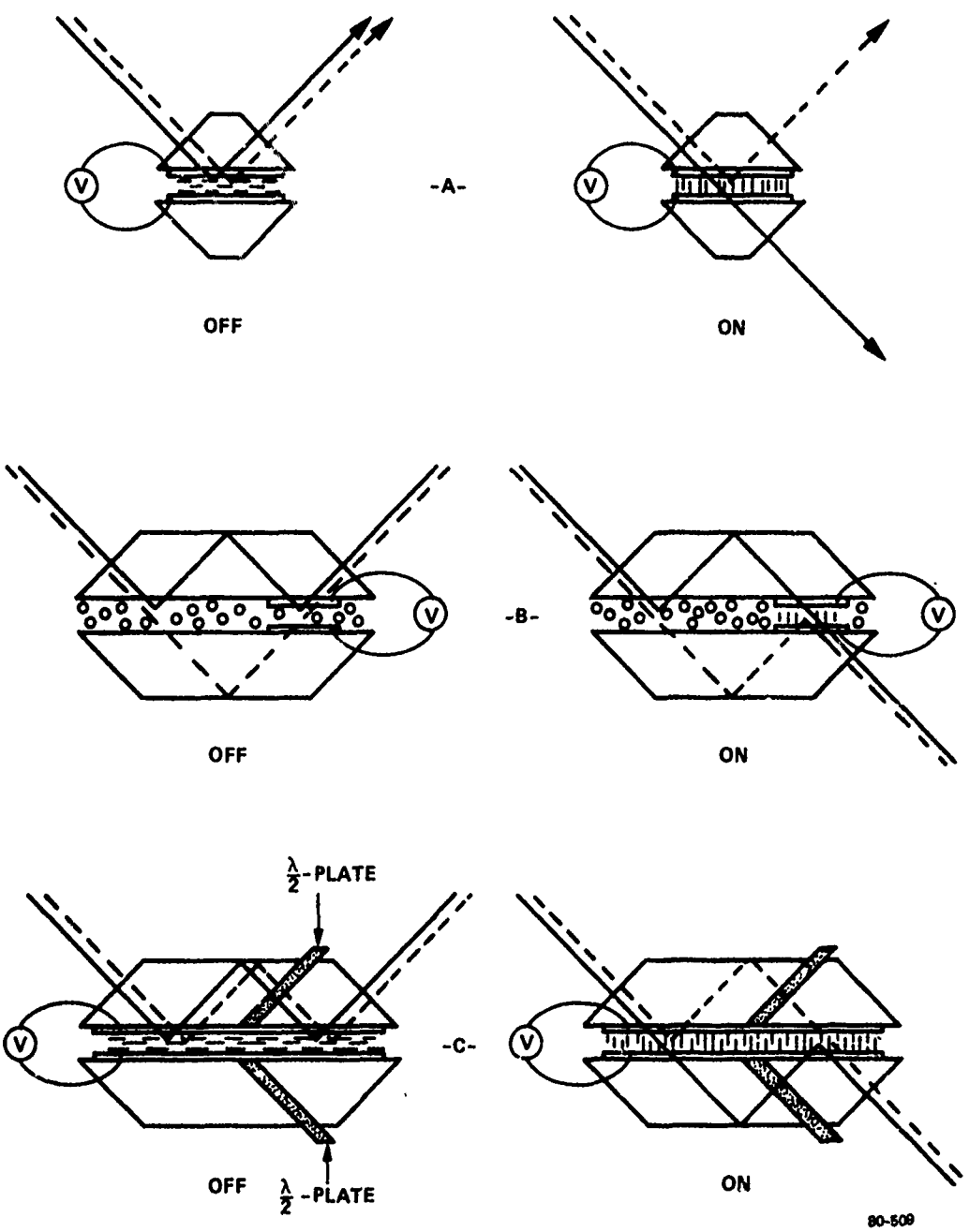

FIG. 6 Structural diagrams (cross-section, side view) of 2 x 2 LC switches illustrating optical ray paths for $E_{||}$ and $E_{\perp}$ polarization components in both voltage states: A) single-pass switch, B) original double-pass switch, C) improved double-pass switch.

SECTION IV

OPTIMIZATION OF MATERIALS

4.1 GLASS PRISM MATERIALS

Three colorless, high-index glass materials suitable for LC switching are readily available in optically polished sheets from the Schott Optical Glass Company, Duryea, PA (sheets that are later cut and polished into prisms). These materials are designated types WG335, WG360, and WG345. Their composition is not given in the Schott data book, but is believed to be barium-flint glass in each case. These prism materials are totally transparent throughout the visible and near-infrared regions out to a wavelength of at least 2.5 microns.

The optical refractive indices are not significantly temperature-dependent, and we have listed in Table 1 the index data supplied by Schott for the 547, 643, and 1014-nm wavelengths. The optical dispersion of these prism materials is shown more clearly in the experimental curves of Fig. 7 where the index values at longer wavelengths have been extrapolated as indicated. Generally, the curves are relatively flat in the 1 to 2 μm region.

4.2 LIQUID CRYSTAL MATERIALS

Among the various manufacturers of liquid crystals, the companies E. Merck of Darmstadt, West Germany and BDH Chemicals, Ltd,. of Poole, England have gained strong marketplace acceptance in the LC industry. The LCs in this contract were supplied by these companies, both of which are represented in the U.S. by EM Industries of Elmsford, NY. These chemical houses make a variety of LCs that are electro-optically active and stable with respect to humidity, UV ambients, and other environmental factors. From the manufacturer's data sheets, we have selected nine LC mixtures that, in our opinion, are desireable for switching; LCs that offer a wide temperature range, low viscosity, high dielectric anisotropy, and high optical

Table 1

Refractive Indices of Schott Optical Glass

Materials Used to Construct Switch

Glass	n_g λ = 547nm	n_g λ = 643nm	n_g λ = 1014nm
WG335	1.624	1.616	1.604
WG360	1.653	1.644	1.629
WG345	1.746	1.734	1.715

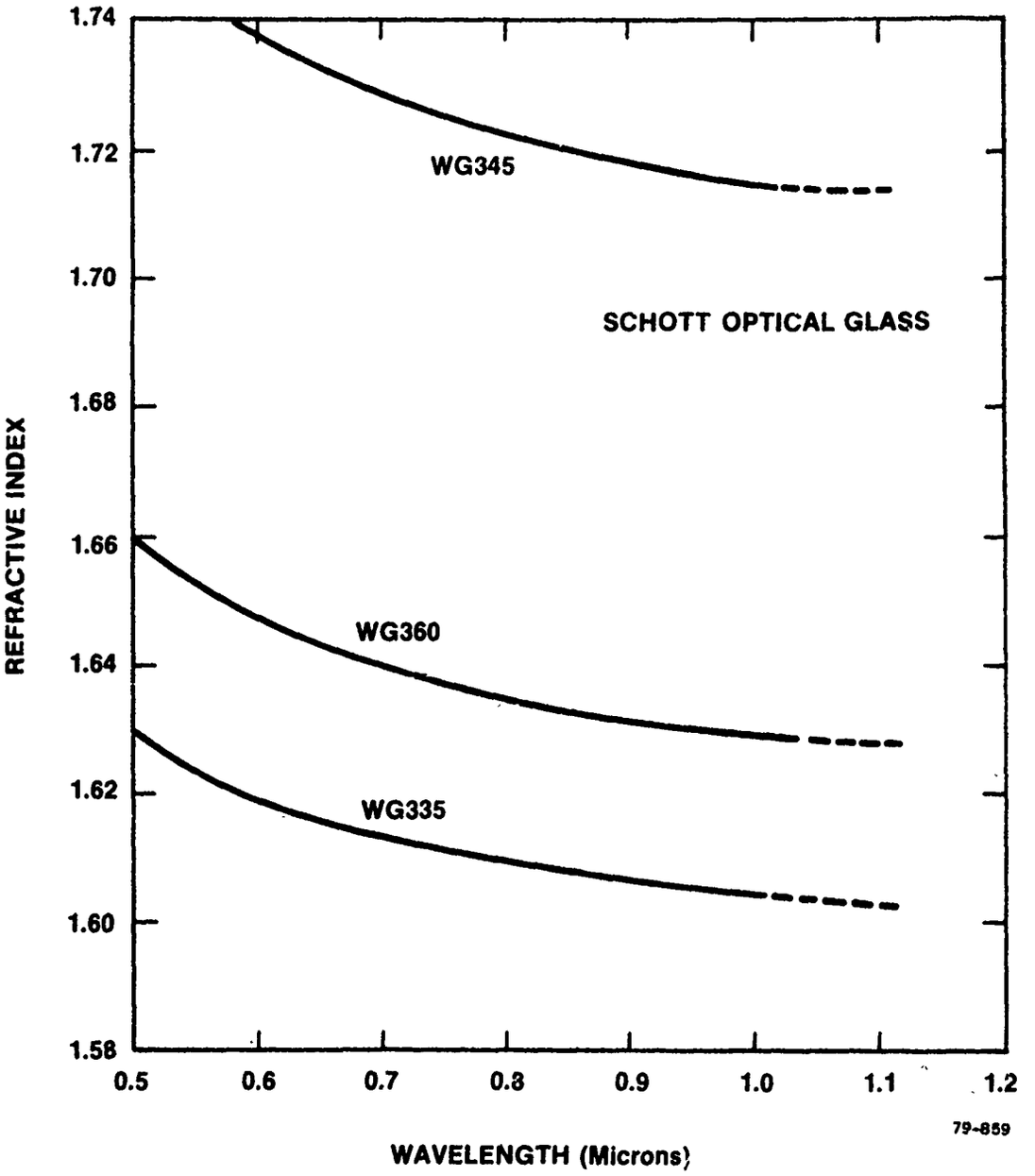

FIG. 7 Optical properties of three commercially available prism materials.

birefringence. The measured properties of these LCs are listed in Table 2, including some estimates for n_o and $\Delta\varepsilon$. The ZLI materials are eutectic mixtures of phenyl cyclohexanes and biphenyl cyclohexanes, while the E-type substances are eutectic mixtures of 4-cyano-4′-n-alkylbiphenals, 4-cyano-4′-n-alkoxybiphenals, and 4-cyano-4″-n-alkylterphenyls.

Considering their optical properties, we note that a thin (4 to 6 μm) film of ordered LC (any of those in Table 2) is highly transparent, that is, more than 95% transmissive to visible and infrared radiation out to a wavelength of approximately 2.5 microns. To a large extent, the optical dispersion of these LCs is like that of the glass. Such data are not available for the Table-2 materials, but we do have dispersion curves, shown in Fig. 8, for the well-known MBBA material, which indicates the characteristics that may be expected from Table-2 substances; that is, slowly decreasing indices that go to fixed, infrared-index values. The implication of Figs. 7 and 8 is that if a specific combination of glass and LC gives optimum switching at a particular wavelength, that optimization will hold at nearby wavelengths.

Turning now to the temperature dependence of optical properties, we note that the LCs in Table 2 have a characteristic response like that illustrated in Figs. 9 and 10 for the representative materials ZLI-1221 and ZLI-1132. As shown, both n_e and n_o decrease slowly with increasing temperature. When the N-I phase transition temperature is reached, the birefringence "collapses" and the index goes to an intermediate value for the isotropic fluid.

Viscosity is a quantity that is relevant to LC switching speed. The temperature-dependence of LC viscosity is presented in Fig. 11 for a typical material, ZLI-1221.

4.3 ELECTRO-OPTIC RESPONSE THEORY

We now consider how a knowledge of physical properties is used to design an optimum switch. We shall focus on the voltage response which is

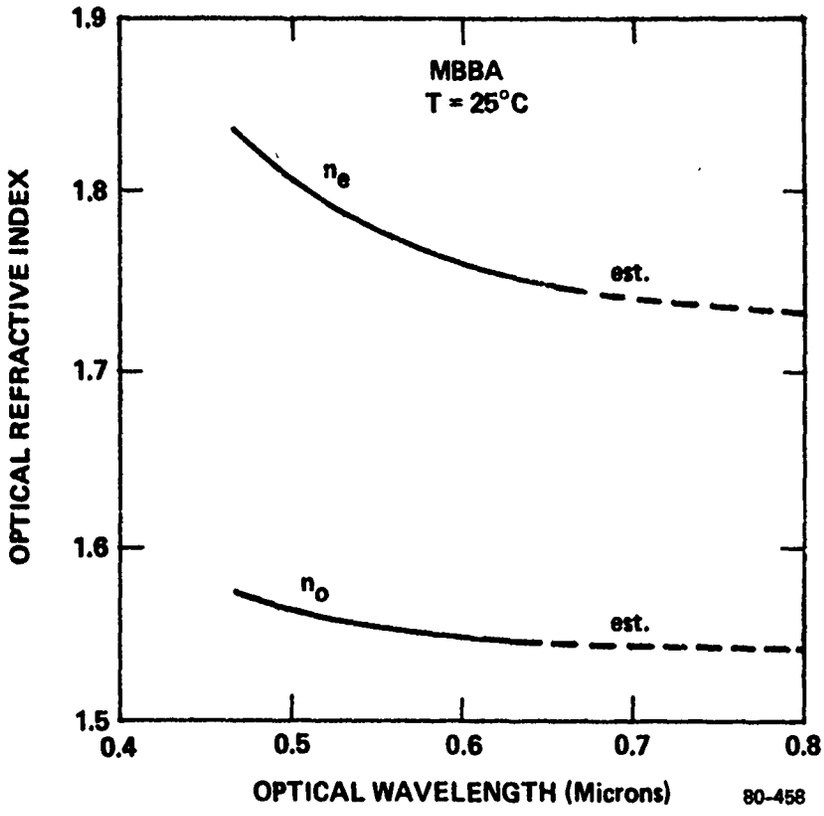

FIG. 8 Dispersion of a liquid crystal, illustrating flattening of curves in near-infrared region. Data taken from M. Brunet- Germain, Compte Rend. Acad. Sci. (Paris), B-271, 1075 (1970).

Table 2. Properties of Nematic LC Mixtures. All are stable and are available from E.M. Industries. Properties measured at 20°C, Indices at λ = 547nm.

Liquid Crystal Type	Maker	n_o	n_e	Δn	$\Delta \varepsilon$	Nematic Temp. Range (°C)	Viscosity (cP)
ZLI 1132	Merck	1.492	1.634	+0.14	+10.3	-6 to +70	27
ZLI 1221	Merck	1.50est	1.63est	+0.13	+ 8.0	-11 to +90	40
ZLI 1294	Merck	1.503	1.663	+0.16	+10.7	-22 to +66	33
ZLI 1344	Merck	1.51	1.69	+0.18	+10.8	-6 to +90	40
E7	BDH	1.522	1.747	+0.225	+13.8	-10 to +61	40
E8	BDH	1.52est	1.767est	+0.247	+13est	-12 to +72	54
E9	BDH	1.52est	1.775est	+0.255	+13est	+7 to +84	96
E60	BDH	1.52est	1.665est	+0.145	+10est	-13 to +63	44
E74	BDH	1.52est	1.698est	+0.178	+10est	-20 to +62	45

est = estimated value

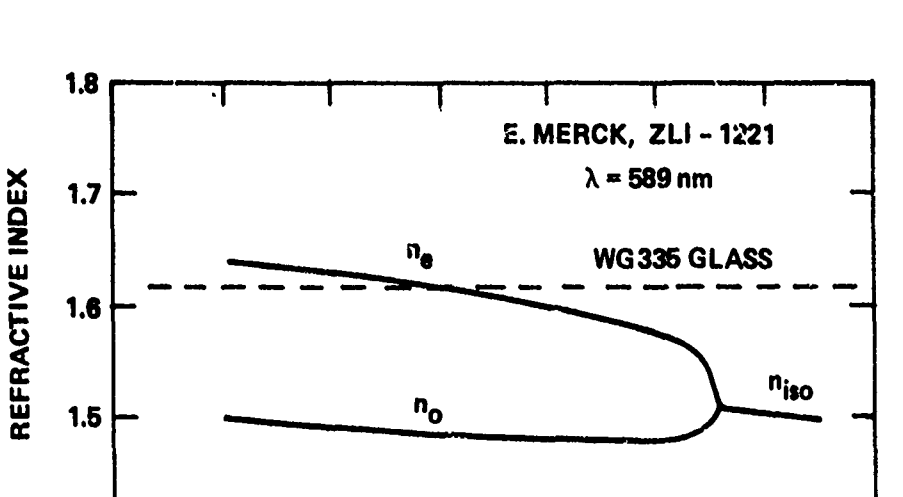

FIG. 9 Optical indices of Merck ZLI-1221 LC as a function of temperature (λ = 589 nm). Index of WG335 glass also shown.

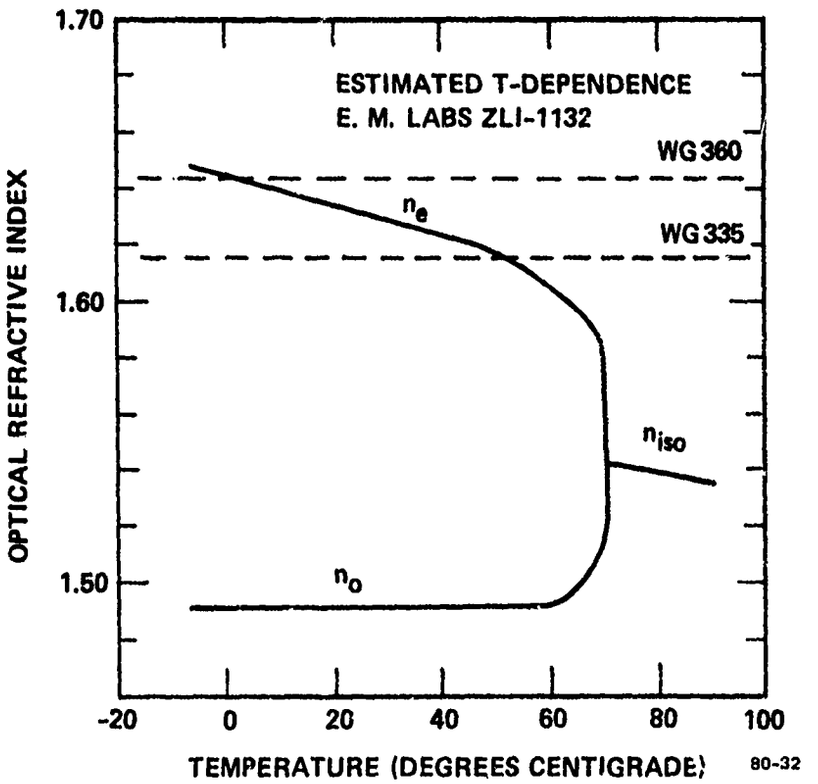

FIG. 10 Optical indices of Merck ZLI-1132 LC as a function of temperature (λ = 633 nm). Data taken from Schadt and Muller, IEEE Trans. on Elec. Dev., ED-27, 1125, (1978). Indices of two glass materials are also shown. At longer wavelengths, all curves are shifted proportionately to lower values.

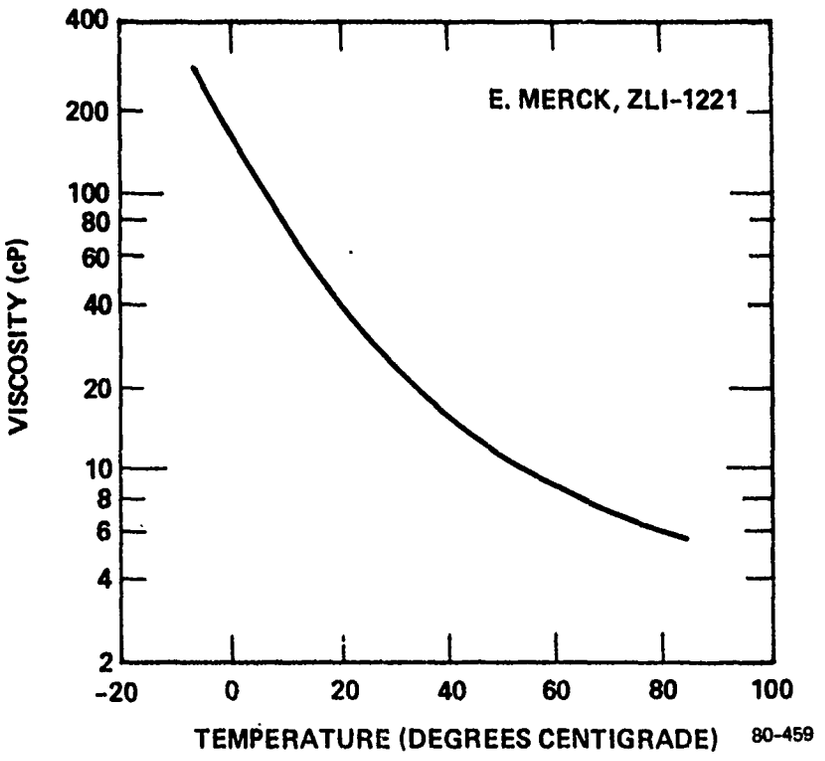

FIG. 11 Viscosity of Merck ZLI-1221 LC as a function of temperature.

an important performance criterion. As voltage is applied, one wants the LC to turn on completely over a narrow voltage range (sharp rise) and the switched light levels should remain constant as the voltage is raised. In other words, the steady-state electro-optical response should have a step-function shape.

We have made an extensive analysis of the turn-on behavior in Appendix A and have found that the switch most closely approaches the ideal step-response when the following relation holds between the glass and LC indices:

$$n_g = n_e \pm 1\% \, n_e .$$

The reason for seeking this equality is to mimimize unwanted dielectric interface reflections, from either $n_g > n_e$ or from $n_g < n_e$, when the switch is partly or totally ON.

When the temperature is changed, nature is not entirely kind with respect to satisfying the above equality, and one finds, as shown in Figs. 9 and 10, that the LC n_e-index varies slowly above and below the constant glass index (indicated by the dashed line). One can match n_g to n_e at a particular temperature, but a small index difference will exist at other temperatures.

4.4 OPTIMUM SWITCHING

The preceeding three sections indicate how an LC switch should be designed. The first step is to choose an LC (for its thermal range or for some other feature). Then, a glass prism material is chosen by picking one whose index n_g gives the best match to n_e over the nematic temperature range. Next, one computes the OFF-state critical angle, $\theta_c = \arcsin (n_o/n_g)$, and one then chooses the prism angle of the glass material to be anywhere from 5° to 16° higher than θ_c, according to the speed-voltage tradeoff discussed in Section VIII. The physical length (L) and height (H) of the glass prisms are determined by the diameter (ϕ) of the microlenses used to couple the fibers; namely, $H \approx \phi$ and $L \approx H/\cos\theta_p$.

We have carried out this procedure for the nine LCs in Table 2 and for three companion glass compositions in Table 1. The results are presented in Table 3 where optimum materials combinations and the resulting θ_c-values are tabulated.

Table 3

Optimum choice of glass prism material for a given LC. Glass selected gives best index match to n_e over LC temperature range. Optical critical angle at λ = 547nm is listed.

Liquid Crystal	Glass	Critical Angle (degrees)
ZLI 1132	WG335	66.7
ZLI 1221	WG335	67.5
ZLI 1294	WG360	65.4
ZLI 1344	WG360	66.0
E7	WG345	60.7
E8	WG345	60.5
E9	WG345	60.5
E60	WG360	66.9
E74	WG360	66.9

SECTION V

SWITCH TECHNOLOGY

This section describes the experimental techniques developed during this contract to make the optical switching devices. We have investigated key aspects of the LC "package" including the electrode films, surface films for LC alignment, means for spacing the prisms a few microns apart, ways of introducing the LC into the device with a uniform molecular texture, and methods for hermetically sealing the switch package.

5.1 TRANSPARENT ELECTRODES

Our early experiments with thin chromium films revealed an inability of the Cr material to meet the conflicting requirements of: 1) less than 5% optical absorption and scattering loss at the wavelength of interest, 2) an electrical sheet resistance of 1500 Ohms/sq or less. We therefore put our electroding efforts into indium-tin-oxide (ITO) which has a history of success in the LCD industry.

A general condition we imposed was that the electrode film should be thinner than $\lambda/4$ at the wavelength of interest, because if $t > \lambda/4$, this film would disturb the glass/LC interface (light would not tunnel through it) and would add spurious reflections, altering the switch properties. We have not verified the deleterious effects of thick films because all our ITO films were less than 500 Å thick,. It would be interesting in the future to test whether a 2000 Å film perturbed the switch properties in a detrimental way.

Highly transparent ITO films were deposited on the $n > 1.6$ Schott glass substrates by means of RF sputtering from a mixed oxide target. The glass prism pieces were placed 7.5 cm from a 6" diam Haseldon target of porous, hot-pressed material: 88% In_2O_3, and 12% SnO_2. After a 1×10^{-6} Torr pumpdown, the target was presputtered for 30 minutes at 90 W in an

80-20 argon-oxygen mixture at 2×10^{-2} Torr partial pressure. After repumping the system to 1×10^{-6} Torr, pure argon flowed in at 2×10^{-2} Torr partial pressure, and the substrates were sputtered for 15 min at a 60 W rf level which produced a clear 400-Å film of ITO with a 1000 to 1500 Ohm/sq sheet resistance. In some cases, the film had a pale brown hue, and it was necessary to increase its optical transmission by annealing, that is, those films were heated in air at 275°C for 10 minutes which increased the electrical conduction as well as transparency.

In the above process, we used the argon-oxygen presputter to restore the target to the same condition at the outset of each run. If oxydation steps such as these are not taken, the target darkens progressively after several runs and the ITO film properties change progressively.

There is some controversy as to whether the above sputtering process is optimal. For example, Fan and Bacher assert (in J. Electrochem, Soc., 122, 1719 (1975)) that high transmission and high conduction in ITO are best achieved with high rf powers, ~500 W, applied for one to two minutes to substrates elevated 2 mm from the rf anode surface (with Pyrex) so that the substrate surface experiences a large temperature-rise during sputtering.

5.2 SURFACE FILMS FOR LC ALIGNMENT

Surface films are deposited on top of the electrodes (or on bare glass in some devices) to provide anchoring forces for the LC at the walls. The LC order induced by surface forces spreads into the "bulk" of the LC by cooperative molecular interaction. One can choose a well-defined surface-ordering direction by a technological procedure such as SiO angle-deposition (or by "rubbing" a polymeric film). This should lead to a uniform, uniaxial LC layer. It is also possible to "dope" the LC with a surfactant-chemical that interacts with a clean, untreated glass surface to produce a well-defined order. However, the surfactant usually leads to homeotropy at V=0 and is not especially useful for getting planar homogeneous order. Therefore, instead of chemical treatments, we used surface treatments in this contract.

As with the electrodes, there is a thickness-constraint on the surface-alignment films; namely, the film thickness should be less than a quarter-wave so that there is no "spurious contribution" to the switch's optical properties. This constraint would seem to rule out polymeric surface films because they typically have a thickness greater than 10,000 $\mathring{A}$ due to the application method; spinning or dipping.

For the foregoing reasons we reverted to the well-known procedure of depositing SiO at an angle of 60° to the substrate. Although it is hard to discern "microgrooves" on a microscopic replica of such a treated surface, the microscopic topography is, in effect, a venetian-blind structure. Some researchers put on two SiO evaporations in succession: a 200-$\mathring{A}$ deposition at 60° followed by a 10-$\mathring{A}$ deposition at 85°, with the substrate rotated 90° about its normal axis between depositions. This produces LC ordering with molecules tilted by a small amount (e.g., 3°) at the walls. The tilted order might be useful in our switch because, for example, it lowers the voltage threshold. However, because of time limitations we did not investigate tilted alignment and instead concentrated on the single SiO evaporation method that generally gives zero-tilt at the walls for 55°-75° deposition in a 100-300 $\mathring{A}$ thickness range. By placing the 60°-oriented substrates 35 cm from a "point-like" baffle-boat source containing powdered SiO, we obtained the desired terraced topography on the glass. A normal-incidence film thickness monitor situated next to the glass was programmed to stop the thermal SiO deposition when a monitor-value of 200 $\mathring{A}$ was reached.

To make a switch, two glass substrates with SiO terraces aligned parallel are assembled. When those substrates were assembled 3 to 4 microns apart, we found that the direction of SiO deposition occasionally lead to a 180° twist in the LC molecular array instead of the desired 0° twist. Specifically, the devices worked best with the prisms assembled ↑↑ rather than ↑↓ where the arrow denotes the SiO incidence direction.

5.3 SPACING, FILLING, AND SEALING TECHNIQUES

Spacing refers to the means of separating the planar prism surfaces by a uniform distance of 3 to 6 microns. A variety of electrically insulating materials are suitable for this job. For example, teflon is available in 6.3-μm strips; but these tend to attract dust and tend to wrinkle during assembly.

As a more reproducible spacing method, we developed the technique of depositing thick-film SiO_2 spacers which has been touched on by other researchers. As in Section 5.2, we again used thermal evaporation of SiO, but here the deposited layer was extremely thick, 40,000 to 50,000 Å, and the deposited material was either SiO_2 or SiO, depending on the deposition rate. The spacer film was deposited through an evaporation mask to define the shape of the spacer "gasket" on the substrate surface.

To get a thick film in a 10-min run, the prisms were placed only 6 cm from the baffle boat source which caused considerable heating of the glass and ITO. In future work on the LC switch package it would be beneficial to deposit spacers on the glass before putting on the ITO so as to "immunize" the ITO from unwanted heat treatment. When making the present SiO_2 spacers, the Infocon quartz-crystal thickness-monitor controlled the deposition and kept the evaporation rate approximately 100 Å/sec.

Half of the spacer gasket was put on one glass prism and the other half put on the other prism. The gasket was not a hermetically sealed loop because that would have necessitated filling the switch with LC through holes drilled in the glass prisms. Instead, we left openings in the SiO_2 stripes, through which LC flowed during filling. The direction of flow seemed important because when the LC traveled along the microterraces, it usually produced a more uniform LC texture than when the LC initially flowed in at right angles to those grooves. (The right-angle flow sometimes produced small voids, air bubbles, and disclination lines). In addition, more homogeneous LC textures were obtained when the liquid was first introduced into the cell in its isotropic phase, rather than its nematic phase.

The empty switch package was heated on a hotplate to 95°C, about 15°C above the nematic-isotropic transition. Then the heated liquid was injected through a side-vent in the gasket using a sterilized pipette.

Hermetic sealing is another important packaging area. In commercial products such as LCD wristwatches, a glass frit seal is often used, but in our laboratory prototypes, we used a simpler procedure to seal the switch. After having deposited the prism spacers, and after the two prisms were clamped together, a small bead of Varian Associates Torr Seal epoxy was applied to the perimeter of the switch package. A 1-mm entry hole and a 1-mm vent hole were left in the epoxy ring. Then the empty switch was placed in a 70°C oven for 50 min to harden and cure the epoxy, following which the LC was added as above. Finally, small amounts of partly cured epoxy were painted on the vent hole and fill hole to complete the quasi-hermetic seal.

SECTION VI

SWITCHING RESULTS

The layout of the experimental 2 × 2 multimode fiber switch is shown in Fig. 12 where the Fig. 3a LC order is employed. Figure 13 is a photograph of a working 2 × 2 device, a laboratory prototype in which microlenses were first attached to fiber ferrules with optical cement, after which those lenses were held in contact with the prism faces with small mechanical fixtures. In a later version of this switch, transparent epoxy (n=1.56) was used to cement lenses to prisms; so the switch was self-supporting. Before they were joined to the prisms, the four fiber-lens "pigtails" were mutually aligned with micropositioners.

The fibers in Fig. 13 are glass-on-glass Corguide step-index fibers with an 85- μm core diameter and an 0.17 NA. Lenses are quarter-pitch Selfoc SLW with a 2-mm diameter and an 0.5 NA.

Figures 14 and 15 present experimental data on the electro-optical performance at λ = 633 nm of a 6-μm layer of Merck ZLI-1132 LC between Schott WG360 glass prisms. The prism angles were 67.0° and critical angle was 65.3°. The polarized-light results of Fig. 14 (where output intensity is plotted vs. the rms level of an 1000 Hz sine wave source) show 95% reflection of $E_{\parallel}$ at V < 0.8 V rms, while the $E_{\perp}$ reflection stays at 91% independent of voltage. Crosstalk for $E_{\parallel}$ is 50 dB below the optical input level in the voltage-OFF state, and with 25 V rms applied, the residual $E_{\parallel}$ reflection is 12 dB below the switched $E_{\parallel}$ transmission. Turn-on begins at 0.8 V rms and reaches the 3 dB coupling point at 5 V rms. The turn-on is oscillatory, but those "spikes" are smoothed out when the optical source has a spectral width of several hundred Angstroms (an LED source). The LC switch is fully ON at 25 V rms.

Turning to the multimode fiber-optical switching of Fig. 15, we see that 35% of the unpolarized multimode light is routed to fiber #4 at 25 V rms,

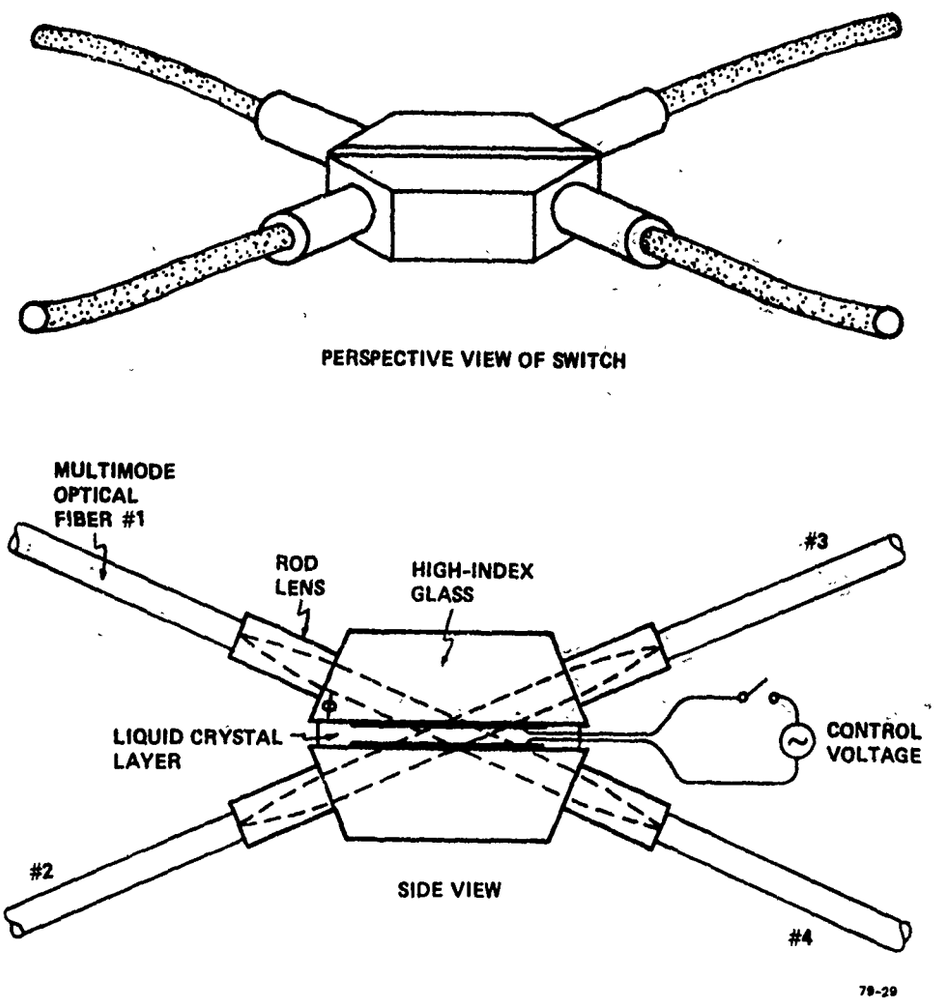

FIG. 12 Structure of fiber-optic LC switch.

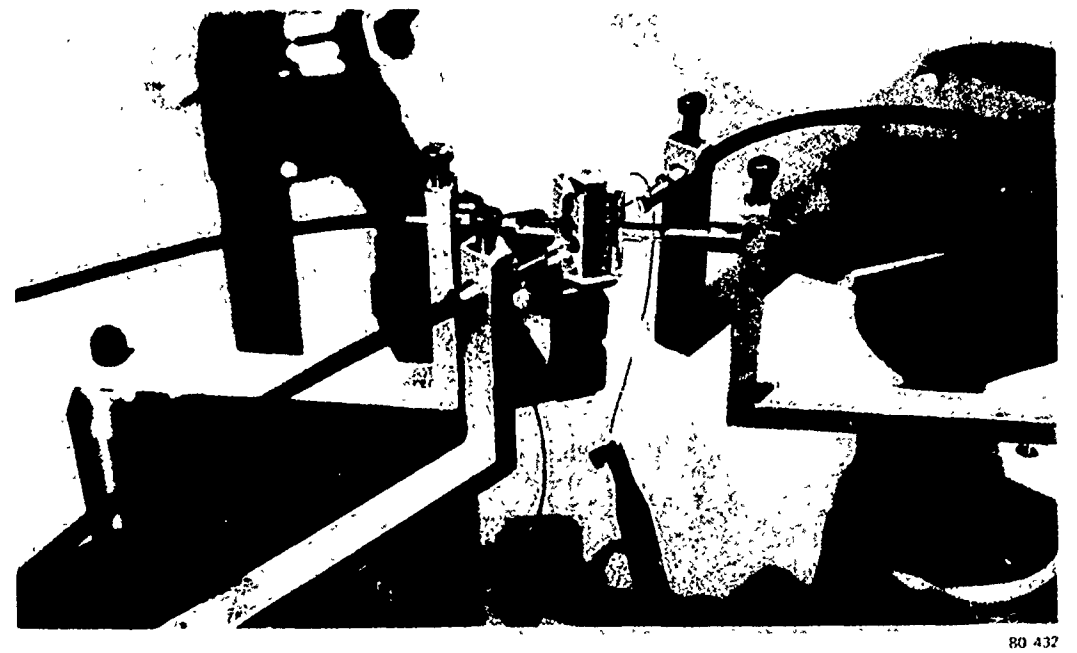

80 432

FIG. 13 Demonstration model of multimode single-pass LC switch.

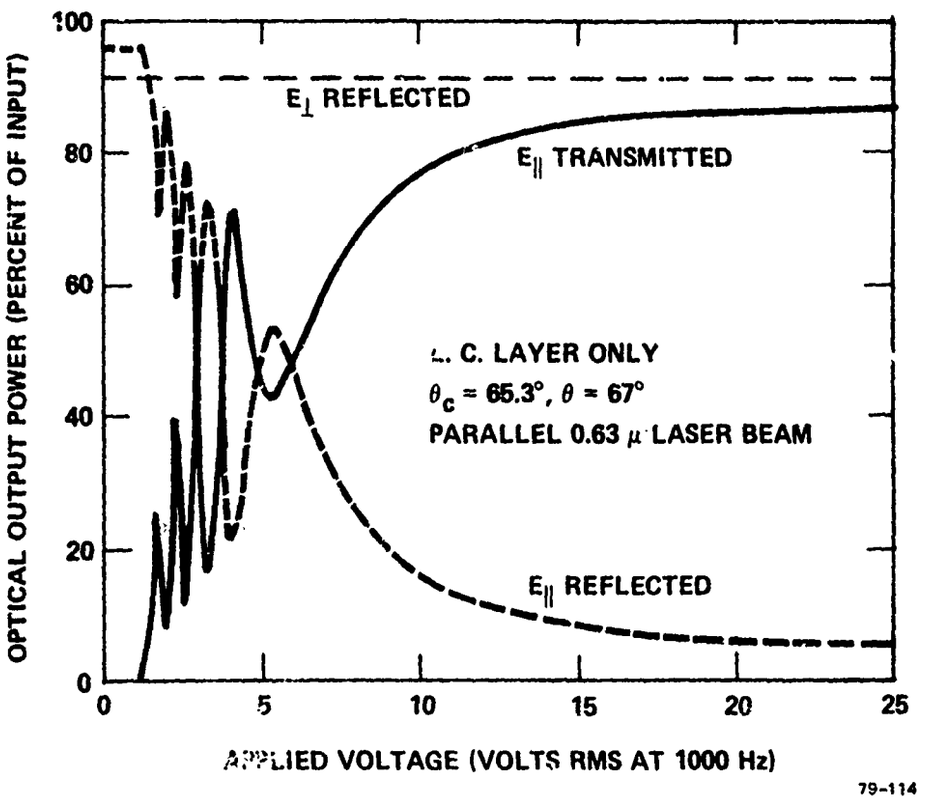

FIG. 14 Electro-optic response of ZLI-1132-LC switch (WG360 glass) to light polarized either in the plane of incidence or perpendicular to that plane. Fresnel losses at in/out glass prism faces have subtracted out.

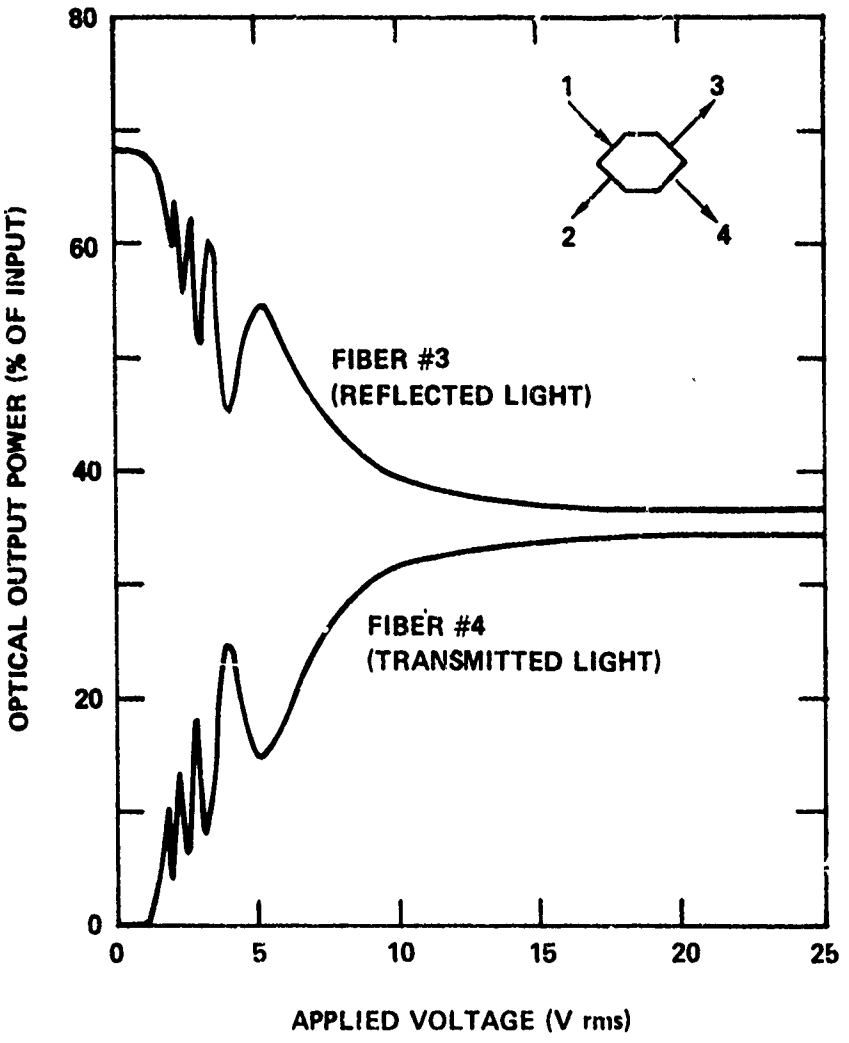

FIG. 15 Experimental response of Fig. 13 fiber switch.

while the fiber #3 output decreases by a corresponding amount. Crosstalk is -45 dB in the OFF state where the optical insertion loss, 10 log P_1/P_3, is 1.6 dB -- a result later improved to 1.0 dB.

Figure 16 shows voltage-response results for a 6-μm film of Merck ZLI-1132 LC between WG335 glass prisms (λ = 633nm). Here, the critical angle was 66.7°, and the prism angles here increased to 71.0°. The results are similar to those for WG360 glass, although the WG335 sample had lossier electrodes and the molecular texture was not entirely uniform in the ON state.

It is interesting to compare the Fig. 14 (or Fig. 16) behavior with what happens in a negative-anisotropy switch. We tested the LC material Merck ZLI-422 for which $\varepsilon_{\parallel} - \varepsilon_{\perp} = -0.5$. Here, the initial order was perpendicular to the WG360 glass walls as in Fig. 3b. We found, as Fig. 17 shows, that the electro-optic turn-on began with nearly equal amounts of light emerging from ports #3 and #4. Then, with voltage exceeding a large (11.5 V rms) threshold, the port #3 output rose to 93%, while the port #4 light level decreased sharply to 3% as Fig. 17 shows. Qualitatively, this agreed with the predicted response: the Fig. 14 sequence in reverse, although the ON-state molecular texture was not uniform in this switch due to imperfect "latent" microgrooves on the prism surfaces. The threshold was as low as 8 V rms in some LC areas.

We developed miniaturized control circuitry for these switches. A small, integrated-circuit chip powered by a miniature 9V transistor-radio battery was set up to produce 5V rms audio-frequency oscillations. The output voltage was stepped up into the 25V rms range by means of an ultra-miniature transformer. To drive the primary of this transformer under a variety of conditions, a buffer transistor (Darlington circuit) was interposed between the oscillator and transformer, althought this current-amplifier stage can be omitted in some cases. Figure 18 shows the electronic control circuit that we built and tested. This was housed in a small control box shown in Fig. 19 (pushbutton to actuate LC) and the actual output waveform at the LC switch terminals is illustrated in Fig. 20. This

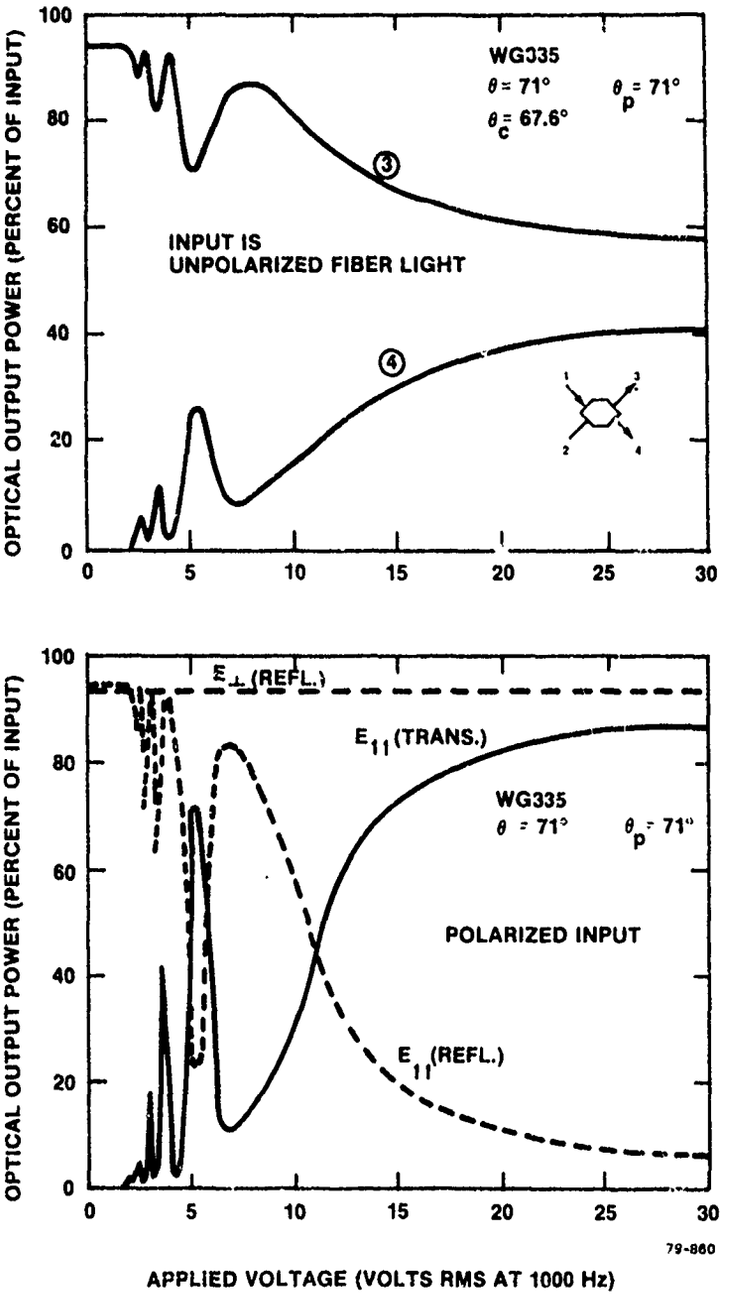

FIG. 16 Electro-optic response of ZLI-1132-LC switch (WG335 glass) to unpolarized 633 nm light (upper curves) and to polarized 633 nm laser beams (lower curves). The 11.3% Fresnel reflection losses at the glass prism faces have been subtracted from observed loss values.

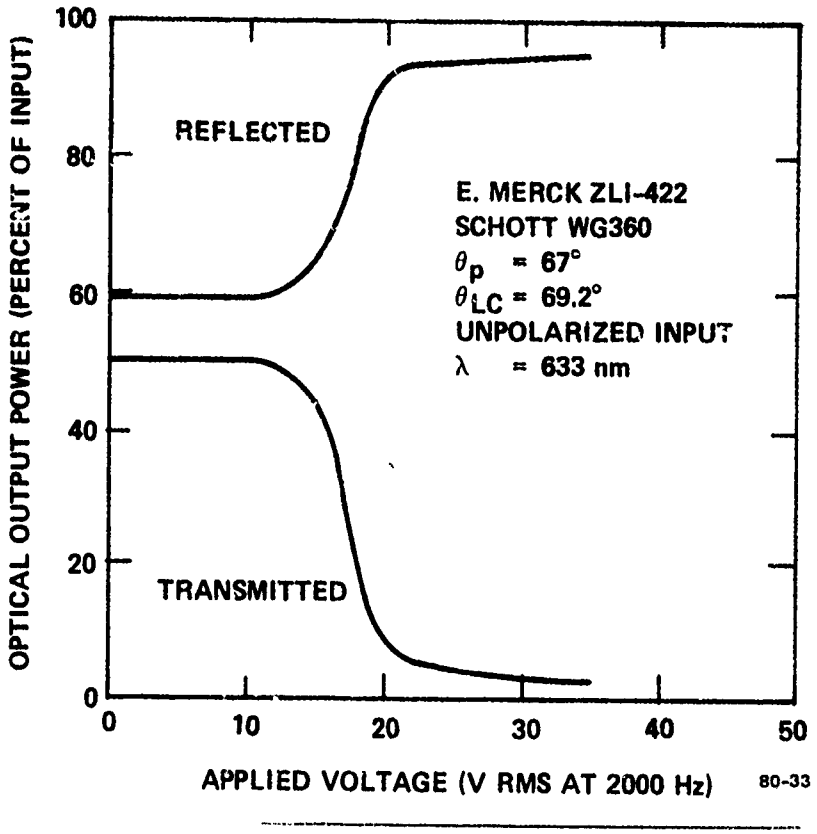

FIG. 17 Electro-optic response of ZLI-422 LC switch (WG360 glass) to unpolarized 633 nm light. The homeotropic LC layer has $\Delta\epsilon = -0.5$.

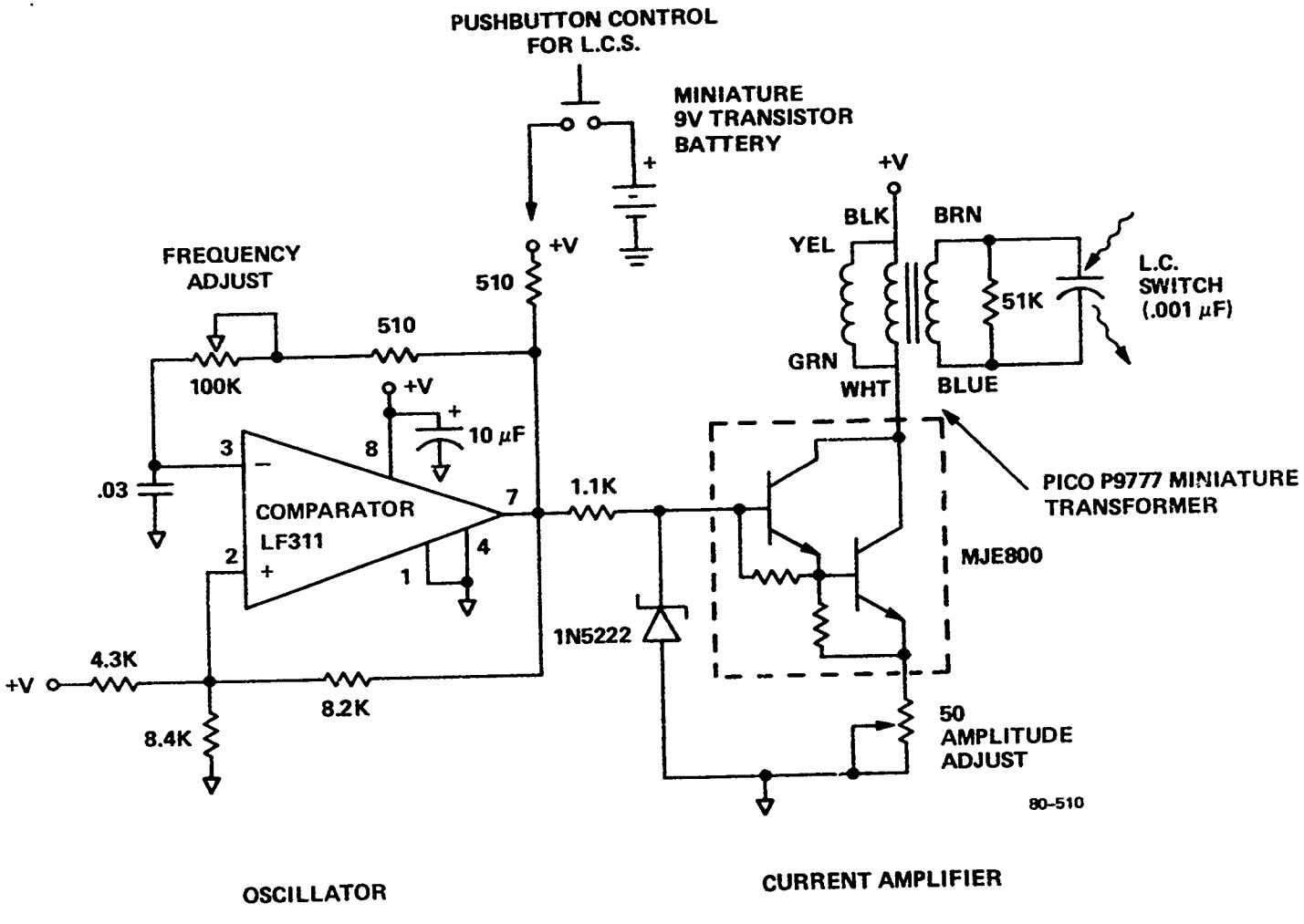

FIG. 18 Circuit diagram for electronic LC controller.

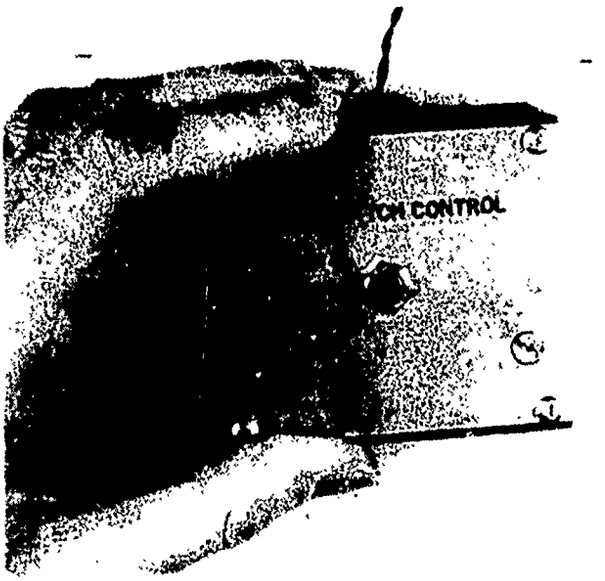

80-35

FIG. 19 Portable, battery-operated control box for LC switch.

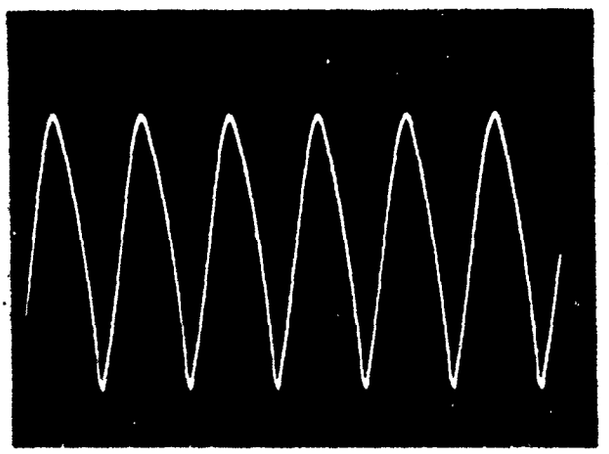

80-36

FIG. 20 Waveform applied to LCS terminals by control box.

controller has successfully operated single-pass and double-pass LC switches. The single-pass devices had a capacitance of 800 to 1200 pico-Farads, while the double-pass switch presented a load of 3000 pF. Our circuit is more elaborate than it needs to be in a commercial product because we have made provision to adjust both the frequency and voltage amplitude.

SECTION VII

FIBER OPTICAL COUPLING RESULTS

The optical insertion loss of the LC switch is comprised of intrinsic LC loss, reflection loss, and optical coupling loss. In practice, the LC scattering loss, electrode loss, and Fresnel interface loss add up to 0.5 dB. The remaining loss, which is 0.5 dB or more, is optical coupling loss -- an optical beam-spreading loss that exists between two fibers that are coupled by a pair of microlenses. We find coupling loss to be the dominant insertion-loss factor at large lens separations and we therefore investigated microlens coupling, theoretically and experimentally, to understand this factor and thereby to minimize it.

7.1 CONCEPTS

Figure 21 illustrates two Selfoc-lens coupling methods for an optical switch. The collimation method (Fig. 21a) was developed just prior to this contract, while the Fig. 21b focusing method is a new and more general technique that was conceived and tested during this contract.

The lenses in Fig. 21a have a length of exactly one-quarter pitch; hence, if the fiber core were an ideal point source, its light would become perfectly collimated. But, because of the finite core size, the output light beam does have a small angular divergence as shown, which leads to coupling loss, especially in cases where the beam diameter exceeds the diameter of the second lens.

The more universal method of Fig. 21b uses lenses whose length differs from a quarter pitch; for example, $0.252p < L < 0.260p$. Here, the fiber light becomes focussed within the "body" of the LC switch and one would choose the lens length to position the minimum waist of the light beam at approximately the midpoint of the switch as shown. (Adjustments in the focal spot positions could also be made with isotropic spacers at the fibers as

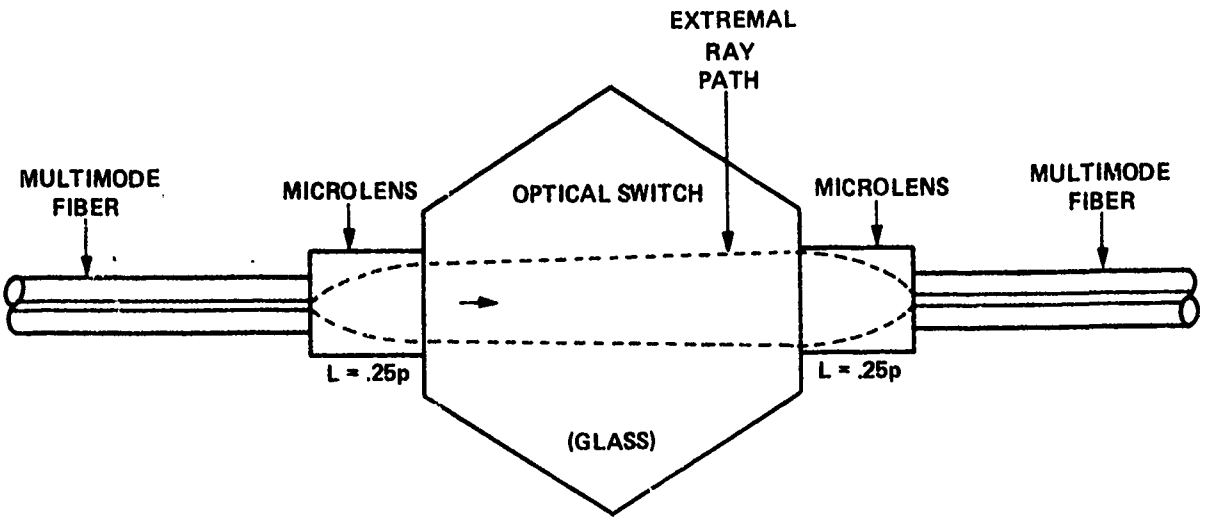

A) COLLIMATION COUPLING

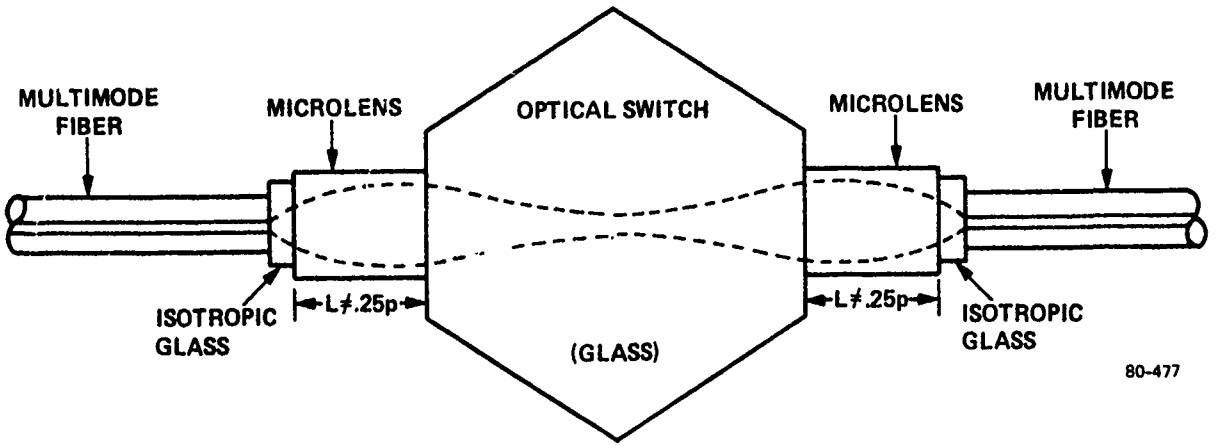

B) FOCUSING COUPLING

FIC. 21 Two means of coupling fibers in an optical switch. Only one of two fiber pairs is shown.

shown). As Fig. 21b indicates, a second lens completes the symmetrical 1-to-1 imaging arrangement that is probably optimal for capturing the light beam and refocusing it with low loss into the core of the second fiber. (We also note that the collimation method is a special case of the focusing procedure).

The two rod lenses are spaced apart (on axis) by a distance S which is equal to the switch length. The switches covered in this contract are 0.7 to 2.0 cm long, and in the future, we may expect more sophisticated LC structures that are 5 to 10 cm long to be developed -- ones that will handle more than 10 fibers for example. In the S > 5 cm cases, it is important to find a way of keeping coupling losses below 1.5 dB and it is here that we believe the focusing method can make an important contribution. We believe that the Fig. 21b method will give significantly lower coupling losses at large S-values than will the collimation method -- this is our central idea -- and we have some preliminary experimental evidence to support this assertion.

7.2 EXPERIMENTAL RESULTS

Our experiment consisted of coupling two 1-m strands of graded-index fibers (63-μm core diam, 0.21 NA) with a pair of wide-angle Selfoc microlenses (2-mm-diam, 0.5 NA) for two different lens lengths. In each case, the input fiber was excited with 633-nm laser light focused into the core by a 40× objective (~0.14-NA Gaussian cone). The on-axis lens separation S was varied and the coupling loss determined at each spacing.

The first set of data was obtained for two SLW lenses that had a length of exactly 0.25 pitch at 633 nm. Then, the experiment was repeated for two 2-mm-diam SLW rod lenses whose length was 0.26 pitch at the same wavelength. The observed loss vs. the air-gap spacing S is plotted in Fig. 22. There, we find that the loss is 0.4 dB when S = 0 for the 0.25-p lenses, with the loss staying at an 0.4 dB plateau as S is increased to 1 cm. Beyond 1 cm, the loss rises quickly. By contrast, for the 0.26-p lenses, the loss started at 1.3 dB for S = 0 and decreased with increasing

S until a minimum value of loss, 0.4 dB was reached at S = 2.4 cm. Visually, we found a minimum optical beam waist at 1.2 cm from the end of the first 0.26-p lens, which correlates with the 2.4 cm minimum-loss lens spacing. Beyond 4 cm, the observed loss increased rapidly. (To find coupling loss in an LC switch, the air separations in Fig. 22 (the abscissae) are multiplied by the 1.64 glass index).

Our ideas about the advantage of focusing coupling seem to be proven by Fig. 22; for example, at S = 4 cm, the coupling loss is 2.9 dB lower in the latter case.

Another important advantage of the Fig. 21b technique is its ability to accomodate large-core fibers. For short-haul applications like distributed computers, fibers with 125-μm to 200-μm D cores (and 0.30 NAs) are often advantageous because of their light-gathering ability. In such cases, one would expect that good fiber-to-fiber coupling would pertain if the microlens diameter were expanded to, say 5 mm, to collect the rapidly spreading beam from the first microlens. But, if we wish to keep the lens diameter fixed at, say 2 mm, we would run into trouble with the collimation technique: specifically, the "break-point" in Fig. 22 where the coupling loss goes up dramatically would occur at smaller lens spacings, for example, at S = 0.4 cm. This would lead to excess ve loss in the switching devices.

The focusing technique appears to offer a remedy, and we feel that 200-μm-D fiber coupling losses below 1.5 dB for S < 2 cm will be achievable with 2-mm-D lenses via Fig. 21b. Stated more generally, the focusing method should offer efficient coupling of large-core, large-NA fibers with 2-mm-D lenses for a variety of switch sizes. This would give our LC switch the capability of handling almost any fiber, making it a "universal" device.

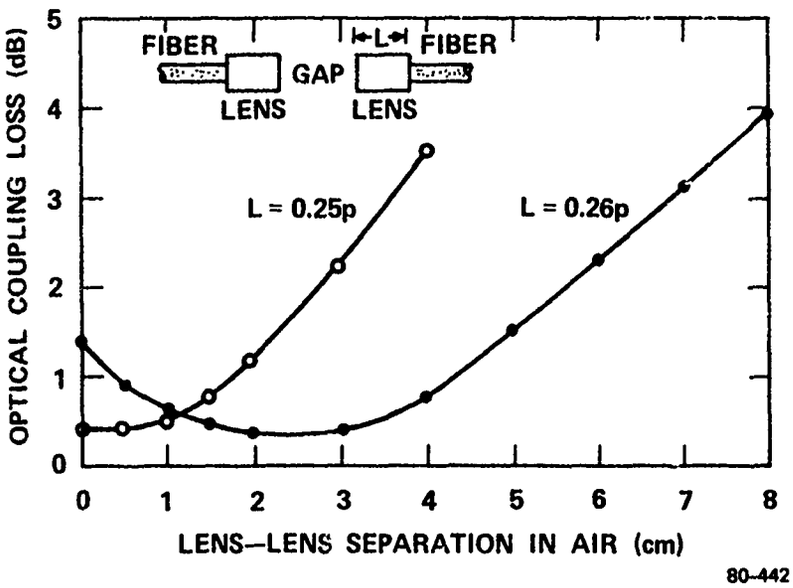

FIG. 22 Observed coupling between multimode fibers as obtained with Selfoc microlenses.

SECTION VIII

IMPROVED SWITCHING SPEED

For the most part, the LC switch properties are excellent, but speed is a limitation. The multi-millisecond electro-optic response times are probably the main disadvantage of the LC approach. During this contract, we devised a new method of speeding up the switch response. An order-of-magnitude improvement was achieved, which represents an advance in the art. This technique is discussed here, beginning with some general comments on response.

Although there is no "flow" as such during an electric-field Freedericksz transition, electric torques are present and the turn-on and turn-off of the LC switch requires physical re-orientation of molecules. Since the LC is a viscous liquid, it is probably fair to say that the fundamental limit on speed is the time it takes for a mechanical or electro-mechanical disturbance to diffuse among neighboring molecules: 10 μs to 10 ms. The well-known electro-optical response times of an LC display at normal incidence are relevant to our field-effect LC switch, apart from the oblique-incidence factors discussed below. The time constants are:

$$\text{rise time} = 4\pi\gamma d^2/\Delta\varepsilon(V^2-V_{th}^2)$$

$$\text{fall time} = \gamma d^2/\pi^2 K_{33}$$

where γ is a viscosity coefficient, d is the LC layer thickness, K_{33} is the elastic bend constant, V the applied voltage, and $\Delta\varepsilon$ the dielectric anisotropy. The rise time and delay time are both voltage-dependent, and we find at conventional ON-state voltages of about 30 V rms that the rise will take about 0.5 ms, which is acceptable in many situations.

The "problem area" is the fall time or "recovery time". This natural decay time ranges typically from 40 to 80 ms. One can exert some control over the fall time due to the prism-spacing factor and the viscosity factor mentioned above (the latter pertaining to chemical composition of the LC). Starting at d = 5 μm, however, the adjustments that can be made by varying d and γ are usually not enough to produce large decreases in the fall time, and some other approach must be found.

We can enumerate four techniques for speeding up the recovery time:

(1) The high-frequency-field method

(2) The in-plane field method

(3) The bias-field method

(4) The incidence-angle method.

The fourth approach is a significant new technique invented at SRC. The other three have been described fairly well in the LC literature, but we shall outline them here to put our method in perspective.

The HF technique refers to the application of an ac erasure-voltage at a frequency of about 100 kHz which drives the LC OFF electrically with torques that return molecules to their initial orientations. This is possible because the dielectric anisotropy of the LC changes from positive to negative at sufficiently high frequencies.

The second method uses a triode electrode structure such as inter-digitated electrodes on one glass surface and a sheet-electrode on the other. Positive molecules are driven OFF electrically by application of a low-frequency E-field in the plane of the LC layer. The other elements of the triode are used to turn the liquid ON with fields normal to the layer.

The third method utilizes thin boundary layers in the LC film near the glass walls where the molecular order changes from the wall alignment to the "bulk" alignment (the LC is not truly uniaxial at a given voltage as per Fig. A1(a)). The thickness of each of the two sub-layers is given by the

coherence length ξ, where ξ is inversely proportional to voltage. A strong bias voltage is first applied, creating boundary layers approximately λ/ξ thick. Then a switching voltage slightly larger than the bias is applied, thereby modulating the coherence length. The altered phase retardation in the LC layer could be sensed with a crossed-polarizer arrangement (not directly applicable to our switch). Because these layers are ultra-thin, they can be altered in as little as 100 microseconds. However, the value of this method for fiber-optic switching is not obvious because the $\lambda/8$ layers are not thick enough (according to tunneling theory) to produce appreciable changes in glass/LC reflection and transmission, although the bias method might give rapid, small-scale changes (partial switching) in our device.

The fourth method is the main subject of this section. Theoretical and experimental evidence led us to investigate the effect of high incidence angles on the transient response. One can imagine various switching devices, as illustrated in Figs. 23a and 23b where the optical incidence angle θ is different, $\theta = \theta_1, \theta_2$, etc. (In each case, the glass prism angle θ_p is the same as θ). We propose that the θ_2 device is faster.

To understand the effect of the angle θ on speed, we need a simple model for the LC such as the uniaxial model in Fig. 24. At a voltage V, the general steady-state situation is a partial switching of $E_{\|}$-light with molecules uniformly tilted at an angle α with respect to the glass substrates, α being a large angle with the switch fully ON, and with α returning to zero after voltage is removed. This is a simple, director-rotation model. The decay of α is rapid when voltage is first taken off; then the rate of change of α decreases as $\alpha \to 0$.

We learned in Appendix A that the switch does not turn on appreciably when α is less that 45°, and that large-scale changes in optical transmission occur when α is in the 45° to 75° range (Figs. A6-A8). We came to the conclusion that high incidence angles (large θ in Fig. 24) would produce fast decay for two reasons: 1) if a large θ is chosen, the

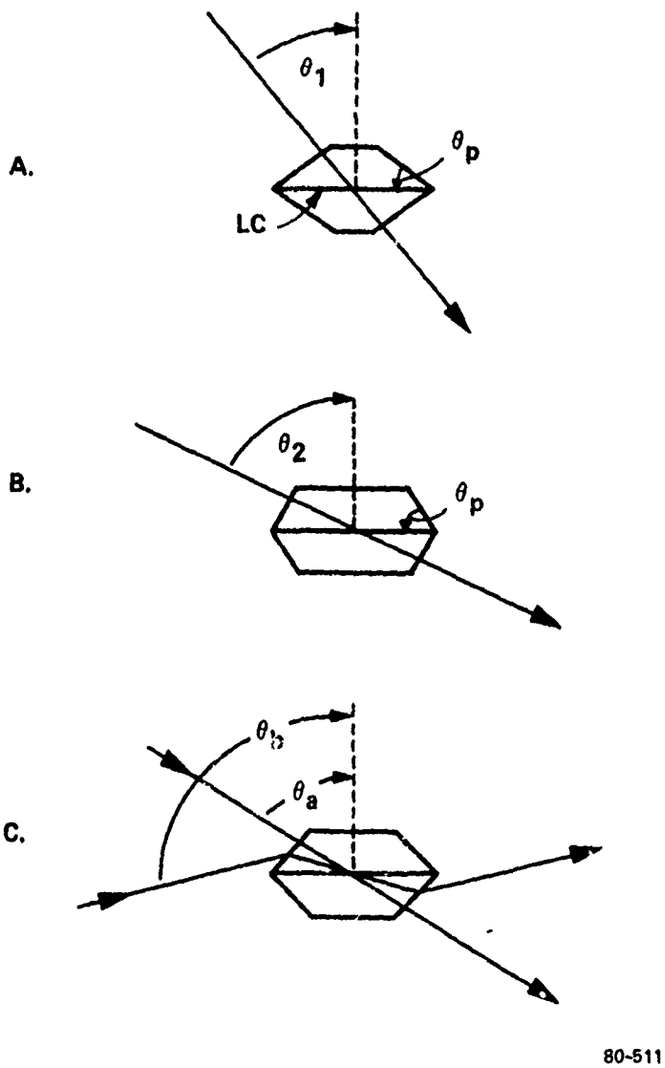

FIG. 23 Structure of 2 x 2 LC switch (side view) showing geometric changes that influence transient response: A) small incidence angle θ_1, B) large incidence angle θ_2, C) method of changing θ in one device.

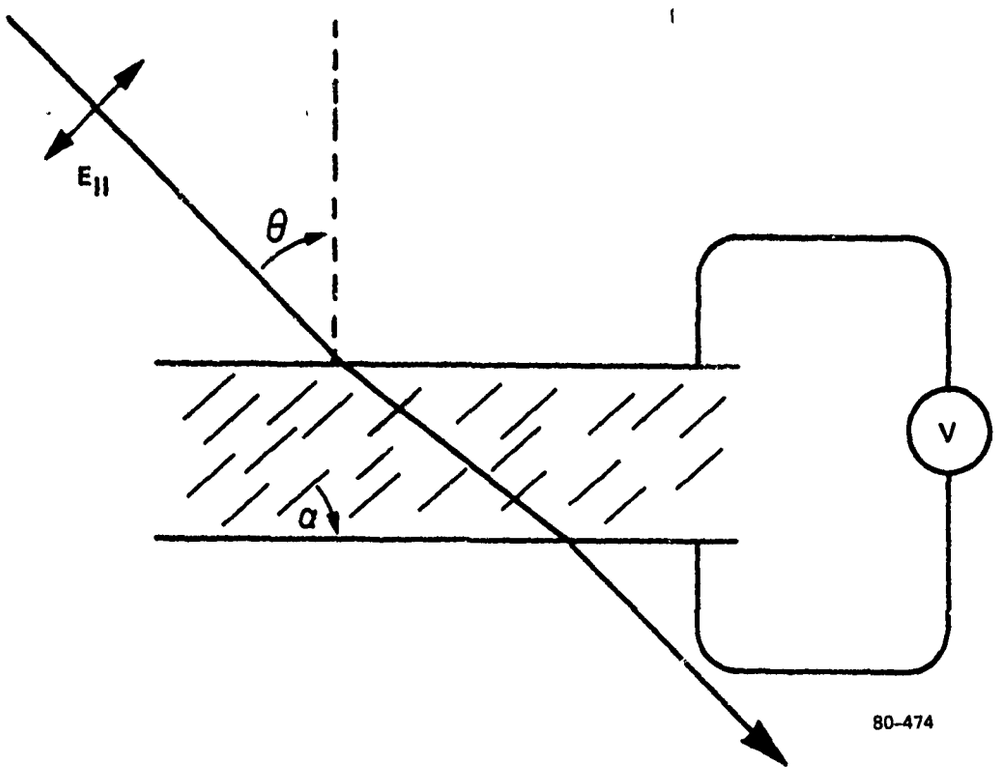

FIG. 24 Simplified model of LC layer at applied voltage V.

optical response will center on a narrow range of large-α values, and 2) the narrower the α-range, the wider the swing in optical transmission produced by a given change in tilt $\Delta\alpha/\Delta t$. Note also that there is a direct linkage between director rotation speed and switching speed because the rotation takes place in the optical incidence plane (Fig. 3). The decay speed-up pertains solely to the $E_{\parallel}$-light. In summary, our idea is to make switches whose prism angle ($\theta_p = \theta$) is 10° to 16° larger than the critical angle (these specific angles are explained below). There are, of course, practical limits on how large θ can be made; for example, the device will become very long as $\theta \to 90^{\circ}$, and $\theta = 80^{\circ}$ might be an upper limit.

8.1 EXPERIMENTAL RESULTS

To prove the above hypothesis, we performed experiments on a $\theta_p = 67^{\circ}$ device as shown in Fig. 23c where a collimated 633-nm laser beam was incident at external angles θ_a, θ_b, etc. where the external angle is related to the incidence θ by means of n_g and θ_p factors.

Figure 25 illustrates the time-dependence of the optical, LC, and electrical waveforms in our LC switch transient-response experiments. The chief quantity of interest is the switched optical transmission (upper waveform). The middle waveform is the effective orientation angle of the nematic director within the LC (a microscopic variable, not directly observable), while the lower waveform shows the ac electrical signal (square wave or sine wave) applied to the LC electrodes for switching. Since we are concerned with the fall time, we set $t = 0$ when the voltage is first gated OFF. We find in our single-pass LC switches an oscillatory decay as shown in Fig. 25. In practice, this decay has an envelope (indicated by the dashed line in Fig. 25), whose form is approximately an exponential. Here, we define the decay time as that time in which the optical output envelope falls to 10% of its initial intensity.

Digressing for a moment to a discussion of the rise time, we see in the experimental result of Fig. 26 (1-ms per division time scale) that the actual rise of switched light (upper trace) is quite fast: 0.4 ms when a 25V rms square wave (lower trace) is applied, representing a typical ON-state drive level. It is seen that the rise is not a significant problem.

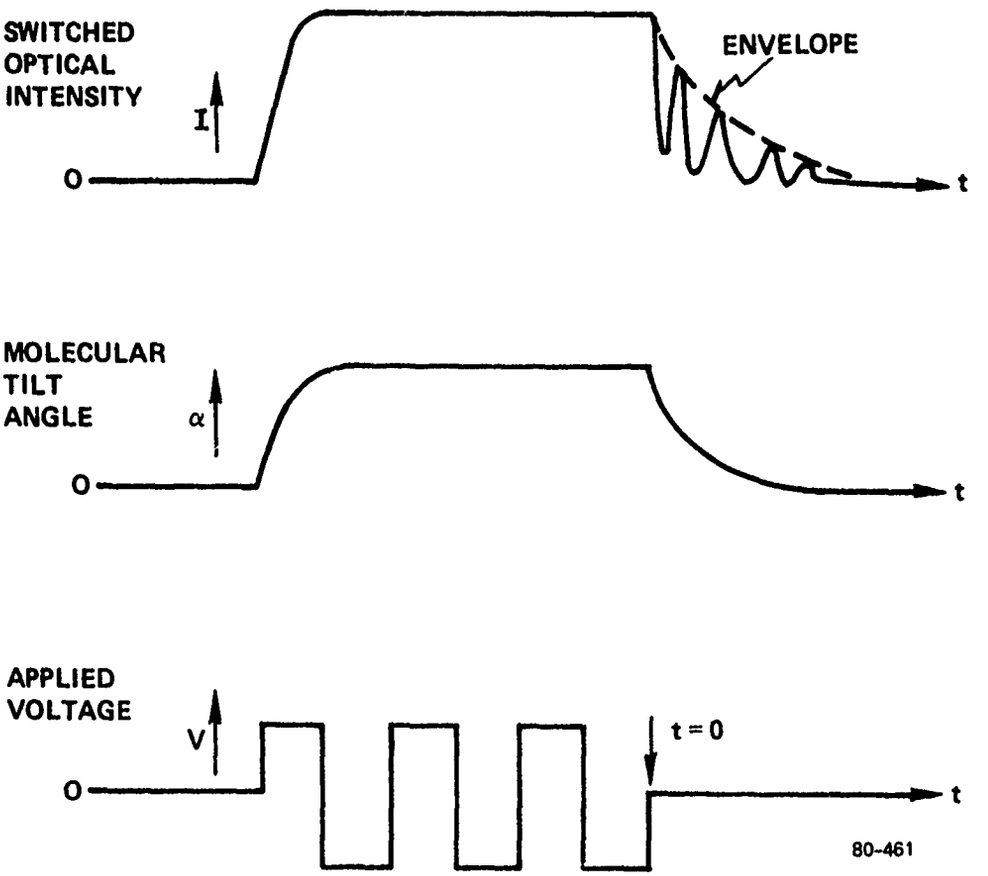

FIG. 25 Waveforms of optical, molecular, and electrical variables during transient response of LC switch.

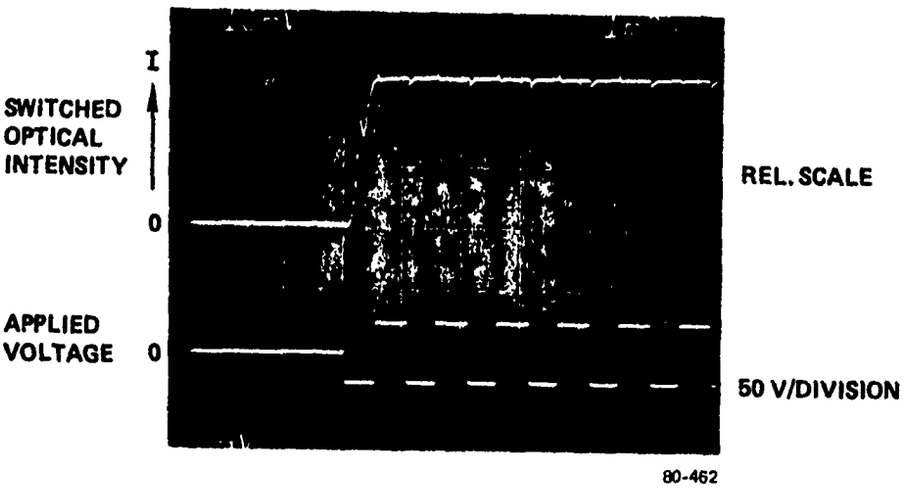

FIG. 26 Observed turn-on of typical LC switch.

The results of our fall-time experiments are presented in the three oscilloscope photographs of Fig. 27. This figure shows what happens to the decay time of a single-pass LC switch ($\theta_p = 67^\circ$, Merck ZLI-1132-LC, WG360 glass, d = 5 μm) as the internal incidence angle is increased from 67° to 73°. (Individual oscillations in the applied 25 V rms square wave are not resolved in the photographs). The time scale is 20 ms per division. For $\theta = 67^\circ$, the decay envelope has a 40 ms time constant. In going to $\theta = 70^\circ$, we see that the recovery time was diminished to 11 ms. Finally, at $\theta = 73^\circ$, we obtain the fast 4-ms response time seen in the lower photograph, a ten-fold improvement in speed for a 6° increment in θ. This response is among the fastest ever deserved for a simple 5-μm LC device with 25 V rms applied. A theoretical analysis will tell us what further improvement may be expected.

8.2 TRANSIENT-RESPONSE THEORY

Figure 24 illustrates a simple LC model, a rotating director in a uniaxially ordered layer, which gave useful insights into steady-state switching (Appendix A) and which should give useful information about the transient decay envelope. (Details about the oscillatory behavior would be derived from a more complex model that took into account O-ray and E-ray interference in the LC).

Only light polarized in the incidence plane is switched ($E_{\parallel}$). Following the discussion of Appendix A, the optical intensity in the single-pass device is:

$$I(\text{trans})_{\parallel} = \frac{\sin^2(2\theta)\,\sin^2(2\theta')}{\sin^4(\theta'+\theta)\,\cos^4(\theta'-\theta)} \qquad (1)$$

where $\theta = \theta_p$ is the structural parameter under consideration, θ' is the refraction angle in the fluid as given by the approximation:

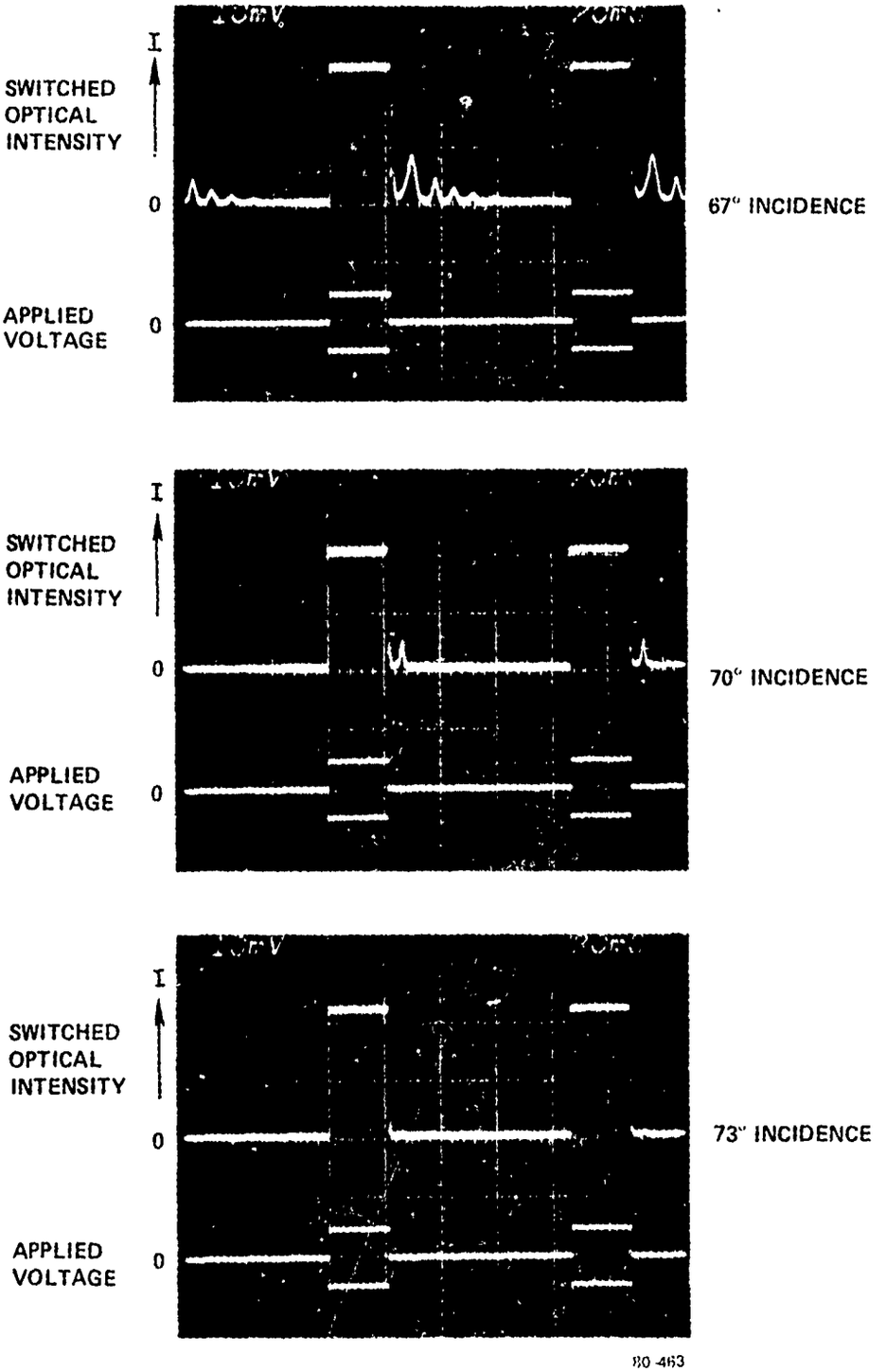

FIG. 27 Observed turn-on and turn-off of 2 x 2 LC switch at three different optical incidence angles. Gated square wave is applied to switch.

$$\theta' \approx \arcsin\left[\frac{n_g\sqrt{n_o^2 \sin^2\alpha(V) + n_e^2 \cos^2\alpha(V)}}{n_o n_e} \sin\theta\right] \qquad (2)$$

The voltage dependence of $I(\text{trans})_{\parallel}$ is contained in the molecular tilt angle $\alpha(V)$, and since the voltage is time varying, Eq. 1 describes the transmission at any instant. The boundary conditions are: $V = V_{max}$ at $t = 0$ and $V = 0$ at $t > 0$. Also, $\alpha = \alpha_o$ at $t = 0$ and $\alpha = \alpha_o f(t)$ at $t > 0$.

We modeled the turn-off by using a simple analytical form for $\alpha(t)$. Although the substitution of a particular $\alpha(t)$ into Eq. 1 is an ad hoc procedure, the calculated results should have validity if there are sound physical reasons for choosing a specific $\alpha(t)$. The use of a simple exponential form for the director time-dependence

$$\alpha = \alpha_o \exp(-t/\tau) \qquad (3)$$

is suggested by the situation within the switch at turn-off; restoring torques from the glass walls opposed by viscous torques in the LC. The voltage-ON tilt angle α_o was determined empirically in Appendix A by curve-fitting to the experimental data of Kahn. There, it was learned that α does not reach 90° in practice and that a typical value is $\alpha_o = 78^\circ$.

Our computation proceeds by putting Eqs. 2 and 3 into Eq. 1 with α_o and τ being free parameters that can be adjusted to give a good fit to the experimental curve. We have solved Eq. 1 with the aid of a computer and have plotted the results for various choices of α_o and τ. Values of τ = 20 to 40 ms were tried because decay times of that order are found in conventional experiments. We also put in values of α_o in the 65° to 80° range as per the Appendix A discussion. We then found that the best fit to the Fig. 27 data was obtained when $\alpha_o = 69^\circ$ and τ = 20 ms. Figures 28 and 29 show the calculated values of the switched light $I(\text{trans})_{\parallel}$ as a function of time in the turn-off situation, with the optical incidence angle θ as a running parameter. The assumed time-dependence of the director

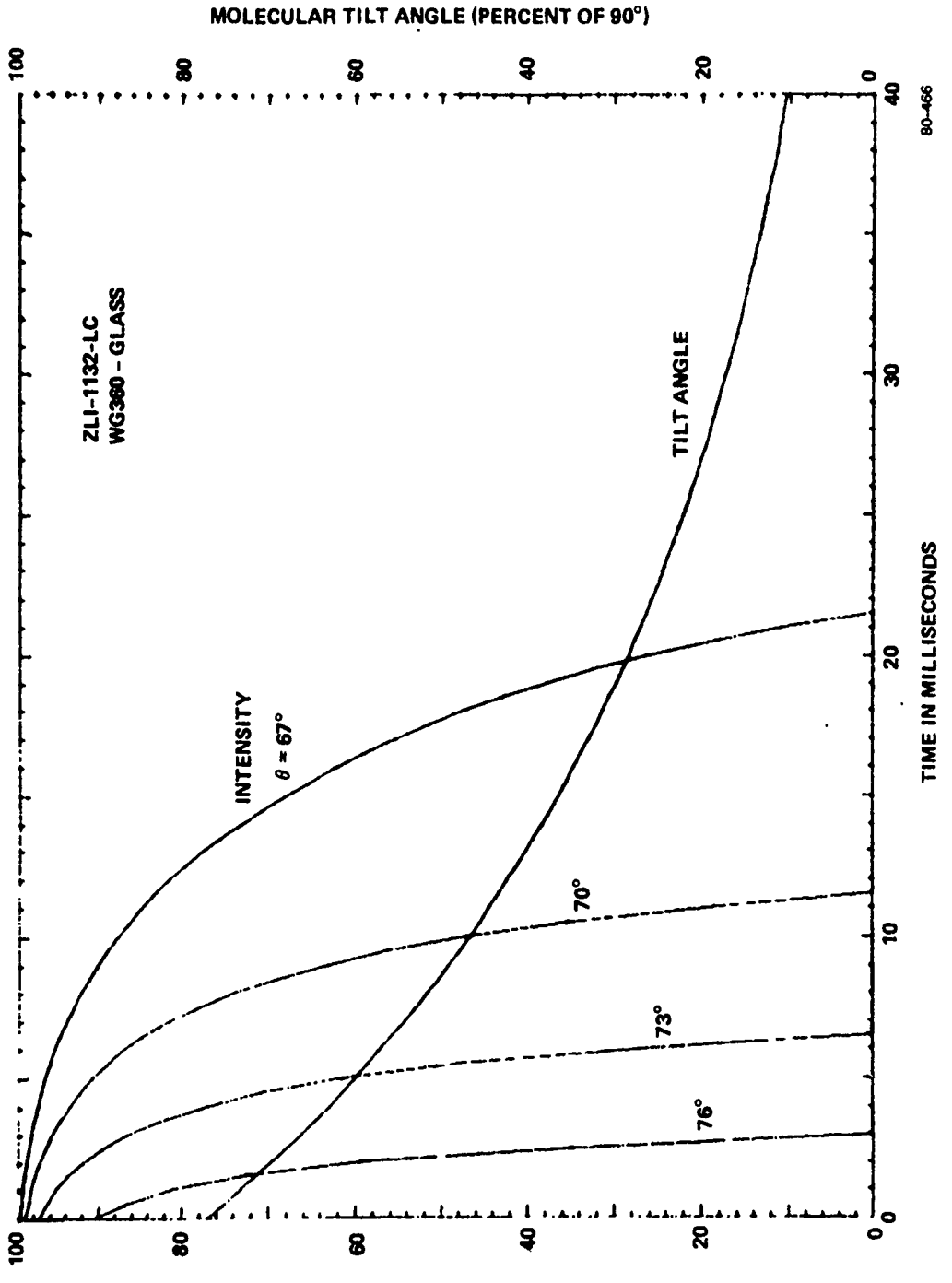

FIG. 28 Theoretical time-dependence of switched light (turn-off behavior) for the optical incidence angles 67°, 70°, 73° and 76°. Assumed $\alpha(t)$ is also shown.

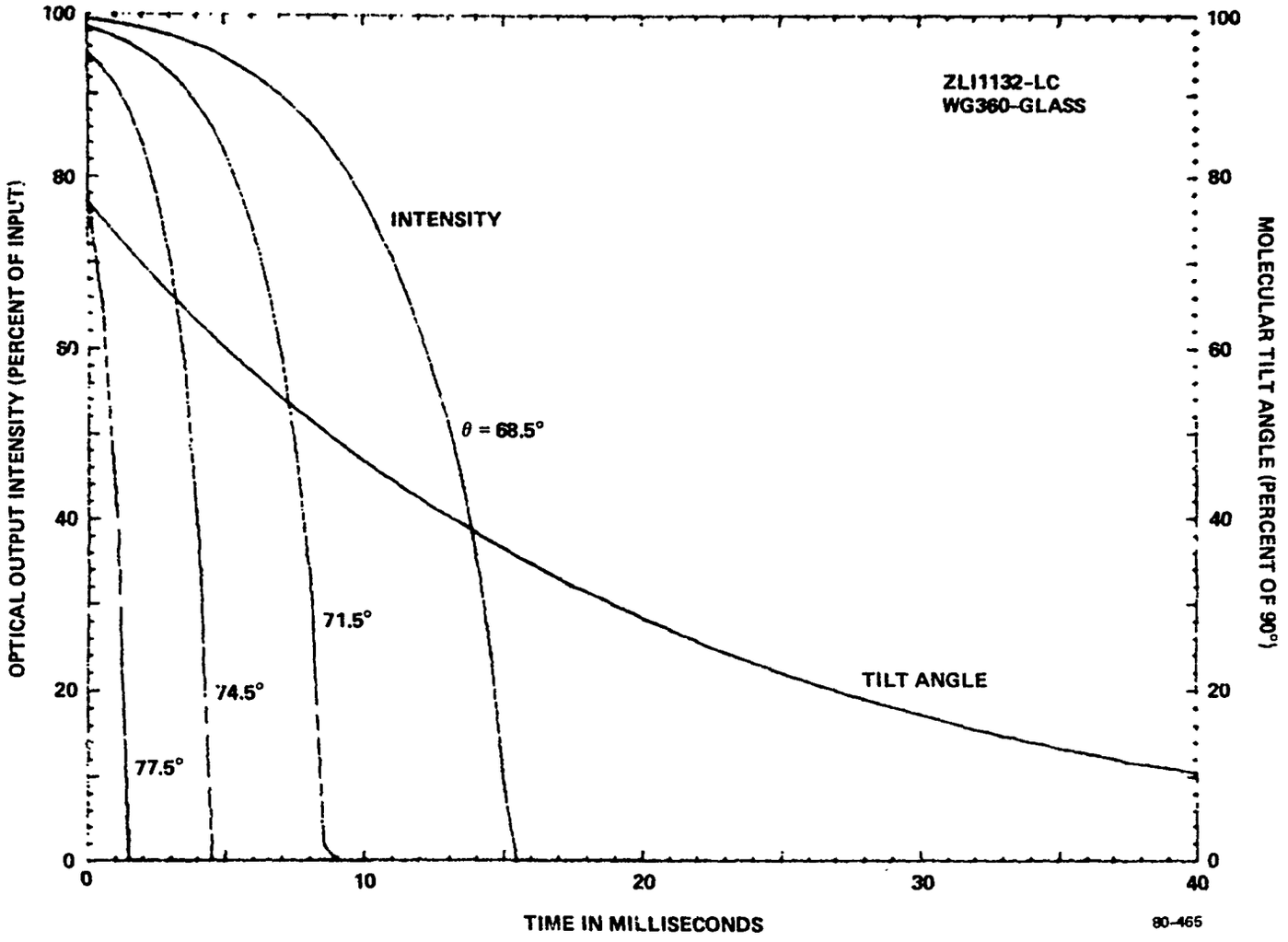

FIG. 29 Theoretical time-dependence of switched light (turn-off behavior) for the optical incidence angles 68.5°, 71.5°, 74.5°, 77.5°. Assumed $\alpha(t)$ is also shown.

tilt $\alpha(t)$ is also shown. Figure 28 indicates what happens when the 67° incidence is increased in steps of 3°, while the Fig. 29 results are for $\theta = 68.5^{\circ}$ stepped up successively in 3° increments. Qualitatively, the curves show a marked decrease in turn-off time with increasing θ.

8.3 COMPARISON OF THEORY AND EXPERIMENT

Experimental and theoretical results have been compared in Fig. 30 where the 90%-down criterion has been used to determine fall times. Over the 67°-73° incidence range, agreement between theory and practice is good, and the theory goes on to predict a further decrease in turn-off time with higher θ; specifically, a 1-ms recovery time at $\theta = 78^{\circ}$ for LC 1132/Glass WG360, which is an incidence angle 12.8° beyond the critical angle. Judging from Fig. 30, there is a high probability that a 1-ms recovery could be attained in practice. Additional predictions of our theory are illustrated in Fig. 31 for the liquid crystal E7 made by BDH Chemicals, assuming that this LC is sandwiched between WG345 glass prisms as per Table 3. The computed decay time for E7 with $\alpha_o = 69^{\circ}$ and $\tau = 20$ ms has a similar θ-dependence; specifically, a fall time of 19 ms at $\theta = 64^{\circ}$, decreasing ten-fold to a 2-ms fall time at $\theta = 77^{\circ}$, an angle 15.5° beyond the critical angle. As in Fig. 30, this is a useful response-time prediction.

The 4-ms result already obtained has practical value and is fully competitive with electro-mechanical fiber switching results. Moreover, because of the Fig. 30-31 results, we feel confident that fiber-optic LC switches with 1 or 2-ms cycling times (ON time + OFF time at room temperature) can be built. The high incidence angle does, however, require a tradeoff in the voltage; namely, as θ is raised, the voltage needed for full turn-on goes up by 50% in some cases. And the 1-ms response might require a doubling of the control voltage relative to the 40-ms geometry.

We have not talked yet about the temperature dependence of the switching speed. Because the viscosity enters into the numerator of the time-constant expressions given above, and because γ has a strong temperature dependence of the sort illustrated in Fig. 11, we estimate that the

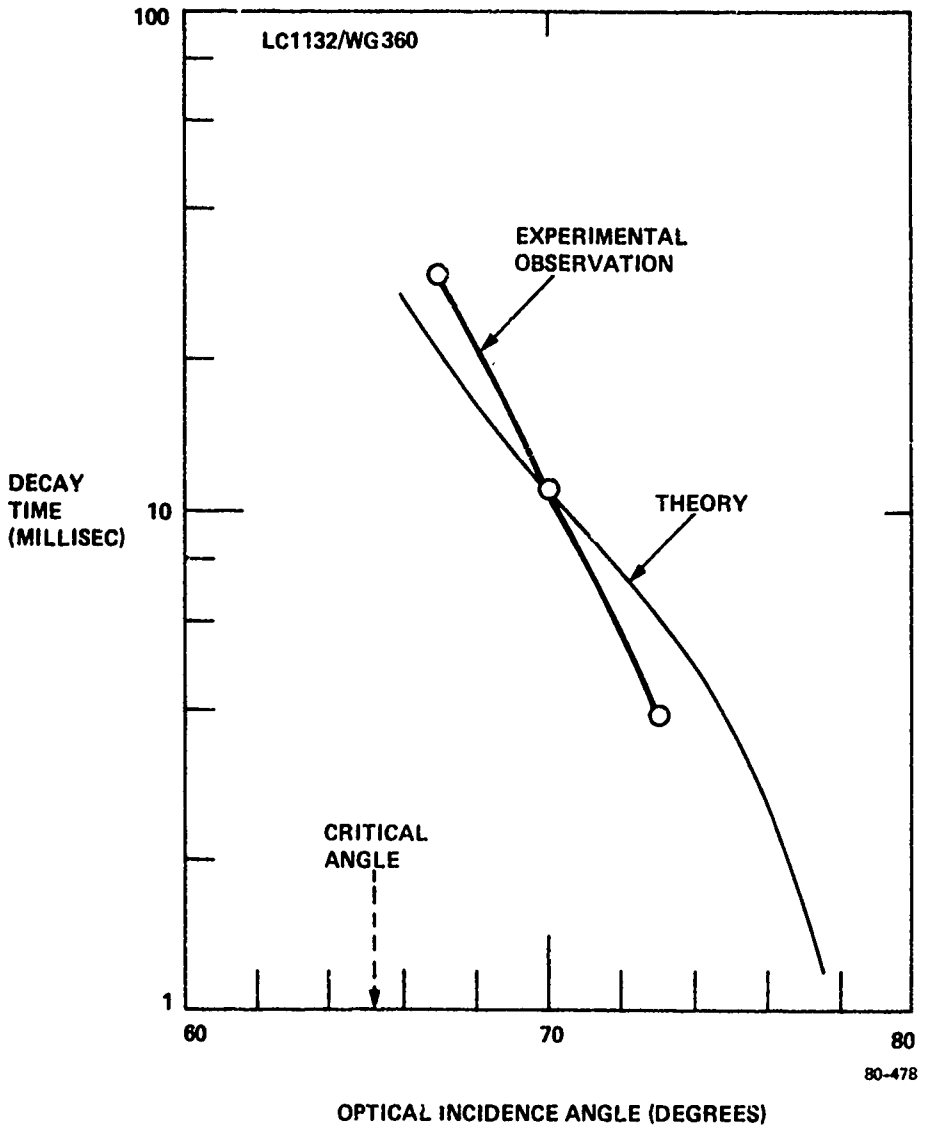

FIG. 30 Experimental and theoretical turn-off times of LC switch (1132/WG360) as a function of prism angle.

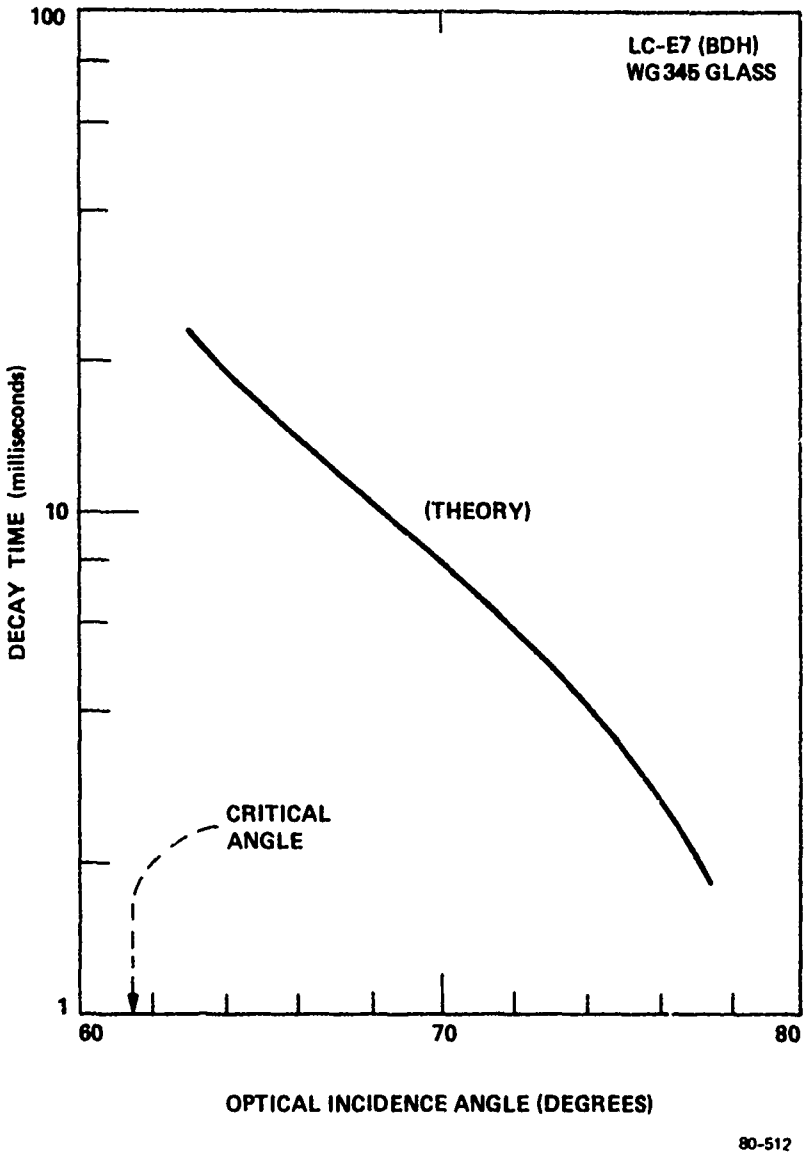

FIG. 31 Theoretical turn-off time of LC switch (E7/WG345) as a function of prism angle.

foregoing transient responses will be modified in accordance with Fig. 11 over the mesophase temperature range. For example, considering temperature extremes, one would expect a 4-fold increase in rise and fall times when lowering T from 22° to 0°C (near the crystal-to-nematic transition point). On the other hand, the LC switch would speed up considerable near the high temperature nematic-to-isotropic transistion temperature; namely, a factor-of-7 reduction in both rise and fall time (sub-millisecond response for both at $\theta = 77^{\circ}$) at T = 80°C compared to room temperature.

As a final comment, we consider whether our $\theta >> \theta_c$ principle for speed improvement applies universally to any uniaxial arrangement of LC molecules. The answer thus far seems to be "no". If, for example, we consider the double-pass switch for which the initial V = 0 order of LC molecules is orthogonal to the incidence plane (Fig. 4), we find a different result. There, the director rotates in a plane normal to the light plane and the transmission of both $E_{\parallel}$ and $E_{\perp}$ light is effected. The influence of $\Delta\alpha/\Delta t$ on $E_{\parallel}$ is not as direct as in the single-pass case. We have preliminary evidence that the fall time is not speeded up appreciably in double-pass structures by increasing θ. This would be explained by the out-of-plane director rotation. At present, the speed-up works best for the Fig. 3 ON/OFF conditions.

SECTION IX

SUMMARY AND CONCLUSIONS--LC RESEARCH

Accomplishments have been made in the following areas on this contract:

(1) Applications of 2 × 2 LC switches in serial data buses and in optical repeater loops have been identified.

(2) A single-pass structure that switches one optical polarization efficiently has been developed. Extremely low crosstalk, -45 dB, is found in the OFF state because total-internal-reflection by the LC is a nearly perfect process.

(3) Optimized materials for switching have been identified. Nine combinations of glass prism material and stable LC material have been found. One such optimum pair is: Schott WG335 glass, plus Merck ZLI-1132 LC. An optimal switch design procedure has been worked out.

(4) Technology has been developed in the areas of electroding, surface-ordering, spacing, filling, and sealing--including the following specific elements: highly transparent 400-Å indium-tin-oxide electrodes, 200 Å of SiO deposited at 60° for LC alignment at walls, 5 μm of SiO_2 deposited in the form of a gasket for prism spacing, LC added to the switch package at 95°C for uniform molecular texture, and an epoxy hermetic seal.

(5) The feasibility of optical switching in the 0.6 to 0.9-μm wavelength range has been demonstrated by self-contained prototype models coupled to four strands of multimode optical fiber, 85 μm-D, 0.17-NA. The measured and extrapolated performance of LC switches is competitive with that of electro-mechanical switches in most respects, and is superior in some respects. We observed an optical insertion loss of 1.0 to 1.6 dB, the lowest reported for an all-electronic switch. Operating voltage was approximately 25 V rms with μA control currents. Crosstalk ranged from -45 to -13 dB, and the optical backscatter was 44 dB down.

(6) Fiber optical coupling with Selfoc microlenses has been investigated and a new focusing-coupling technique has been conceived and tested in an air-gap experiment. Our results indicate that we will be able to get low coupling losses in large switches; less than 1.5 dB in switches as long as 5 cm. Also, we anticipate with this method low coupling losses with large-core, large-NA fibers such as 200-μm-D, 0.3 NA.

(7) A significant improvement in switching speed has been obtained with a novel technique invented at SRC. The idea is to build the LC switch with a relatively large prism angle, approximately 12° to 15° higher than the optical critical angle. We found experimentally that a 6° increase in optical incidence angle gave a factor-of-ten reduction in fall time, 40 ms to 4 ms, starting at $\theta_p = \theta_c + 1.7^{\circ}$. There is evidence, both experimental and theoretical, that 1-ms switch cycling times (ON time, plus OFF time) are feasible at room temperature for our fiber-optical LC structures.

With regard to future work, we would recommend further effort in the following four areas:

(1) Additional technology development. Thicker ITO electrodes, 1000 to 1500 Å, should be tested to see they offer more stability than the 400-Å films. Methods of LC alignment, filling, and sealing should be optimized.

(2) Environmental testing and additional transient response testing. This would include operational tests over the 0° to 80°C temperature range in which the transient response and the steady-state response characteristics would be measured. It would be useful to cycle the switches ON and OFF 10^5 to 10^6 times to obtain lifetime information and reproducibility data.

(3) Wavelength tests. Although we fully expect that the switch will operate properly at the long wavelengths that are now becoming popular for long-distance communications, it would be worthwhile to verify that the switching performance is good at $\lambda = 1.3$ μm and at $\lambda = 1.6$ μm.

(4) Larger, more complex switching arrays. A logical extension of the present work would be to increase the size and functional complexity of the fiber optical switch. A useful project would be to design and build LC structures for $1 \times N$ and $N \times M$ fiber switching (multi-pole and matrix switching). These switches would require two or more layers of LC.

MAGNETIC STRIPE DOMAIN RESEARCH

SECTION X

BACKGROUND

Magneto-optic materials represent the major potential competition to electro-optic materials in the field of multimode optical switching. Their use, however, has been severely restricted because of the limited optical transparency of crystals containing iron. In the far infrared, many of these materials display excellent figures of merit but are quite inefficient in the wavelength region where present fiber optic sources and detectors operate.

The most promising materials to date for magneto-optic applications are the rare-earth iron garnets. They display large figures of merit in the region between 1.2 and 2.0 μm, and, if their properties are suitably enhanced by shifting the peak in the figure of merit towards lower wavelengths, these materials will prove extremely valuable for multimode optical switching. A materials development program requires a detailed understanding of the garnet structure and how it may be modified to achieve the desired physical properties.

Rare-earth iron garnets have the general formula $A_3B_2(B'O_4)_3$ where the A cations are in eight fold coordination with the oxygen anions, B' cations are in four-fold coordination with the oxygen anions. These sites are commonly referred to as the dodecahedral, octahedral and tetrahedral sites, respectively. The rare-earth cations occupy the dodecahedral sites, while iron occupies both the octahedral and tetrahedral sites in the usual case. However, departures from this usual case are common, and, depending on the relative ionic sizes of the cations involved, some small fraction of the rare-earth cations (especially the heavier ones) are known to occupy octahedral sites in addition to the dodecahedral sites.

Diluting the iron garnet structure with bismuth is known to increase the Faraday rotation at wavelengths from .6 to 1.0 μm. Bismuth occupies

the dodecahedral sites and for that reason can be considered a substitute for the rare-earth cations in the garnet composition. When bismuth is present, the Curie temperature of the garnet is higher than one expects on the basis of the observed lattice constant. The relative sizes of the rare-earth cations present also affects the Curie temperature. Hence, the larger rare-earth cation, the higher the temperature. Finally any dilution of iron with non-magnetic cations reduces the net magnetization of the garnet via reduction of the Curie temperature.

It has been proposed that the higher Faraday rotations observed with bismuth substituted rare-earth iron garnets is associated with the increase in superexchange between octahedral iron and tetrahedral iron. No doubt this is at least partially correct, as can be evidenced by experimental data. However, this theory is contradicted by the fact that other rare earth cation combinations have been prepared and evaluated which should also generate an increased super exchange in the iron sublattice, but do not yield the desired Faraday rotation effects.

Experimental evidence of the role of bismuth in producing the large Faraday rotation was obtained by observing that bismuth substituted yttrium iron garnet had much larger Faraday rotations than the pure yttrium iron garnet. Further, a linear dependence of Faraday rotation on the concentration of bismuth present was observed in the calcium bismuth vanadium iron garnet system, where increased concentrations of bismuth produced a steady increase in Faraday rotation. This point is important and formed the main point in Sperry's plan to develop improved magneto-optic switching materials.

In the past, at least three proposed mechanisms have been made in attempts to explain the magnitude of the induced Faraday rotation on bismuth substituted iron garnets. First, that the $S_o \rightarrow {}^3P_1$, transition of trivalent bismuth is responsible, second, that a charge transfer transition occurs between the ferric ion $3d^5$ state and the $6S^2$ state of trivalent bismuth and third, that an oxygen to ferric ion transition occurs. There are published reports which indicate that each of these mechanisms have merit. However, absorption studies tend to rule all three approaches as

unsuitable for explaining the observed Faraday rotation effects. Namely, the origins of transitions in iron garnets above 20,000 cm^{-1} (21,640, 23,100, 25,600 and 27,400 cm^{-1}) were observed to be of such intensity and width to be precluded from being crystal field transitions. In addition, dilution of the iron sublattice by non-magnetic cations indicated these transitions to be pair transitions involving octahedral and tetrahedral iron. However, it was evident that bismuth affects this transition in some manner.

In summary, although the origin of magneto-optic line-shapes of the crystal field transitions is understood, this is not the case for the strong pair transitions above 20,000 cm^{-1}. It remains to be determined which model of these transitions allows the excited state configurations to be established. Only when this is determined will the true role of the bismuth cation in obtaining higher Faraday rotation garnets be known. Once the role of bismuth is established the selection of the optimum Faraday rotation bismuth rare-earth iron garnet composition will be a more straightforward task.

Since the primary stumbling block to the widespread application of magneto-optic switching devices has been the lack of suitable materials in the visible and near infrared regions of the spectrum, emphasis must be placed upon materials development before any significant time is spent on device considerations. It is for this reason that the magneto-optic portion of the first year of the contract was spent exclusively in materials development and materials evaluation.

In the development of useful magneto-optic materials having a large figure of merit (θ_F/α) several important requirements must be met:

(1) The material should have the largest possible Faraday rotation (θ_F).

(2) The optical absorption coefficient (α) should be as low as possible.

(3) The saturation magnetization should be low (to allow for reasonable magnetic control fields).

The magneto-optic material consists of a thin magnetic garnet film deposited via liquid phase epitaxial methods onto a non-magnetic garnet substrate.

Since all available evidence points to the fact that the amount of Faraday rotation is proportional to the concentration of bismuth ions, the basic emphasis of Sperry's program was to incorporate higher concentrations of bismuth in the cation position of the garnet structure of the magnetic film.

However, bismuth is too large to fit into the normal iron garnet structure without producing lattice mismatch stress between the magnetic film and the substrate. Although the introduction of small species into the magnetic film appears to be a possible technique to compensate for the large size of the bismuth cation, experiments at SRC have already shown that such an approach decreases the Faraday rotation. Consequently, the only feasible approach is to match the lattice size of the bismuth substituted iron garnet film to that of the substrate and to introduce components into the substrate to achieve a concomitant expansion in its lattice size.

As new stripe domain magneto-optic materials are developed using the techniques described, they must be evaluated to determine which properties are enhanced by each approach. The continual feedback between material development and material characterization in house at Sperry selected those techniques which produce magneto-optic materials with the highest figures of merit in the wavelength region of interest. The material properties to be determined as a function of wavelength (.4 to 1.6 μm) are: the index refraction, n; the absorption coefficient, α; the Faraday rotation, θ_F; and the figure of merit, M.

The index of refraction measurements were made using a method reported by Hacskalyo[1], in which the Brewster angle φ_b of the material is determined experimentally using an eclipsometer and a monochromatic light source. The refractive index is then simply determined from the relation

$$n = n_o \tan \varphi_b$$

where n is the refractive index of the sample and n_o is the refractive index of air.

The absorption coefficient is determined from a knowledge of the thicknesses and refractive indices of the garnet and its substrate together with the amount of transmission of light through the garnet/substrate composite. By following a method outlined by Hunt[2], which details a general theory for treating magneto-optic scattering (both reflection and transmission) from multilayer structures comprised of magneto-optic and dielectric materials, the absorption coefficient is found.

The Faraday rotation may be simply determined by noting that the ratio of the intensity of the first order diffracted beam to the zeroth order beam is given by

$$I(1)/I(0) = (4/\pi^2)\tan^2\theta_F t$$

or

$$\theta_F = (1/t)\tan^{-1}\left(\pi/2\sqrt{I(1)/I(0)}\right)$$

where t is the garnet thickness. The figure of merit is calculated by taking the ratio of θ_F/α.

SECTION XI

SUMMARY OF RESULTS

Liquid-phase epitaxial films of bismuth substituted rare-earth iron garnet were deposited on non-magnetic garnet polished substrates. The optimum composition was grown on gadolinium gallium garnet and its magneto-optic behavior determined.

Increased concentrations of bismuth were incorporated in rare-earth iron garnet films deposited on gadolinium scandium gallium garnet polished substrates. Faraday rotations of 60,000 degrees per centimeter were recorded for representative LPE films of this type. Refractive index and absorption curves were determined for typical LPE magneto-optic films. Although the basic mechanisms and ultimate properties of bismuth substituted rare-earth iron garnet films were not determined completely during this twelve month contract, significant and original technical progress was achieved which merit further investigations and support.

SECTION XII

SUBSTRATE PREPARATION

Gadolinium gallium garnet (111) substrates are available commercially. Other crystallographic orientations have been grown in this laboratory. However, the lattice dimensions (12.383Å) of 3G limit the concentration of bismuth that can be incorporated and, as a consequence, the desired magneto-optic figure of merit cannot be realized. We have grown samarium gallium garnet single crystals which possess a lattice parameter of 12.43; unfortunately, this material exhibits considerable absorption in the wavelength region of interest. These data are shown in Figs. 32 and 33 which depict absorption curves for gadolinium gallium garnet and samarium gallium garnet.

Garnet substrate single crystal growth experiments were conducted with the objective of obtaining large unit cell non-magnetic material. The larger than gadolinium gallium garnet unit cell (12.383Å) substrates are demanded if higher Faraday rotation magneto-optic thin films are to be prepared with the quality and perfection required by optical processing devices. Since there are no available commercial sources for substrate wafers other than <111> gadolinium gallium garnet, crystal growth experiments had to be conducted at Sperry Research Center.

There are a number of different approaches that can be used to formulate garnet compositions whose lattice parameters are greater than that of gadolinium gallium garnet. In the selection of appropriate compositions, several important factors must be considered. These considerations include that the material must be (1) non-magnetic; (2) optically transparent at the wavelength under examination; (3) capable of production by single crystal growth methods and (4) amenable to wafer processing procedures.

Referring to gadolinium gallium garnet as the base material in which the gadolinium cations occupy the dodecahedral garnet sites and the gallium cations occupy the octahedral and tetrahedral sites, several substitutions

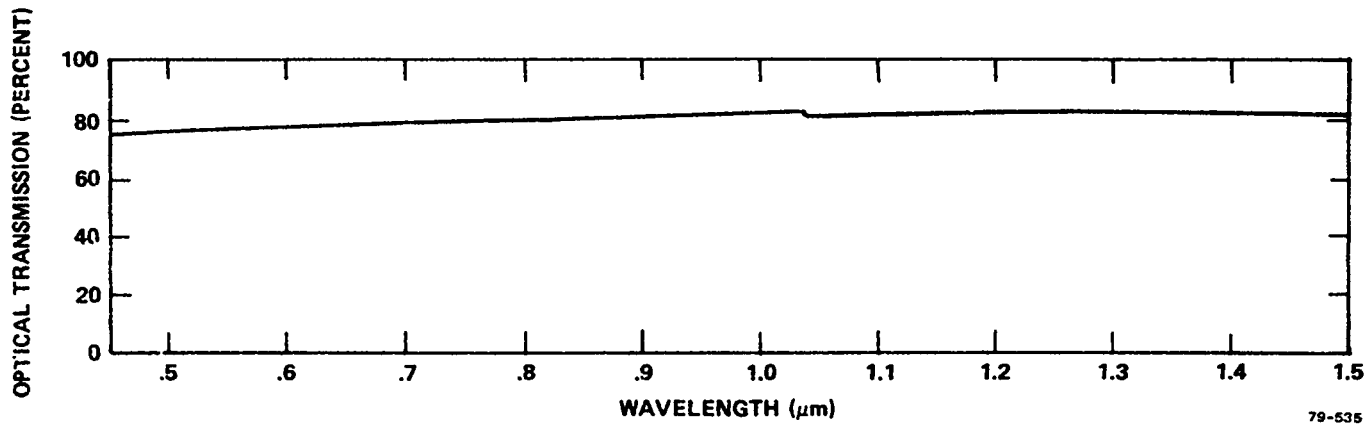

FIG. 32 Transmission curve for gadolinium gallium garnet substrate single crystal as a function of wavelength.

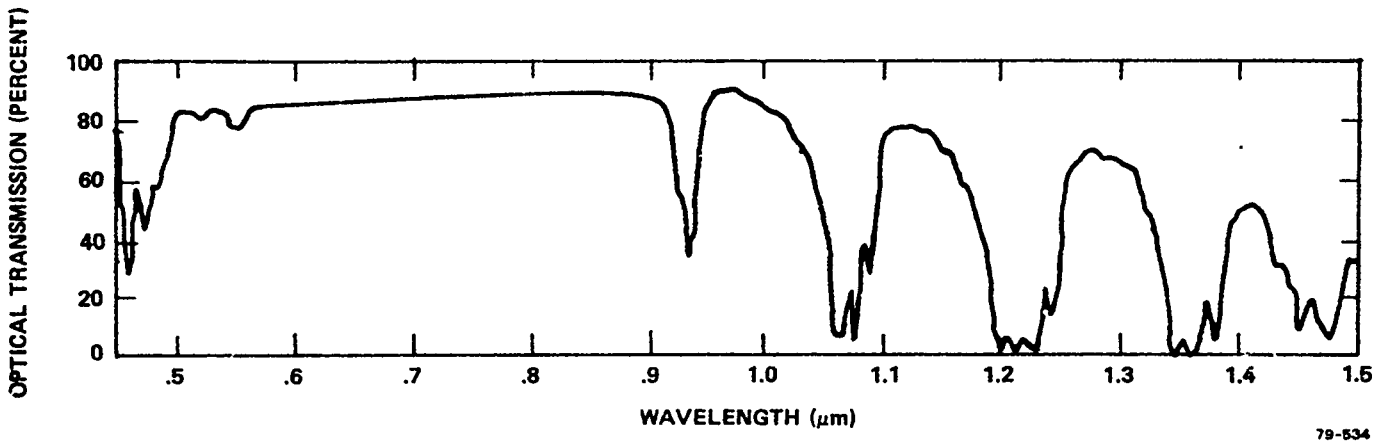

FIG. 33 Transmission curve for samarium gallium garnet substrate single crystal as a function of wavelength.

come to mind which should yield lattice parameters larger than 12.38Å. The garnet structural formula can be written $A_3B'_2(BO_4)$, which translates into $Gd_3Ga_2(GaO_4)_3$ for gadolinium gallium garnet. During this report period, the substitution of scandium for gallium in the octahedral site was investigated. Initially, garnet phases were prepared by solid state reactions and the lattice parameters measured by x-ray powder diffraction techniques. Since chemical analyses of the final products were not carried out, it is pointed out that all substituted garnet compositions cited herein are melt or beginning compositions. On the basis of the solid state reactions, the phase $Gd_3Sc_2(GaO_4)_3$ should be stable and has a lattice parameter of approximately 12.60Å. Since this phase has the largest lattice parameter observed to date for a colorless non-magnetic garnet, Czochralski direct melt single crystal growth studies were conducted.

An rf heated iridium crucible 5cm i.d. by 5cm high was used to contain the appropriate molten oxides which had a melt composition of $Gd_3Sc_2(GaO_4)_3$. This formula assumes complete substitution of scandium for gallium in the octahedral site of the garnet lattice. The binary oxides of six-nines purity were intimately mixed and placed in the iridium crucible. The temperature was raised until the charge had melted. The crucible was refilled and the charge remelted until the molten level was six-to-eight millimeters from the top of the crucible. The melt was then used for crystal growth experiments. A 3G seed was used for the initial single crystal growth experiment. Subsequent experiments utilized seed material prepared from melts of the same composition.

Single crystalline boules of centimeter dimensions were grown. Unfortunately, not all of the slices survived the wafer polishing operations; however, wafers adequate for liquid-phase epitaxial deposition experiments were obtained. Further refinements in growth procedures such as withdrawal rates, rotation rates, composition and ambient gaseous environment will be made in an attempt to obtain strain-free large single crystals of scandium substituted gadolinium gallium garnet.

Representative single crystalline boules were oriented crystallographically along the <111> direction and cut into 0.020-inch wafers. These wafers were lapped and polished to a surface finish using colloidal sillica as the final polishing medium. This process is done in-house as the technique was determined and proven-in in the bubble memory materials program.

SECTION XIII

LIQUID-PHASE EPITAXY FILM GROWTH

The substrate wafers were subjected to a rigorous cleaning procedure prior to use in an LPE experiment. The magnetic stripe domain garnet films were grown under isothermal conditions from supersaturated solutions contained in pure platinum vessels. Film growth was conducted 10° to 20°C below the initiation of nucleation temperature. The solution was recycled to 150° to 200°C above the saturation temperature after each epitaxial growth experiment.

Optimum conditions for LPE growth of bismuth substituted rare earth iron garnet films deposited on scandium substituted 3G wafers have not been achieved to date. More research must be performed before a precise set of reproducible LPE conditions can be stated with certainty. However, experimental procedures have been determined for the deposition of device quality magneto-optic-garnet films which possess Faraday rotation values greater than that reported in the available literature. The results of evaluation measurements of representative films are described in Section XIV.

SECTION XIV

MAGNETIC STRIPE DOMAIN EVALUATION

Faraday rotation measurements of rare-earth bismuth iron garnet thin films were made. On the basis of these results, the optimum magnetic stripe domain material that could be deposited lattice-matched to 3G was determined. Table 4 lists the important parameters for a representative magneto-optic film that was investigated. Included in the table are the wavelength region examined, per cent transmission, absorption coefficient, Faraday rotation and the calculated figure of merit.

A Faraday rotation curve for a 9.6 μm-thick magnetic stripe domain thin film is shown in Fig. 34. The figure of merit for this film has been included in the same figure for comparison.

Table 5 lists the thickness and Faraday rotation of the sample films deposited in expanded lattice garnet substrates. The thickness was calculated from optical interference patterns obtained on a Beckman Model 5270 spectrophotometer. The Faraday rotation measurements were made using a Gaertner ellipsometer as a polarimeter. The films were placed in a water-cooled magnetic coil capable of providing fields of up to 2000 Oe, which is sufficient to saturate the magnetic domains in the direction parallel to the light path.

Table 5

Thickness and Faraday Rotation of Rare Earth Bismuth Iron Garnet Films on $Gd_3Sc_2Ga_3O_{12}$ Substrates

Film No.	Thickness (μm)	θ_F(deg/cm @ 633nm)
1	1.9	3.05×10^4
2	4.7	2.70
3	3.3	3.35

Table 4

Magnetic Stripe Domain Results for a
Rare-Earth Bismuth Iron Garnet Thin Film

λ(nm)	%T	$\alpha(cm^{-1})^*$	α(dB/μm)	θ_F (deg/cm)	FM† (deg/dB)
800	63.5	236	0.102	7100	6.96
820	64.0	232	0.101	6600	6.53
840	63.7	235	0.102	6150	6.03
860	62.4	246	0.107	5750	5.37
880	60.7	260	0.113	5300	4.69
900	58.9	276	0.121	5000	4.13
920	58.1	283	0.123	4700	3.82
940	58.7	277	0.121	4350	3.60
960	60.4	263	0.114	4100	3.60
980	63.4	237	0.104	3800	3.65
1000	67.3	206	0.0894	3500	3.91
1020	72.3	169	0.0734	3350	4.56
1040	76.5	140	0.0608	3050	5.02
1060	79.8	118	0.0512	2800	5.47
1080	82.2	102	0.0443	2600	5.87
1100	83.5	93.9	0.0408	2400	5.88
1120	84.4	88.3	0.0383	2200	5.74
1140	84.9	85.3	0.0370	2000	5.41
1160	85.3	82.8	0.0360	1800	5.00
1180	85.4	82.2	0.0357	1600	4.48
1200	85.5	81.6	0.0354	1400	3.95

* $\alpha = \frac{\ell n(1/T)}{t}$; t = 19.2 μm (2-sided film, 9.6 μm each side)

† FM = Figure of Merit

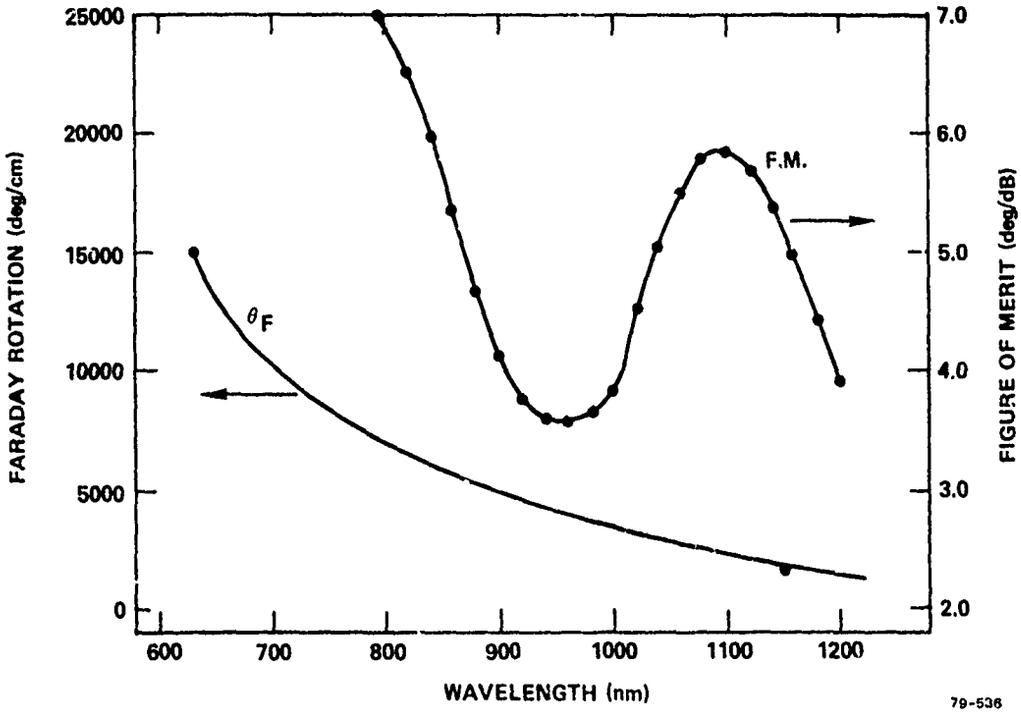

FIG. 34 Faraday rotation and figure of merit curves for a rare-earth bismuth iron garnet as a function of wavelength.

Further LPE studies have yielded LPE magneto-optic garnet films which exhibit Faraday rotation values of 6×10^4 degrees per centimeter at 633 nm. These results are the highest figures recorded for LPE garnet films.

The index of refraction for a typical bismuth rare-earth iron garnet composition film was determined as a function of wavelength. Table 6 lists these results for a bismuth substituted rare-earth iron garnet LPE magneto-optic thin film.

Table 6

Refractive Index vs. Wavelength for $(Lu,Pr,Bi)_3 Fe_5O_{12}$

λ,nm	n
500	2.441
600	2.344
700	2.291
800	2.258
900	2.237
1000	2.222
1100	2.211
1200	2.203
1300	2.197
1400	2.192
1500	2.188

SECTION XV

OPTICAL DIFFRACTION EXPERIMENTS

The magneto-optic diffraction in two of the most recent samples was measured at a wavelength of 633 nm. First, the magnetic domains in the film were "straightened" by applying an H-field in the plane of the wafer, plus a small bias field at right angles to the film. Next, a collimated He-Ne laser beam was incident normally on the wafer and the intensity of the first-order and zero-order diffracted optical beams was recorded. The incident beam strength I_{inc} was also determined where we define $I_{inc} = I-I'$, in which I is the intensity of the beam falling on the wafer, and I' is the intensity of the beam reflected back towards the laser. The reflected intensity I' was typically 25% of I, and about 2/3 of I' came from the first surface of the wafer with 1/3 coming from the second surface (internal reflection).

The following results were obtained: For sample #1, whose composition was $Gd_{.0047}\ Bi_{.5555}\ Fe_{.1935}\ O_{12}$, with a film thickness of 7.3 μm, the optical diffraction was

$$\frac{I_1}{I_{inc}} = 2.6\% \qquad \frac{I_{-1}}{I_{inc}} = 2.6\% \qquad \frac{I_o}{I_{inc}} = 36.0\%$$

For sample #2, whose composition was the same, and whose film thickness was 5.9μm, we found

$$\frac{I_1}{I_{inc}} = 2.4\% \qquad \frac{I_{-1}}{I_{inc}} = 2.4\% \qquad \frac{I_o}{I_{inc}} = 41.6\%$$

Using the equation

$$\frac{I_1}{I_{inc}} = e^{-\alpha t} \left(\frac{4}{\pi^2}\right) \sin^2(\theta_F t)$$

to describe the first-order diffraction, we can estimate the absorption coefficient α for each sample using the measured values $\theta_F(633)$ = 31,233 deg/cm for #1 and 35,381 deg/cm for #2. We find that the optical loss values are $\alpha(633) \approx 1165$ cm^{-1} for #1 and approximately 1290 cm^{-1} for #2. The absorption loss is expected to be much smaller at the near infrared communications wavelengths.

SECTION XVI

CONCLUSIONS

Magneto-optic garnet films were deposited on commercial 3G substrates, and SRC grown 3G and gadolinium scandium gallium garnet material. Garnet transparent substrates which possess lattice parameters as large as 12.59Å were prepared, grown and fabricated into substrate wafers. Epitaxial polished substrate surfaces were prepared at SRC according to procedures documented and proven in bubble memory research investigations.

Optical absorption, film thickness, lattice parameter, index of refraction and Faraday rotation measurements were performed on typical epitaxial films as a function of wavelength. Faraday rotation values greater than that reported previously in the available literature for LPE magneto-optic films were determined. To obtain high quality films which possess these properties, it was necessary to utilize garnet substrates with expanded lattice parameters.

Although significant progress was achieved during the contract period in magnetic stripe domain research, much remains to be accomplished. Before the superior performance magneto-optic garnet thin film can be identified, without completing a trial and error lengthy research project, the important mechanisms should be determined. The length and scope of this research project was not sufficient to even attempt to address this fundamental and important question. It is felt that sufficient progress and promise was achieved during the contract period. The difficult and complex problem of what fundamental mechanisms play important roles in the Faraday rotation of magneto-optic garnet thin films should be the subject matter of a longer term, future research effort.

ACKNOWLEDGMENT

We gratefully acknowledge the expert technical assistance of F. A. Bradlee in the preparation and fabrication of substrate single crystals and polished wafers and F. G. Garabedian in the single crystal growth of nonmagnetic garnet and liquid-phase epitaxial deposition of thin films. Thanks are given to W. R. Bekebrede for X-ray orientation, film thickness, lattice parameter, index of refraction, and Faraday rotation measurements and to A. B. Smith and W. G. Goller for Faraday rotation studies.

REFERENCES

1. Hacscaylo, M., J. Opt. Soc. Ad., 54, 198 (1964).
2. Hunt, R. P., J. Appl. Phys., 38, No. 4, 1652 (1967).

APPENDIX A

THEORY OF LIQUID CRYSTAL SWITCHING

LIST OF ILLUSTRATIONS

LIST OF ILLUSTRATIONS (CONT.)

APPENDIX A

THEORY OF L.C. SWITCHING

Figure A1(A) represents the actual LC orientation in our switch at an applied voltage above threshold, $V > V_{th}$. The nematic LC layer is uniform in the x-z plane with 0^{o} twist, both at $V = 0$ and $V > V_{th}$. Initially, at $V = 0$, molecules are parallel to the walls with 0^{o} tilt or a very small tilt. In an electric-field Freedericks transistion, the nematic director w ll have a nonuniform orientation $\alpha(V, z)$ as illustrated in Fig. A1(A), where $\alpha \approx 0$ near $z = 0$ and $z = d$, with reaching a maximum at $d/2$, the midpoint of the layer. There are boundary layers at the walls where α changes rapidly. These are quite thin, especially at high voltages; thus we shall not make serious errors in our calculation by using in our model the uniform ordering of Fig. A1(B), where (V) is independent of z. The boundary layer correction will be taken up in the future.

Assuming a uniform LC layer embedded in an isotropic, high-index glass medium, we now calculate the intensity of light transmitted through the LC, which is the switched portion in a single-pass device. Figure A2 shows the incident, reflected, and transmitted optical beams, as well as the angles of incidence and refraction, θ and θ'. Since the uniform birefringent LC film is like a uniform plate of uniaxial crystal, the light traveling in the LC will be divided into its orthogonal, normal modes (shown by dotted and solid lines in Fig. A2). These O-ray and E-ray modes are designated as $E_{\parallel}$ and $E_{\perp}$ where the subscripts denote optical polarization in the plane of incidence and normal to it, respectively.

We choose the incidence angle $\theta_{\perp}$ for $E_{\perp}$ to be greater than the critical angle $\theta_{c}(\perp)$ for total internal reflection, $\theta_{c}(\perp)$ being independent of voltage as discussed below. Hence, there is no transmitted E-ray light

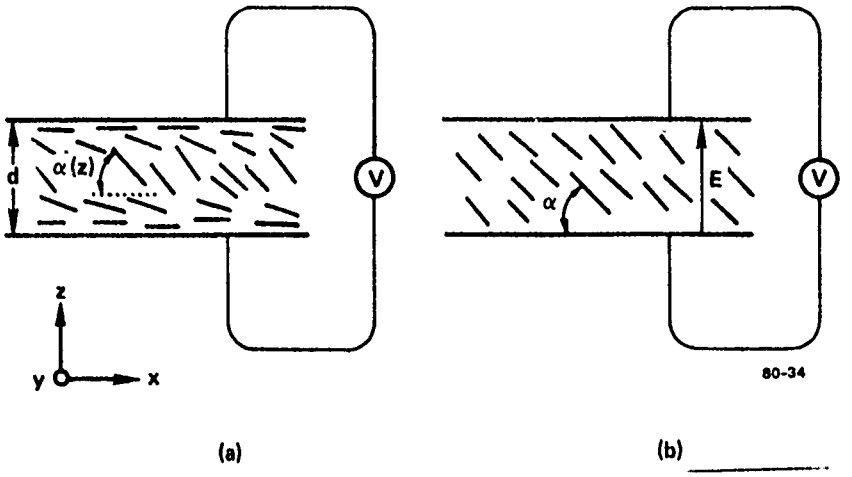

FIG. A1 Orientation of nematic LC molecules within the switched layer: (a) actual; (b) theoretical model.

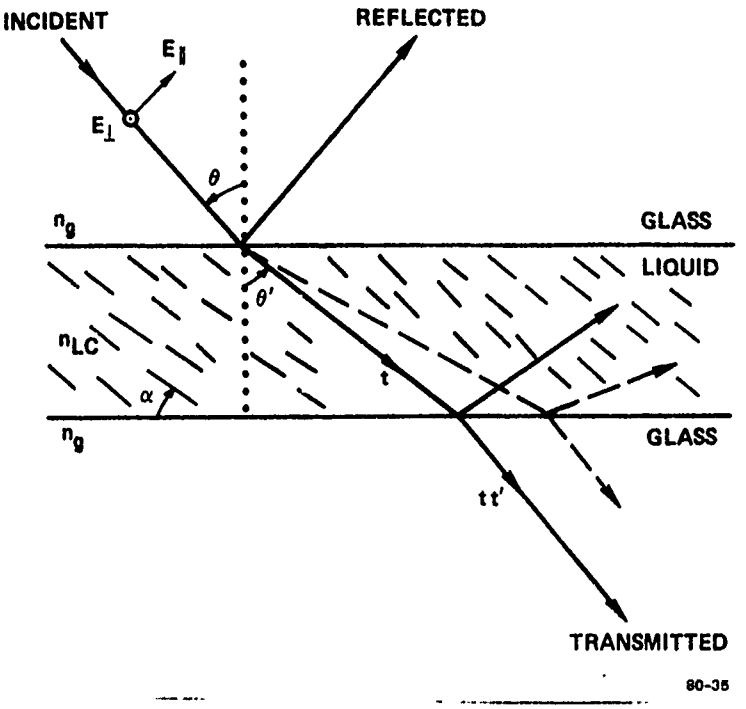

FIG. A2 Optical ray diagram for oblique incidence on birefringent LC sandwiched between high-index glass prisms.

at any voltage, and there should be no interference between O-ray and E-ray beams at the switch output. However, in practice, we do observe oscillations in the switch-output light (vs voltage in the steady state and vs time in the transient decay). This may be due to the fact that the LC optic axis does not tilt exactly in the plane of incidence when voltage is applied. So, an improved theory would include this O+E interference. (Another explanation for the oscillations may be $+\alpha$ and $-\alpha$ tilting of molecules within the same switch, which could be put into the present theory without difficulty.)

Returning to Fig. A2, the transmissivity of a plane-parallel plate is discussed in Born and Wolf, Principles of Optics, 2nd revised edition, MacMillan, New York, 1964 (Sec. 7.6.1). Following their approach, the transmitted amplitude at the first interface is t, while at the second interface (birefringent-to-isotropic) a fraction t' of the new input is transmitted. Hence, the total complex amplitude that emerges from the switch is tt' as shown. Multiple reflections and interference effects have been neglected in Fig. A2. Denoting tt' as $\mathcal{T}$, we note that the transmitted intensity is $\mathcal{T}$ times its complex conjugate: $I(\text{trans}) = \mathcal{T}^2$.

We now turn to Sec. 1.5.3 of Born and Wolf where the transmission coefficients $\mathcal{T}_{\parallel}$ and $\mathcal{T}_{\perp}$ for $E_{\parallel}$- and $E_{\perp}$-light are presented (the Fresnel formulae for oblique incidence). These are used in our model. We concentrate on the $\parallel$-component because in our switch the molecules are usually configured (see QSR-1) to give total reflection of the $\perp$-component irrespective of V. Using Born and Wolf's Eq. (35) for $\mathcal{T}_{\parallel}$ we find that

$$I(\text{trans})_{\parallel} = \frac{\sin^2(2\theta)\,\sin^2(2\theta')}{\sin^4(\theta'+\theta)\,\cos^4(\theta'-\theta)} \qquad (1)$$

where θ is the incidence angle in the glass and θ' the propagation angle in the LC stratum. Using Snell's law of refraction, we have

$$\theta' = \arcsin (r \sin\theta) \tag{2}$$

where $r = n_g/n$

in which n is the effective refractive index of the LC at θ' and $\alpha(V)$. From the theory of crystal optics and from the index ellipsoid of the liquid crystal, we find that $n_{\parallel}$ and $n_{\perp}$ are:

$$\left.\begin{aligned} \left(\frac{1}{n_{\parallel}}\right)^2 &= \frac{\cos^2(\theta' - \alpha(V))}{n_o^2} + \frac{\sin^2(\theta' - \alpha(V))}{n_e^2} \\ n_{\perp} &= n_o \end{aligned}\right\} \tag{3}$$

The incidence is quite oblique in our switch; usually θ is 67 to 77°. Hence, we shall not make large errors in the computation if we assume $\theta' \approx 90^\circ$ in the index relation (3). In that case, we get

$$\left(\frac{1}{n_{\parallel}}\right)^2 \approx \frac{\cos^2 \alpha(V)}{n_o^2} + \frac{\sin^2 \alpha(V)}{n_e^2}$$

or, in other words

$$\frac{1}{n_{\parallel}} \approx \frac{\sqrt{n_o^2 \sin^2\alpha(V) + n_e^2 \cos^2 \alpha(V)}}{n_o n_e} \tag{4}$$

Substituting (4) into (2) gives

$$\theta' \approx \arcsin\left[\frac{n_g \sqrt{n_o^2 \sin^2\alpha(V) + n_e^2 \cos\alpha(V)}}{n_o n_e} \sin\theta\right] \quad . \qquad (5)$$

If (5) is substituted into (1), the resulting expression for $I(\text{trans})_{\parallel}$ is a messy combination of trigonometric functions. Nevertheless, $I(\text{trans})_{\parallel}$ can be evaluated easily with a computer and we have done this for several combinations of glass and LC materials. The Univac computer automatically plots transmitted light as a function of θ, α, or V — whichever independent variable is chosen.

The materials chosen were glass types WG335, 360, and 345, plus liquid crystals 1132 and E7. These liquids are phenylcyclohexanes and biphenyls, respectively. The refractive indices of the glass were obtained from the Schott filter glass data book, and the LC indices are given in the article by Schadt and Muller, IEEE Trans. Electron Devices ED-27, 1125 (1978). For LC1132, we considered behavior at room temperature and at a temperature near the critical point, $T_c = 70^\circ C$. At $\lambda = 633$ nm, the indices are

Glass WG335, $n_g = 1.617$ at $T = 20^\circ C$

Glass WG360, $n_g = 1.644$ at $T = 20^\circ C$

Glass WG345, $n_g = 1.734$ at $T = 20^\circ C$

LC1132 $n_o = 1.492$, $n_e = 1.634$ at $T = 20^\circ C$

LC1132 $n_o = 1.493$, $n_e = 1.605$ at $T = 60^\circ C$

LC E7 $n_o = 1.522$, $n_e = 1.746$ at $T = 20^\circ C$

We first calculate $I(\text{trans})_{\parallel}$ from Eqs. (5) and (1) as a function of incidence angle from $\theta = 50^\circ$ to $\theta = 90^\circ$ for several values of α, namely, $\alpha = 0^\circ$, 15°, 30°, 45°, 60°, 75°, and 90°. The results for LC1132 are presented in Figs. A3-A5. Next, we compute $I(\text{trans})_{\parallel}$ as a function of

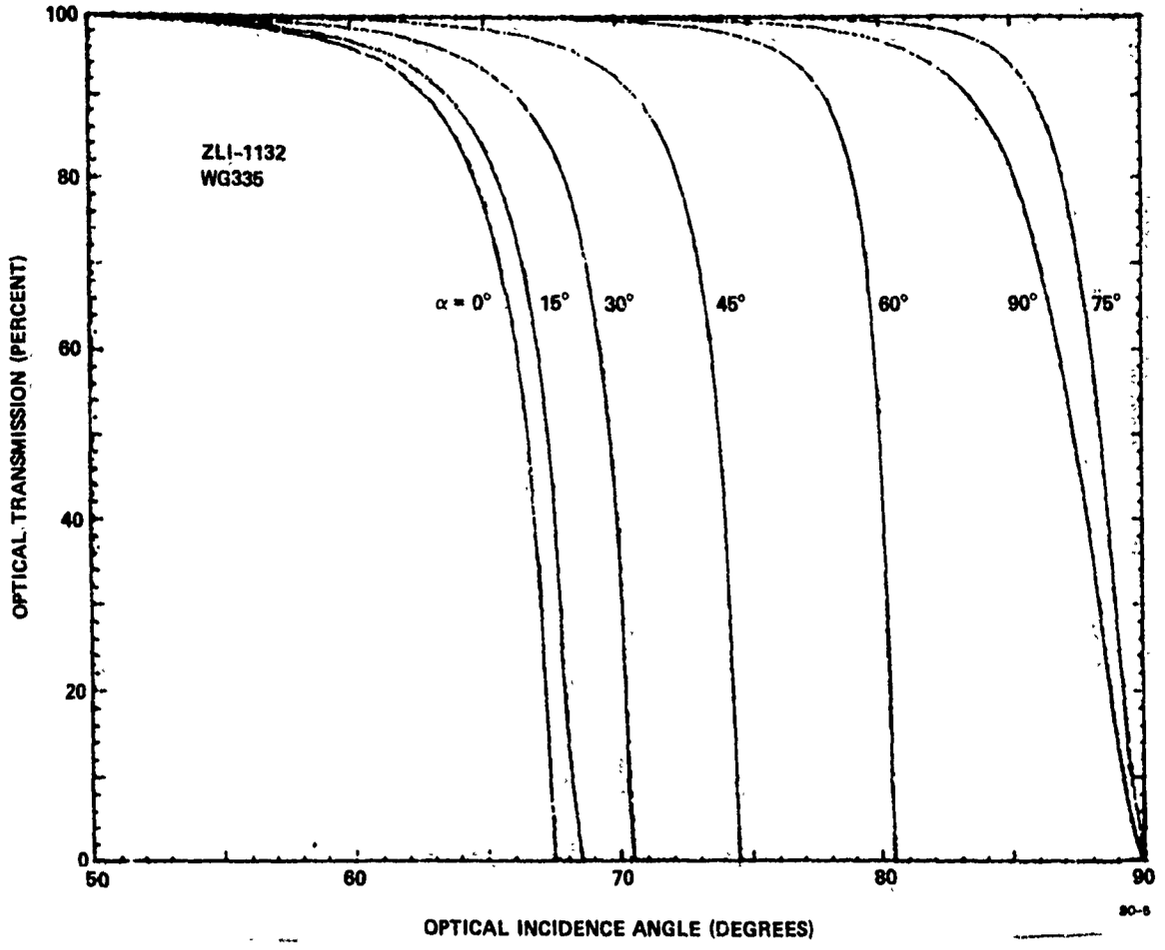

FIG. A3 Switched light vs. θ for glass-335/LC-1132.

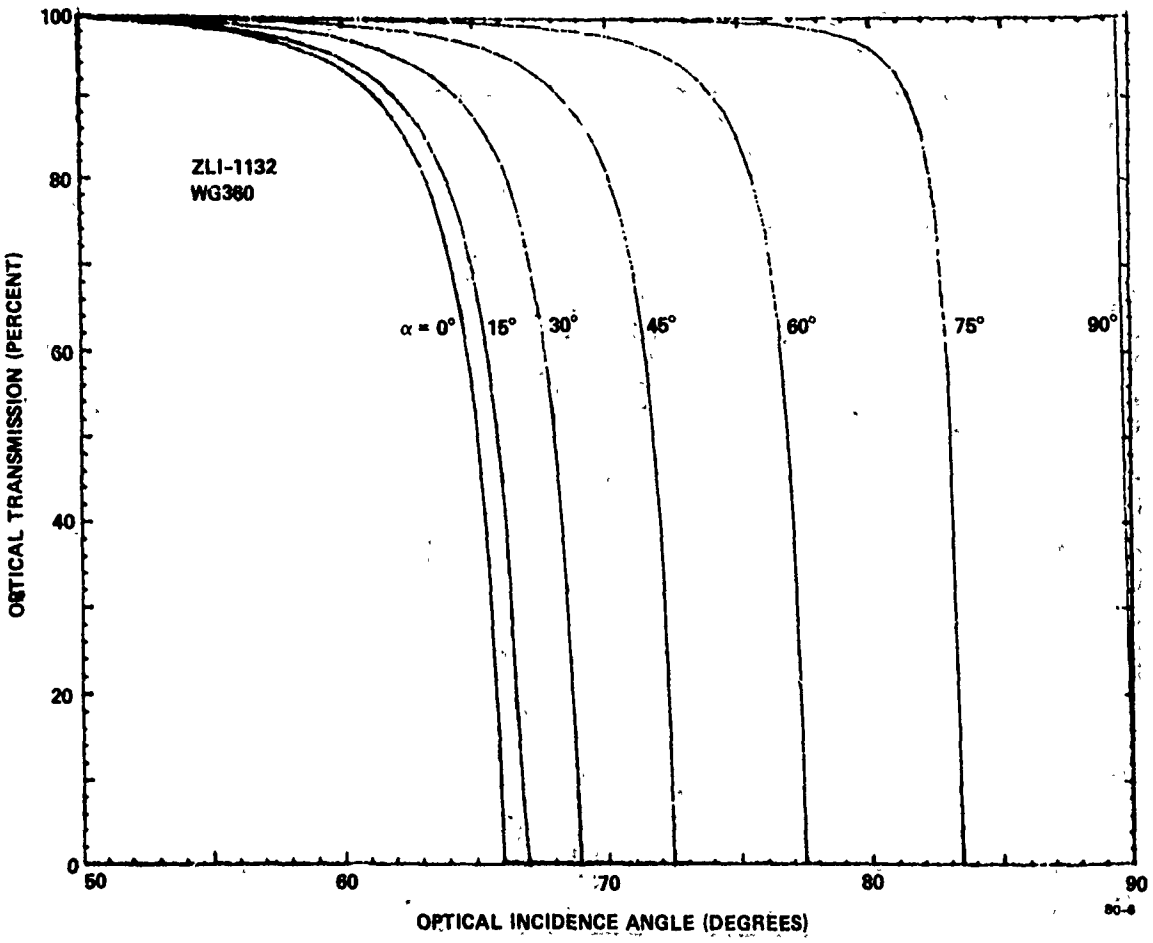

FIG. A4 Switched light vs. θ for glass-360/LC-1132.

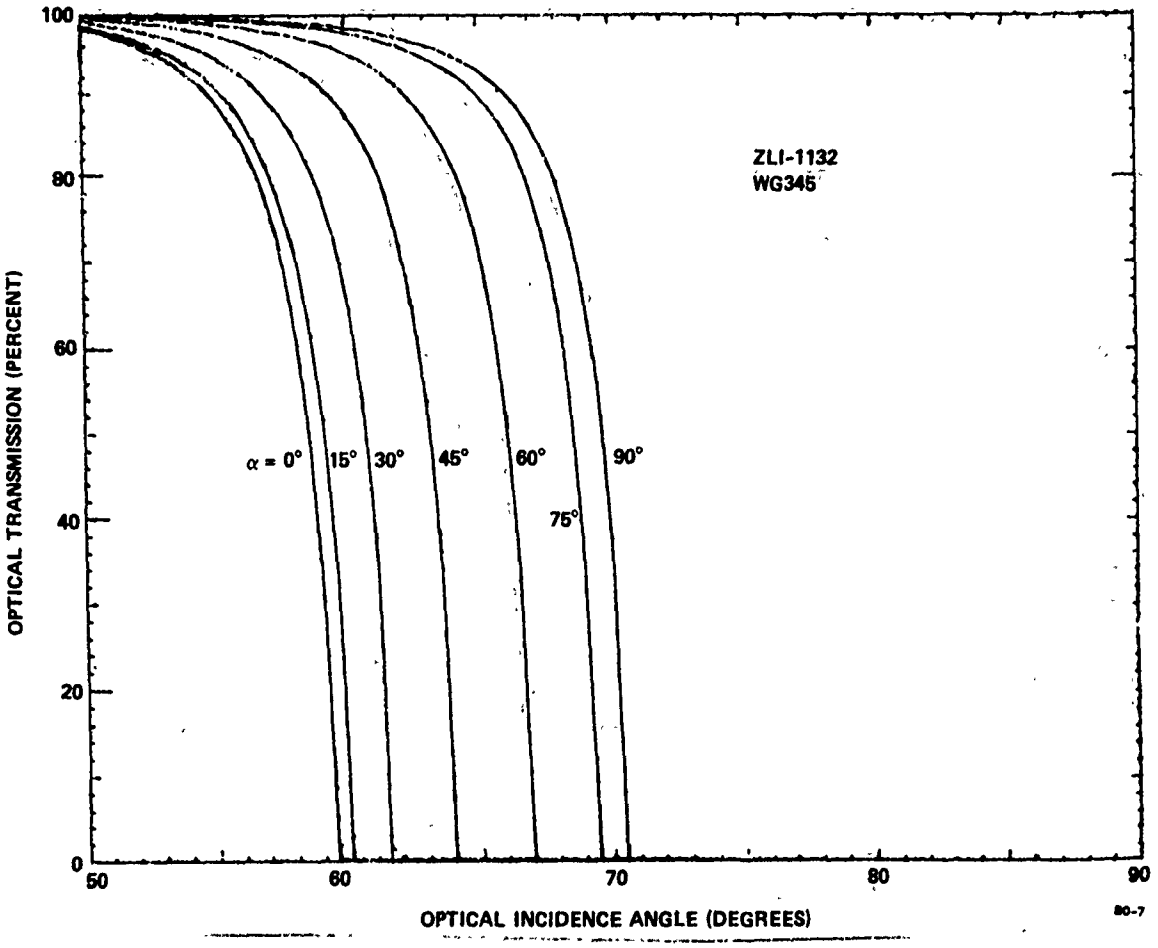

FIG. A5 Switched light vs. θ for glass-345/LC-1132.

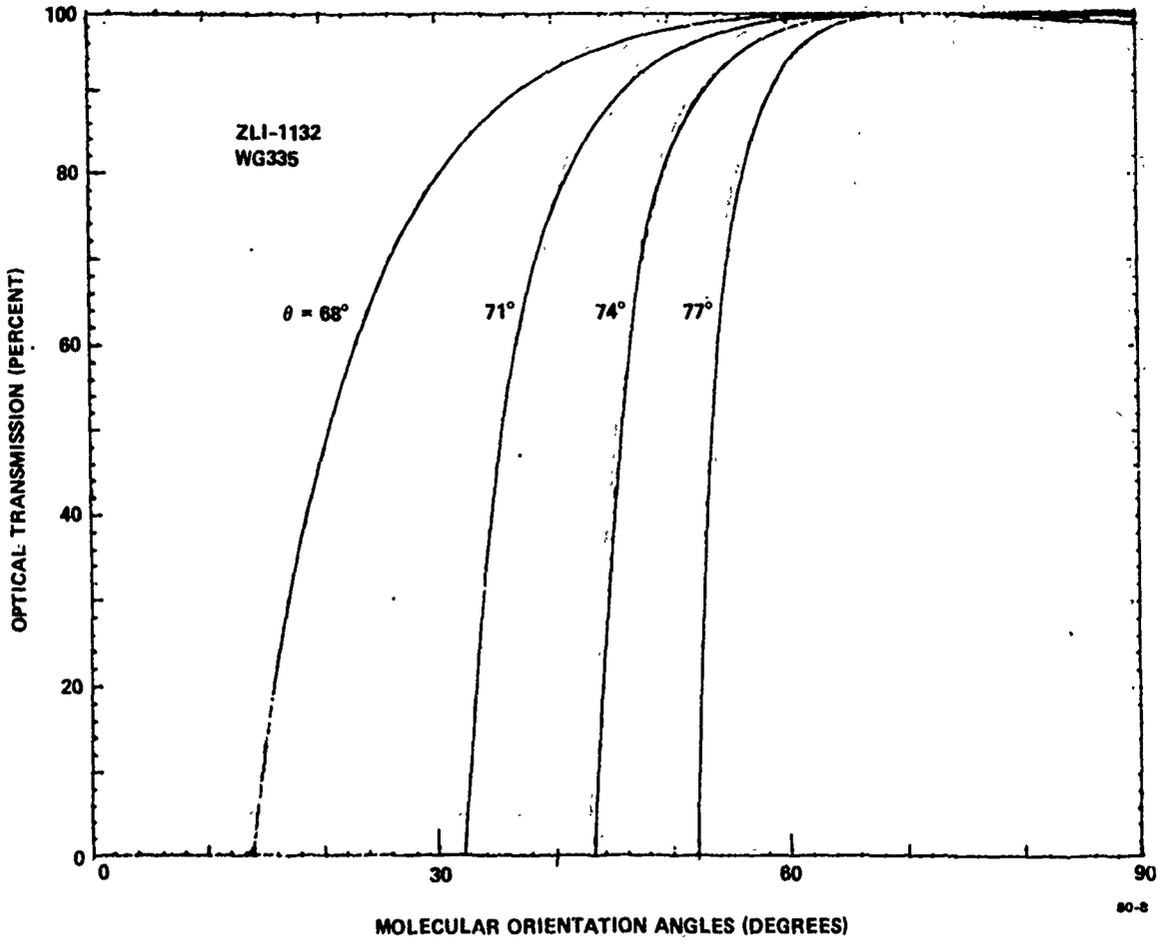

FIG. A6 Switched light vs. α for glass-335/LC-1132.

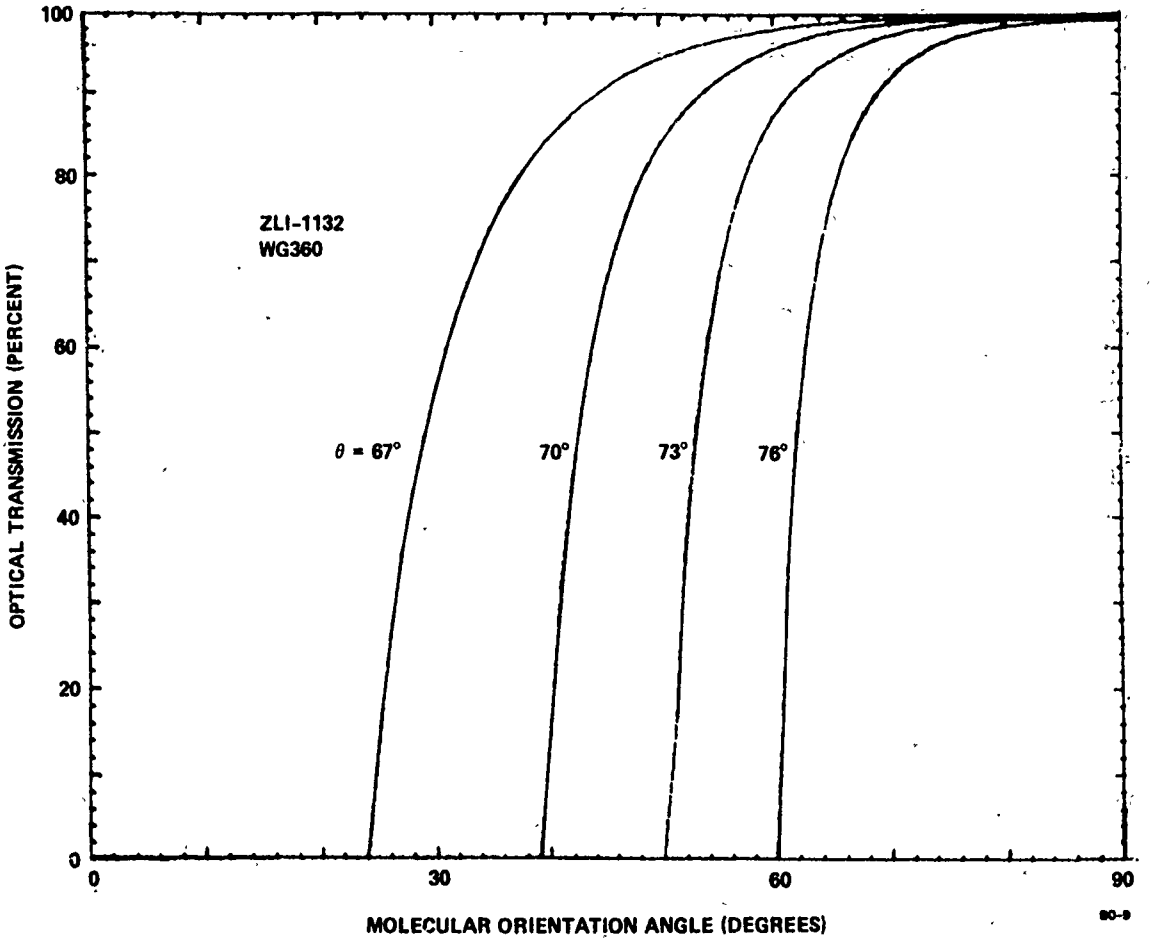

FIG. A7 Switched light vs. α for glass-360/LC-1132.

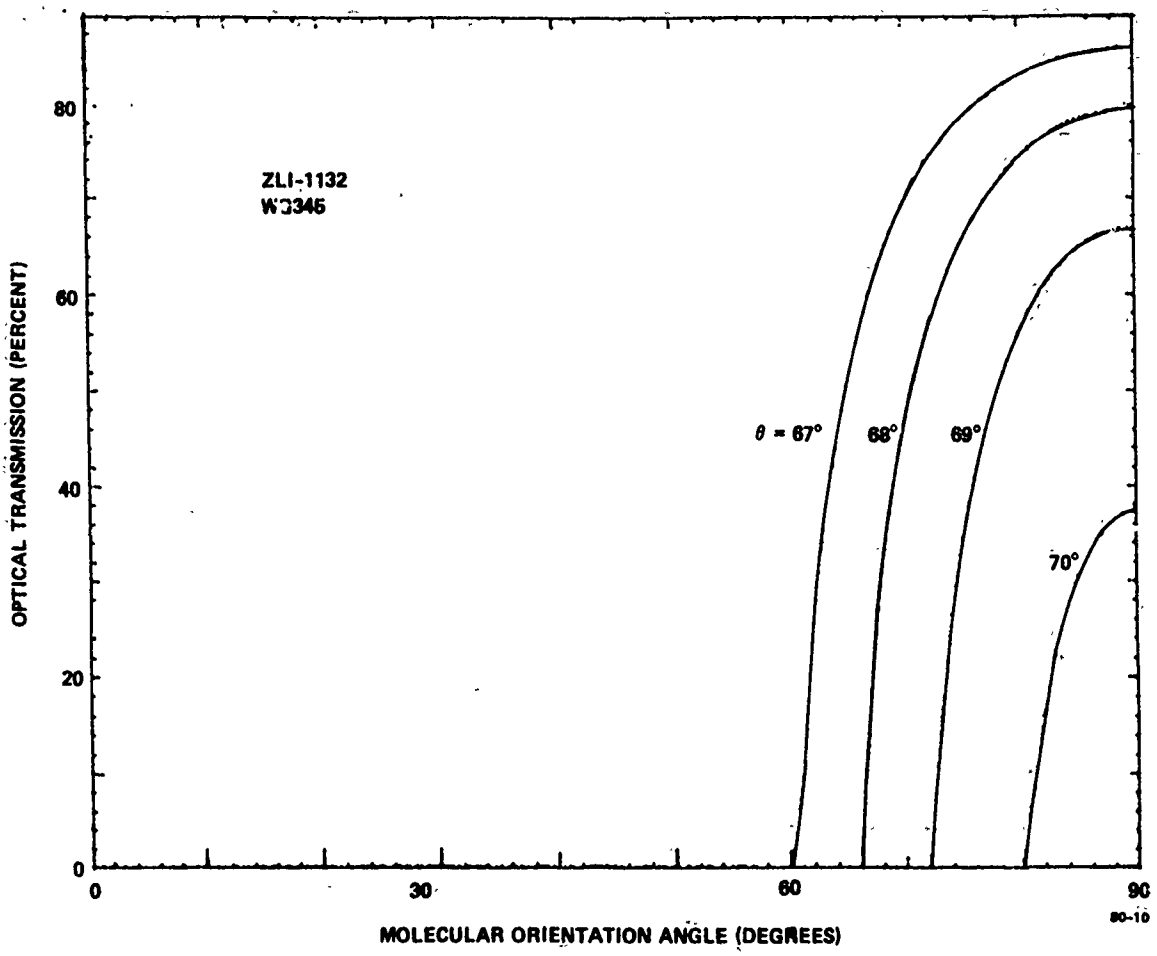

FIG. A8 Switched light vs. α for glass-345/LC-1132.

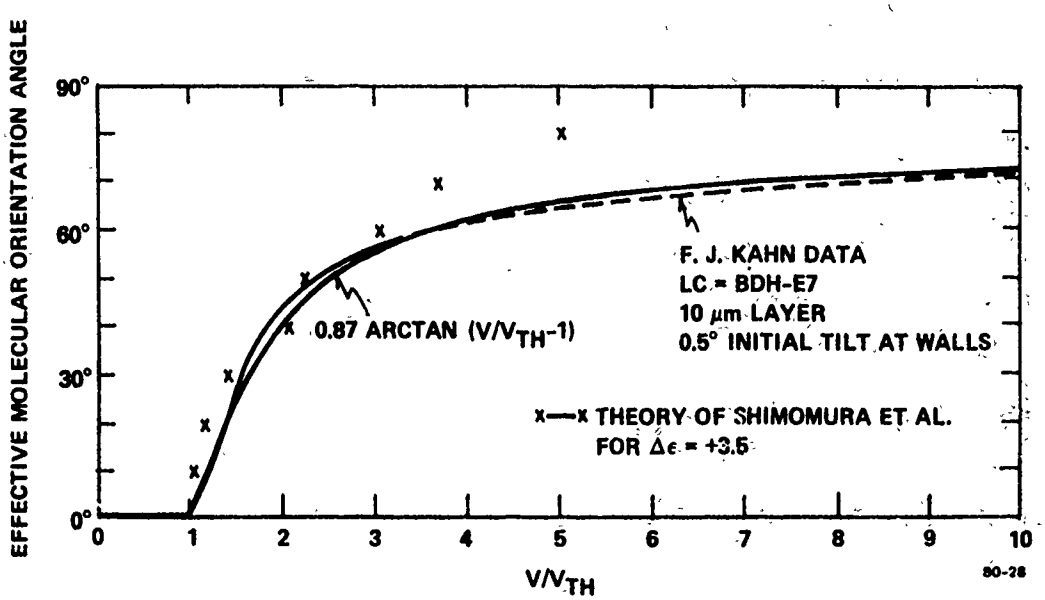

FIG. A9 Molecular tilt angle as a function of normalized voltage.

molecular tilt angle, α = 0 to 90°, for several values of incidence angle in the 67 to 77° range. As above, this was done for LC1132 and the three glasses, as shown in Figs. A6-A8. For the highest index glass (Fig. A8), the turn-on is "postponed" to the highest α-range.

Finally, we computed the voltage response of our switches. With the foregoing model, it is necessary to introduce an analytical form for $\alpha(V)$. To make a realistic choice, we examined the LC literature to see whether experimental work had been done on molecular orientation vs applied voltage, and we found data taken by F. J. Kahn (J. Molec. Cryst. Liq. Cryst. 38, 109 (1977)) on a 10-μm layer of LC-E7. By measuring capacitance of the layer over a range of voltage, Kahn was able to determine the effective molecular orientation $\alpha(V, d/2)$ at the midplane of the layer. His measurements extend from V = 0 to 4 V rms and we have extrapolated his results (dashed line) to 10 V rms as shown in Fig. A9. There are also some theoretical calculations by Shimomura et al. (Japan. J. Appl. Phys. 15, 1479 (1976)) for a 10-μm film of MBBA-BBCA indicated by X-symbols in Fig. A9, but the agreement with Kahn's data is not good. For convenience, it is useful to normalize the applied voltage V with respect to the threshold voltage V_{th} and this has been done in Fig. A9. For our theory, we fitted Kahn's curve in Fig. A9 with several trial functions, keeping those functions simple. As illustrated, we found that the experimental curve could be fitted accurately with the function

$$\alpha(V) = 0.87 \arctan[(V/V_{th}) - 1] \quad , \tag{6}$$

and we therefore adopted this relation. Admittedly, our model is inexact, unlike the theories of Shimomura and Berreman but, because we have introduced an empirical $\alpha(V)$ relation, we feel that our theory will give reasonably accurate predictions for the turn-on characteristics of LC switches.

Using α from (6) as the argument of the $\sin^2$ and $\cos^2$ functions in (5), we put θ' of (5) into (1) and calculated, with the aid of a

Fortran program, the voltage response I(trans(V)). Switched light has been plotted as a function of normalized voltage over the range $0 < V/V_{th} < 20$ for three glasses and for two liquids (at 20°C and 60°C for LC1132), with the results displayed in Figs. A10-A17.

After examining these figures, we infer that the relative size of n_g and n_e is important in determining the shape of the turn-on. Specifically, when n_g is much larger than n_e, the switch turns on slowly and at high voltage. When $n_g \simeq n_e$, the device turns on steeply at low voltages and the throughput remains near 100% as the voltage is increased. When n_g is less than n_e, the turn-on is quite rapid at very low voltage, but then the optical transmission "sags" at higher voltages due to unwanted reflections at the glass/LC interface.

The glass/LC combinations that give step-like turn-on (the best combinations) are WG335/1132 and WG345/E7. In LC1132, the index n_e decreases as $T \to T_c$, which explains why WG335/1132 is a better match over the nematic temperature range than WG360/1132.

Looking at the turn-on from another viewpoint, consider the critical angle $\theta_c(\parallel)$ and note that $\theta_c \to \arcsin(n_e/n_g)$ as $\alpha \to 90^\circ$. Now if θ_c is close to 90° for large α, say $70^\circ < \alpha < 90^\circ$, then, from Figs. A10-17, the turn-on will have the desired step-shape; therefore, we shall plot θ_c vs α to see when this preferred behavior occurs. Setting $\theta' = 90^\circ$ in (2) and using (3) we find

$$\theta_c(\parallel) = \arcsin \frac{n_o n_e}{n_g \sqrt{n_o^2 \sin^2\alpha + n_e^2 \cos^2\alpha}} \quad ; \qquad (7)$$

$$\theta_c(\perp) = \arcsin(n_o/n_g) \quad .$$

It is useful to examine the effect of temperature changes on θ_c, and so we have estimated the temperature dependence of n_o and n_e for LCs 1132 and E7 by analogy with the curves given in Fig. 3 of Schadt and

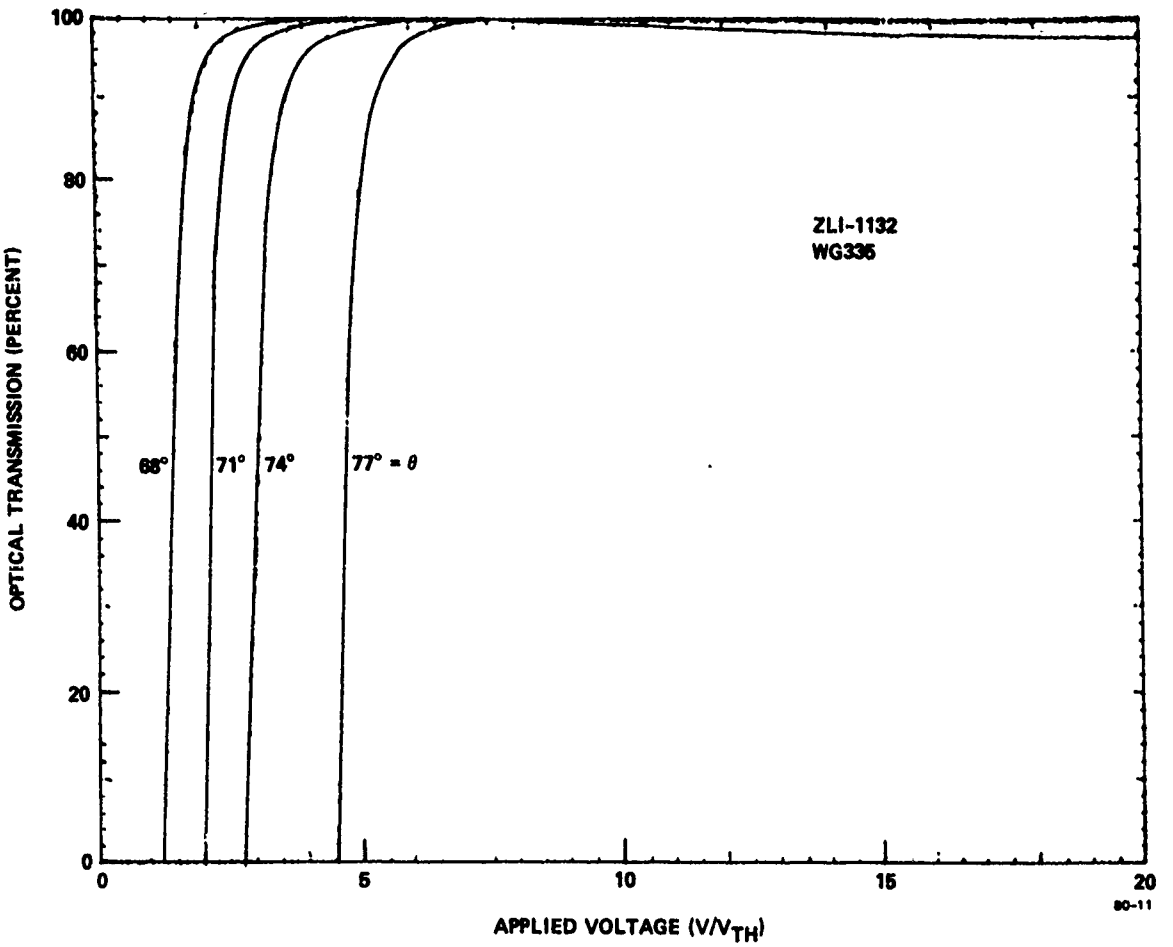

FIG. A10 Switched light vs. V/V_{TH} for glass-335/LC-1132.

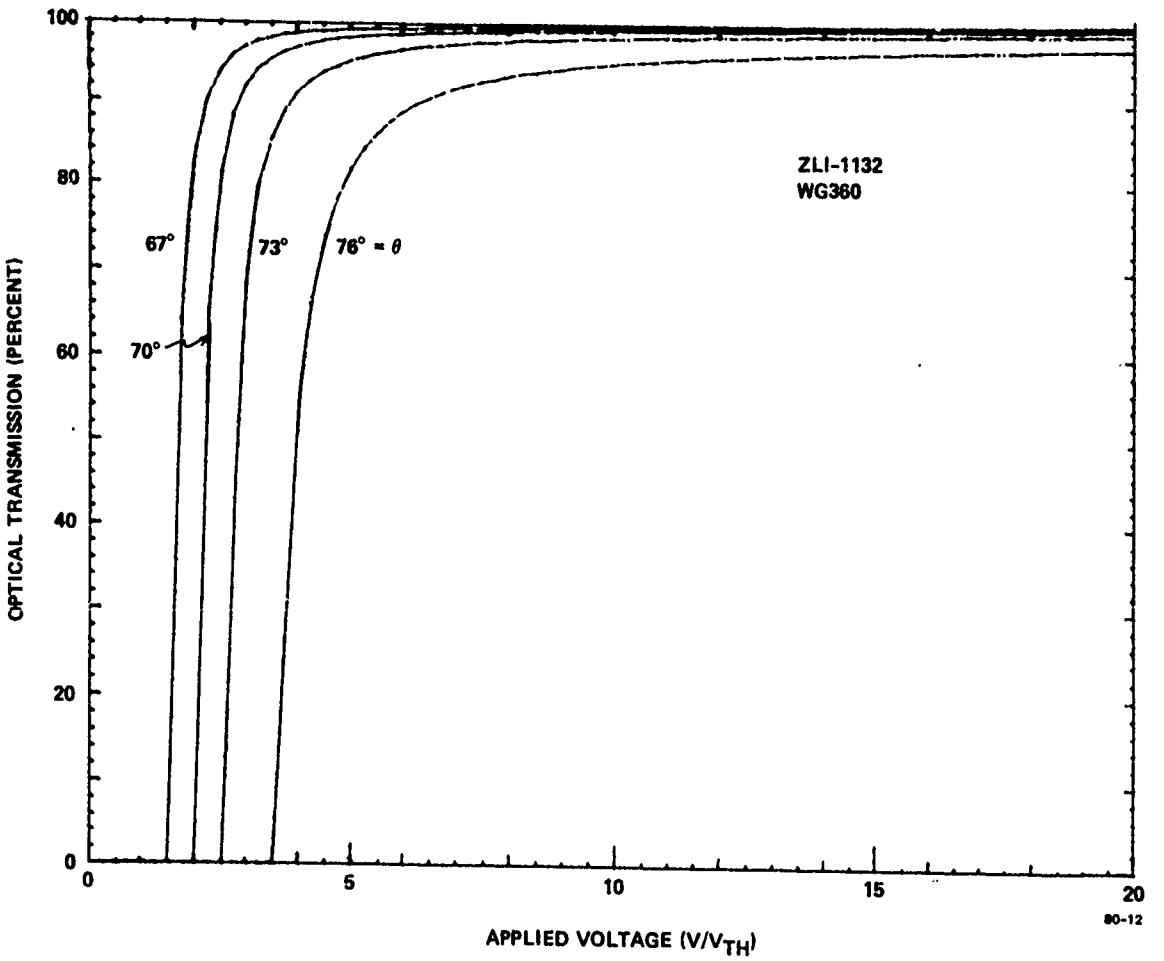

FIG. A11 Switched light vs. V/V_{TH} for glass-360/LC-1132.

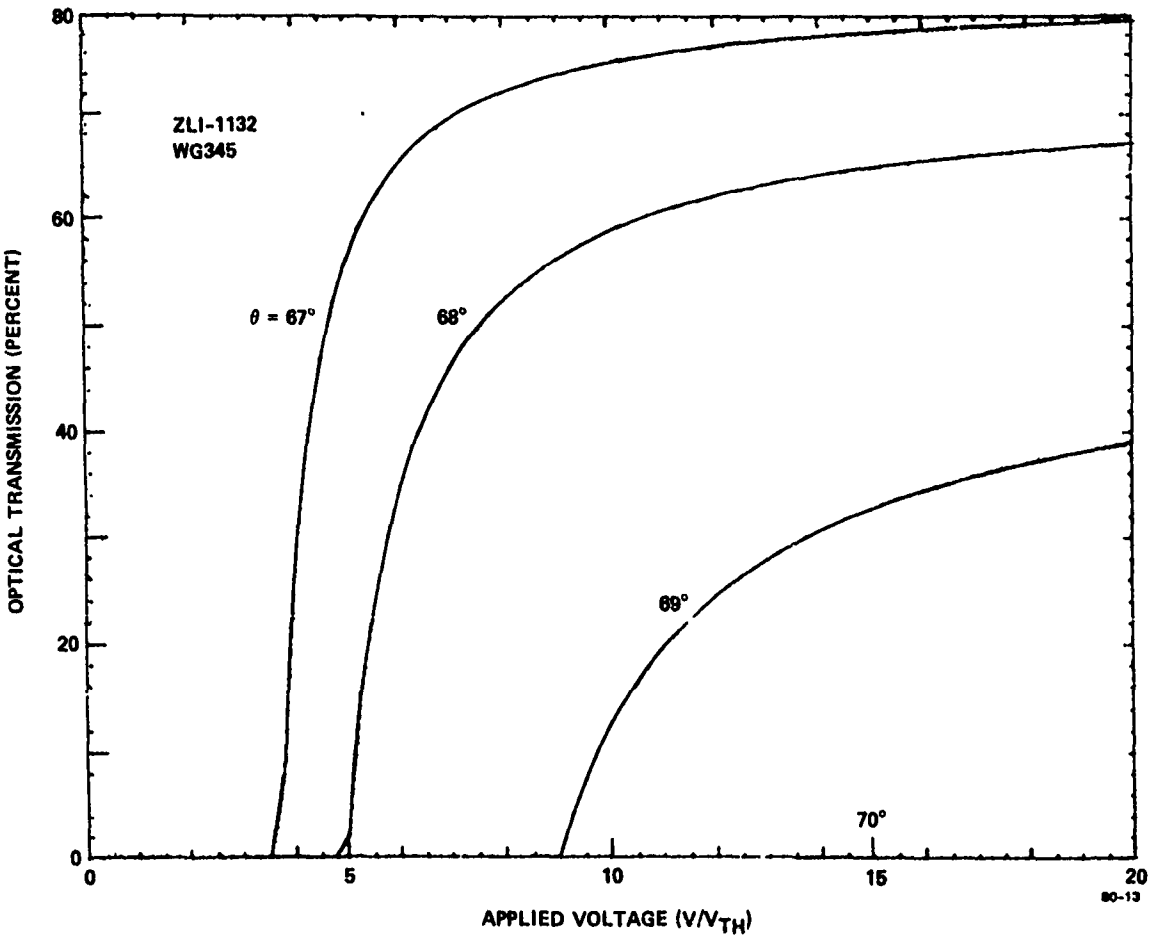

FIG. A12 Switched light vs. V/V_{TH} for glass-345/LC-1132.

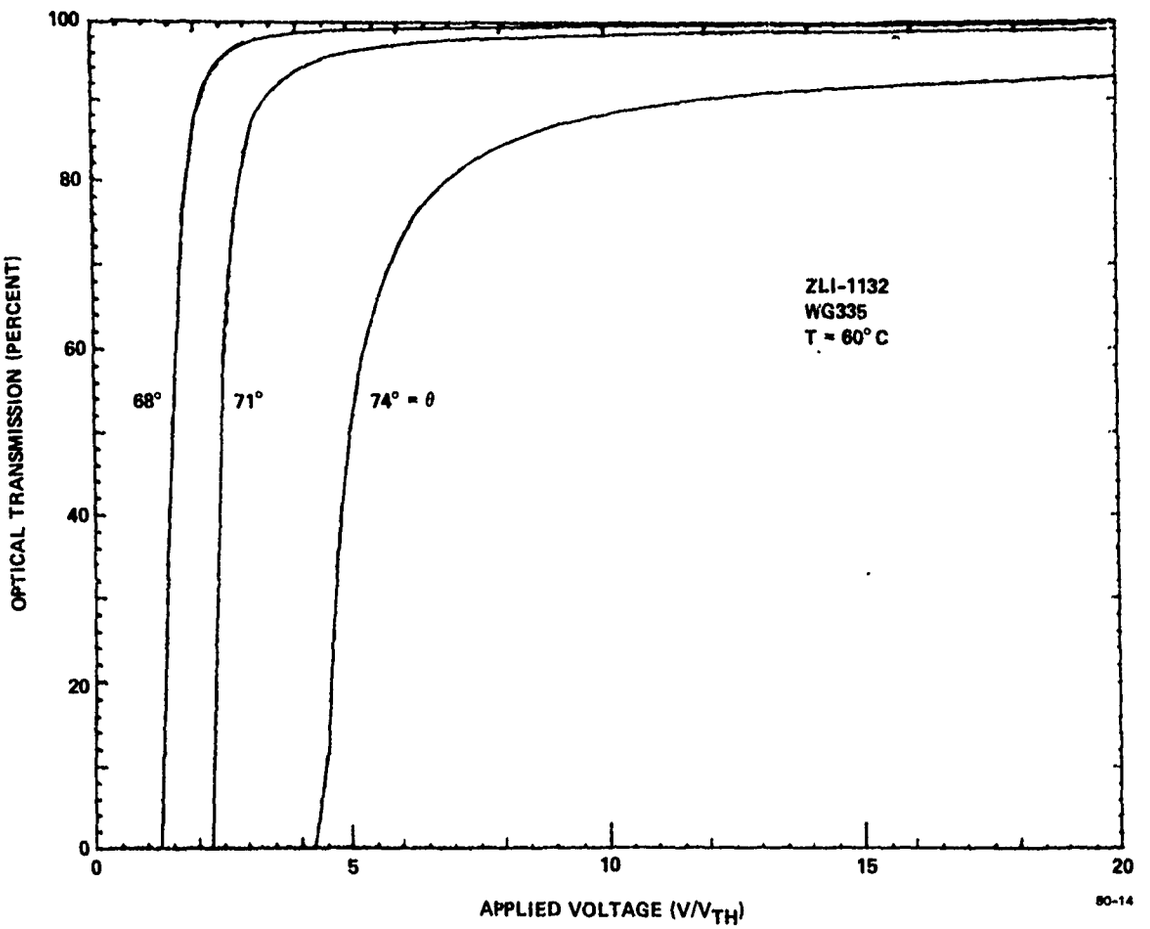

FIG. A13 Switched light vs. V/V_{TH} for glass-335/LC-1132 at 60° C.

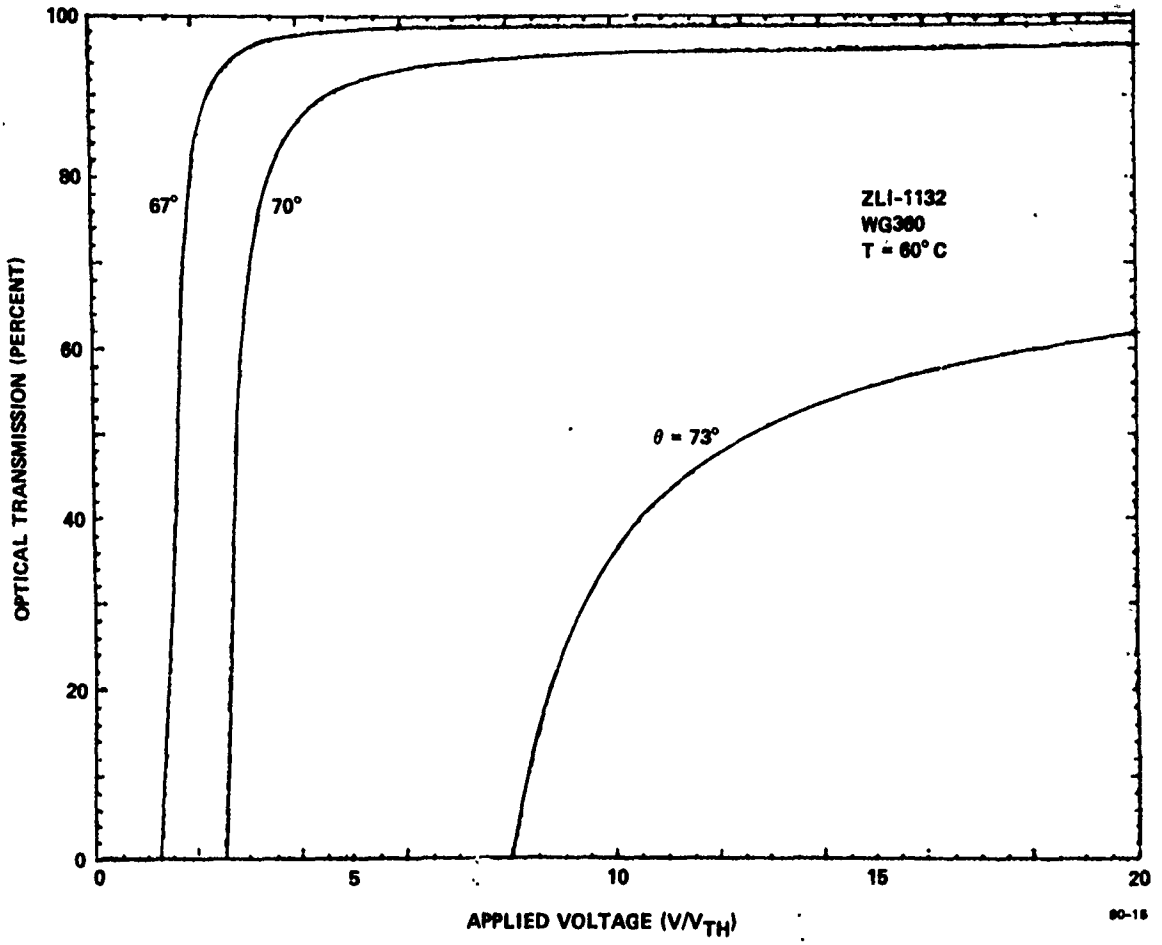

FIG. A14 Switched light vs. V/V_{TH} for glass-360/LC-1132 at 60°C.

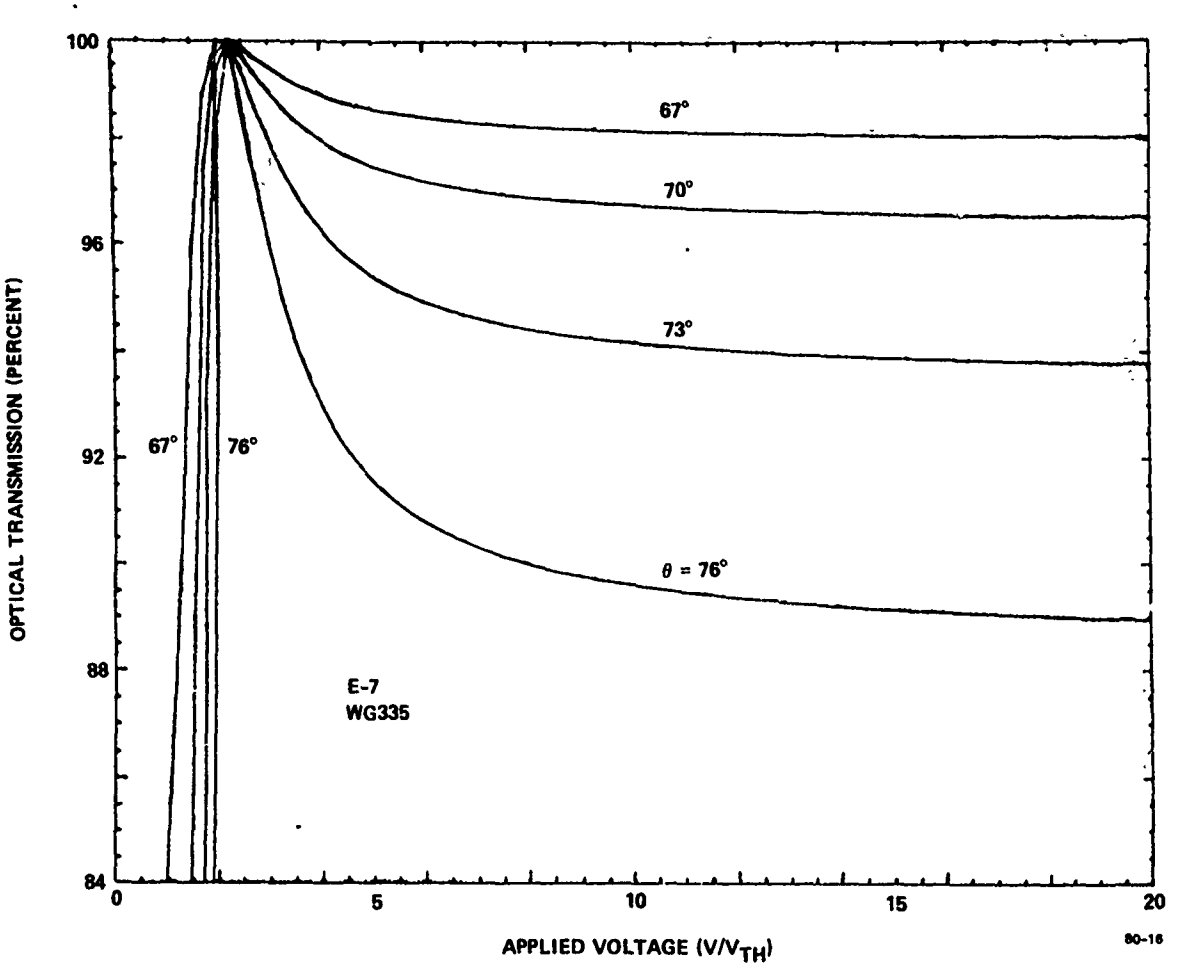

FIG. A15 Switched light vs. V/V_{TH} for glass-335/LC-E7.

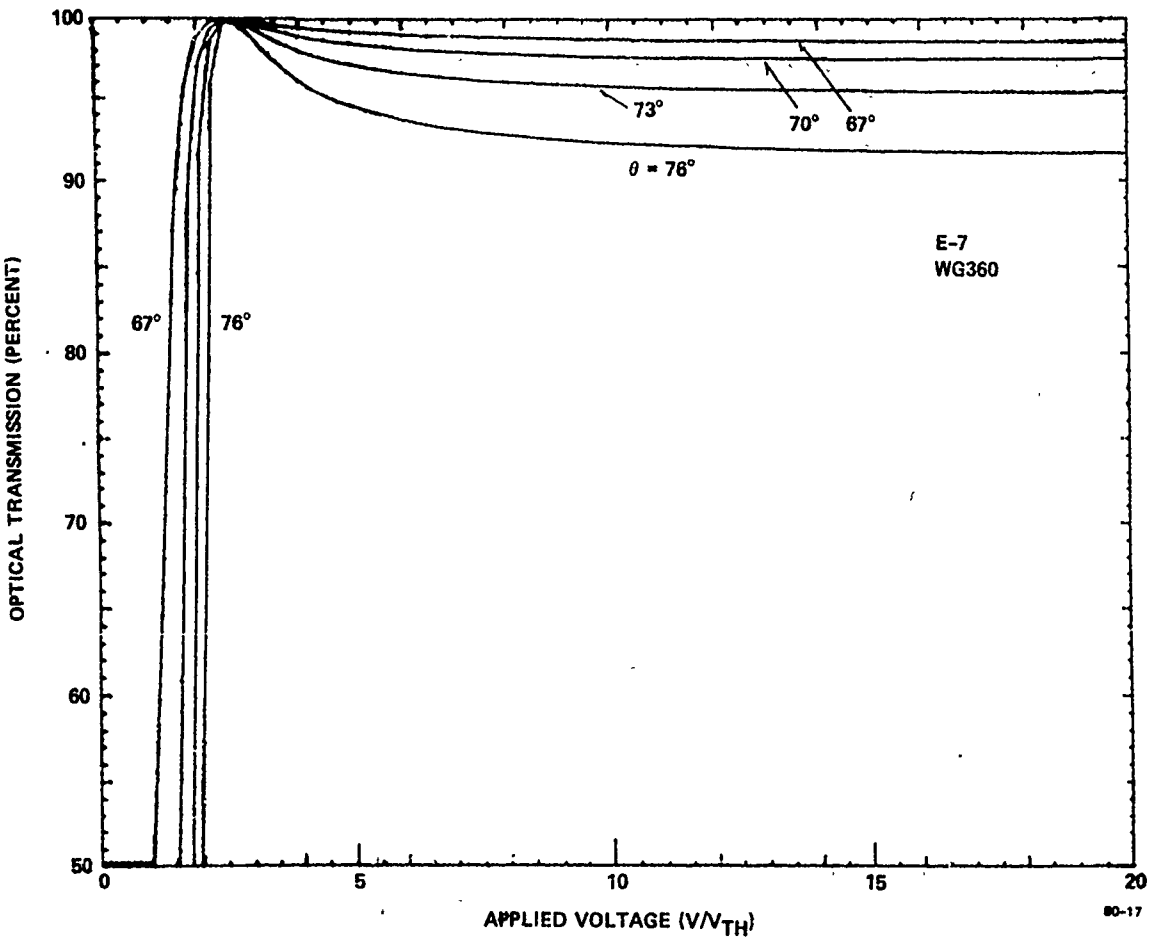

FIG. A16 Switched light vs. V/V_{TH} for glass-360/LC-E7.

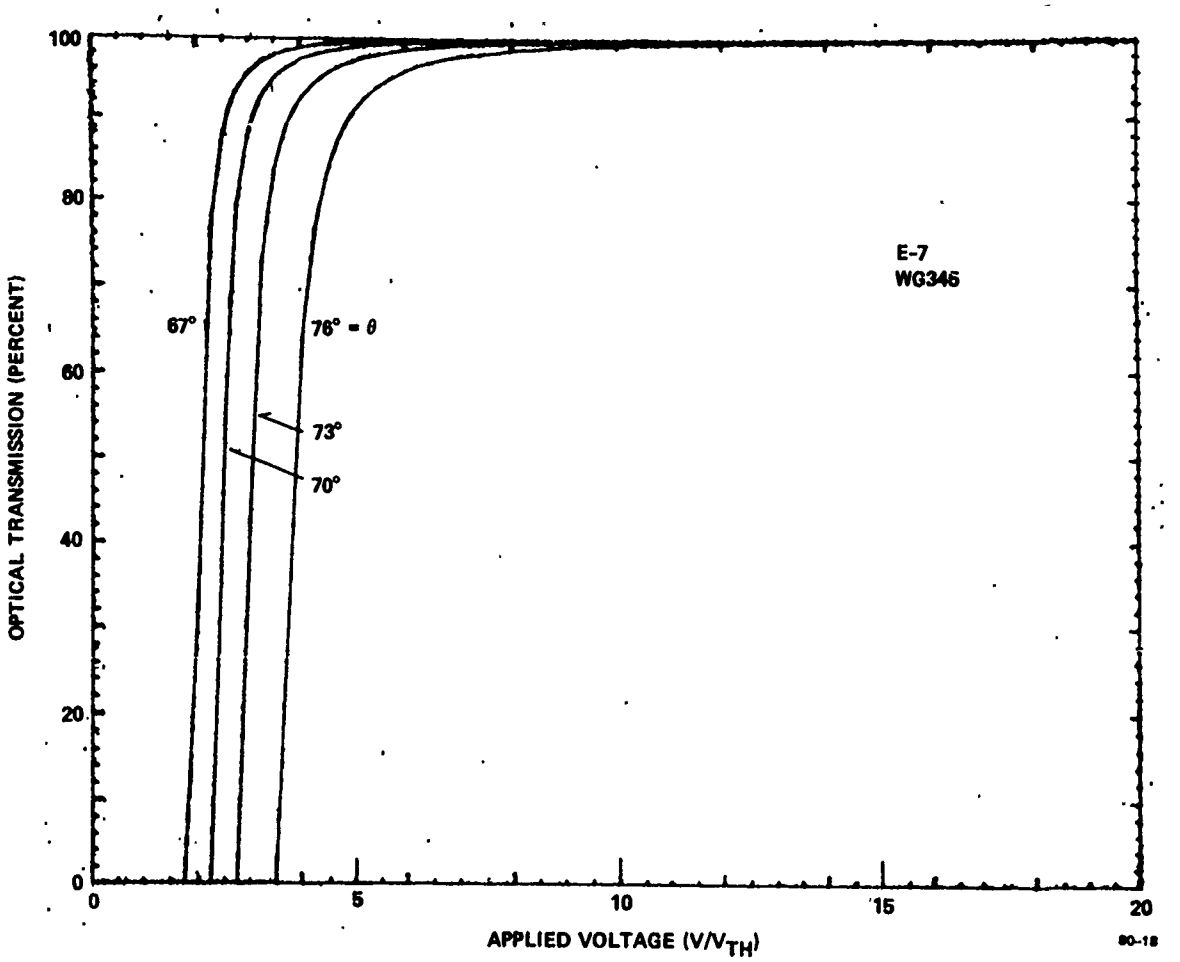

FIG. A17 Switched light vs. V/V_{TH} for glass-345/LC-E7.

Muller (see Fig. A18). Our estimates are

LC 1132	$n_o = 1.492$,	$n_e = 1.645$	at T =	0°C
	$n_o = 1.492$,	$n_e = 1.634$		20°C
	$n_o = 1.492$,	$n_e = 1.624$		40°C
	$n_o = 1.493$,	$n_e = 1.605$		60°C
	$n_o = 1.502$,	$n_e = 1.594$		66°C
LC E7	$n_o = 1.522$,	$n_e = 1.800$	at T =	0°C
	$n_o = 1.522$,	$n_e = 1.746$		20°C
	$n_o = 1.523$,	$n_e = 1.720$		40°C
	$n_o = 1.525$,	$n_e = 1.680$		57°C

The nematic-isotropic phase transition takes place at 70°C in 1132 and at 59°C in E7.

Substituting the above index values in (7), we have plotted θ_c as a function of α from $\alpha = 0$ to 90° for the foregoing temperatures as illustrated in Figs. A19-A24. Here, we find that the $\theta_c(\text{II})$ values are closer to 90° over the nematic phase when $\alpha > 70°$ for 335/1132 and 345/E7 than for the other glass/LC combinations. This reiterates the Fig. A10-A17 result from another standpoint.

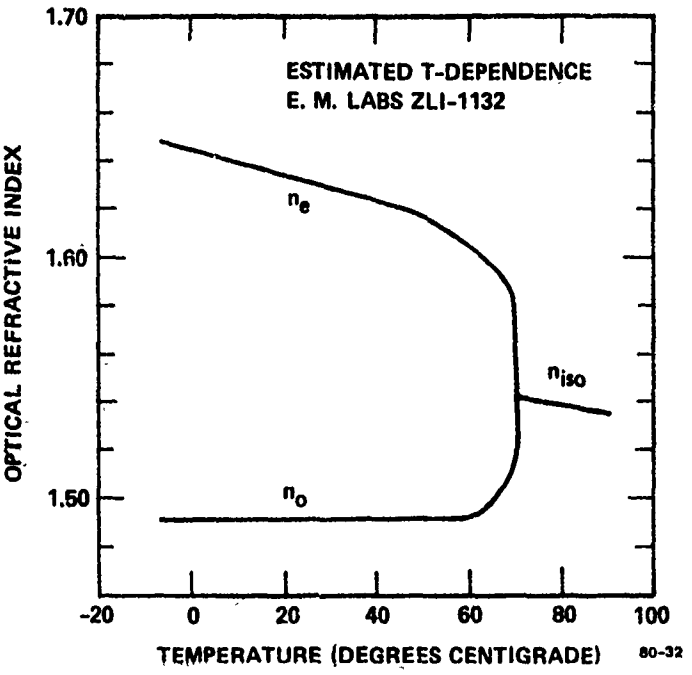

FIG. A18 Temperature dependence of n_o and n_e for LC-1132 estimated by emulating curves in Fig. 5 of Schadt and Muller.

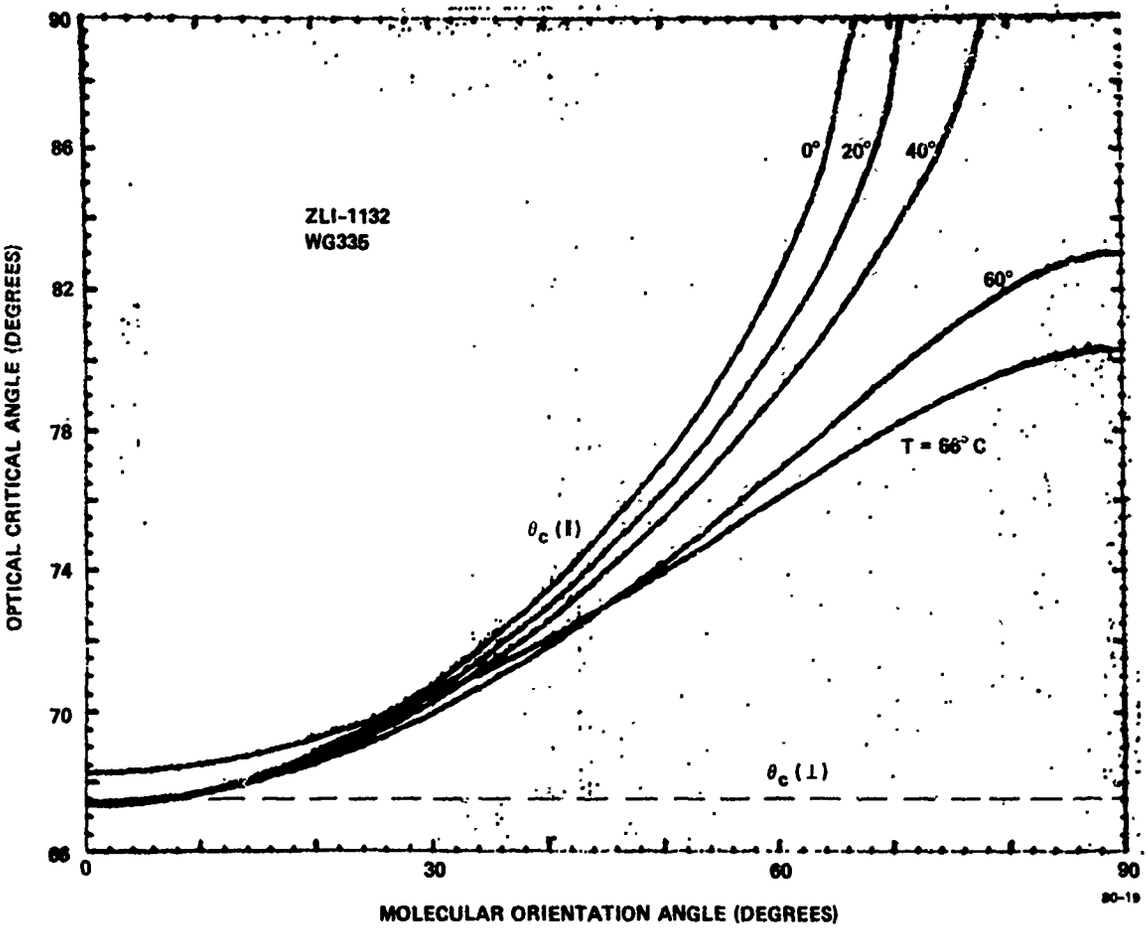

FIG. A19 Critical angle vs. α for glass-335/LC-1132.

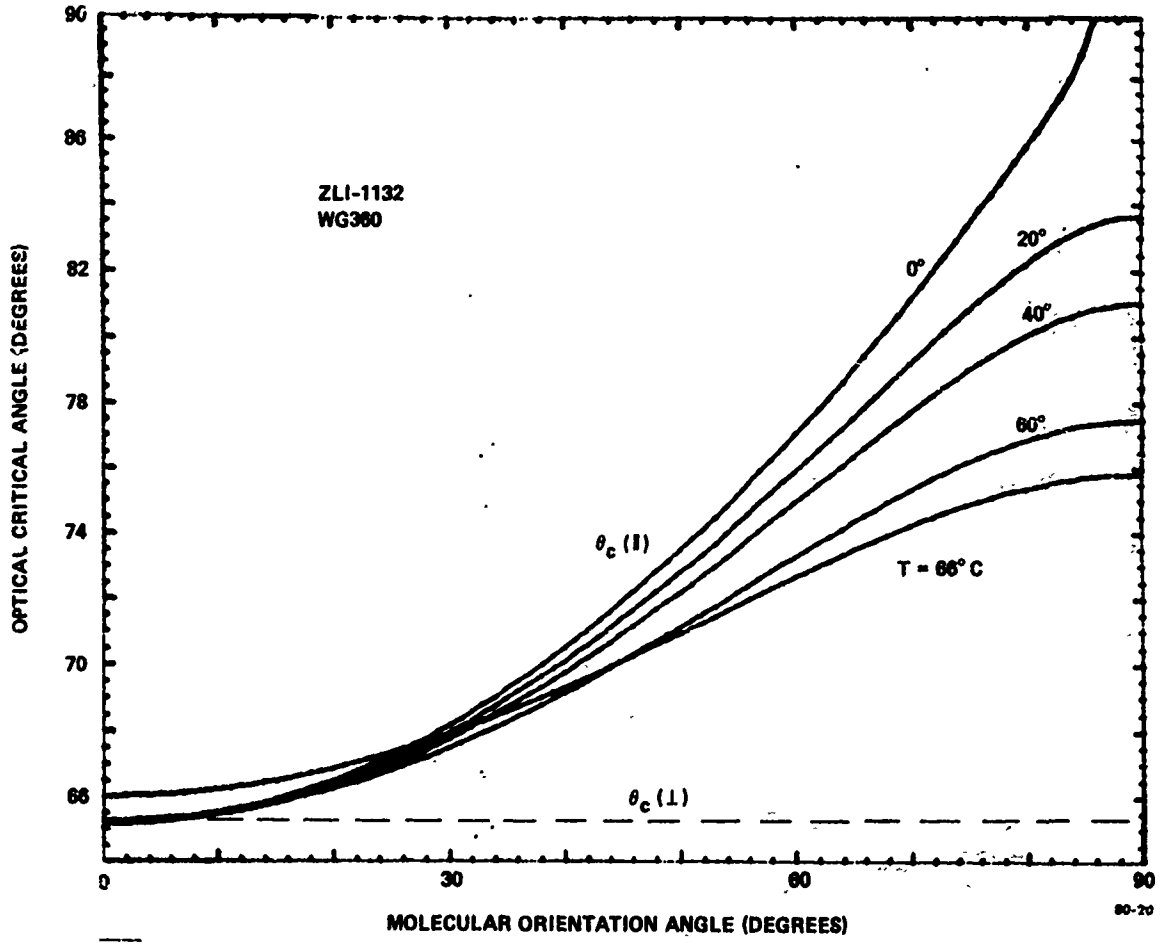

FIG. A20 Critical angle vs. α for glass-360/LC-1132.

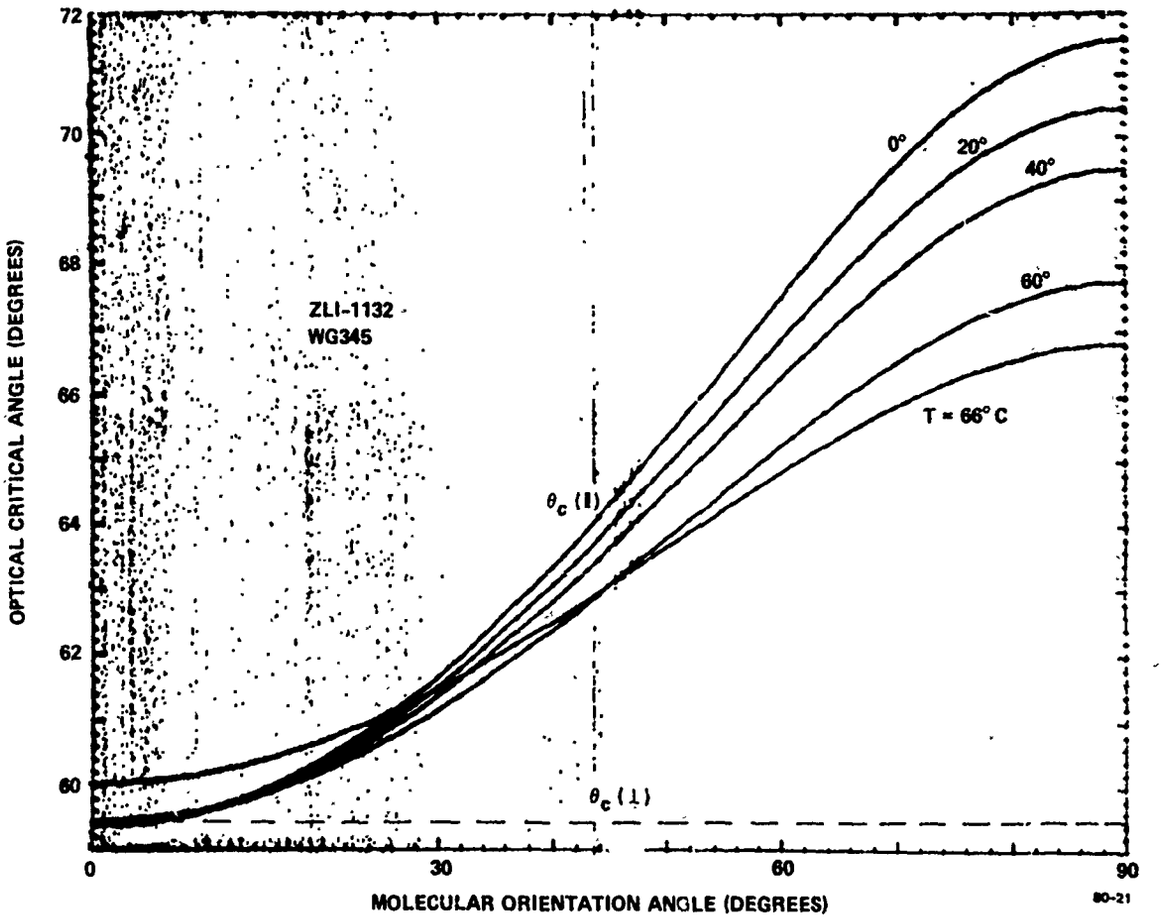

FIG. A21 Critical angle vs. α for glass-345/LC-1132.

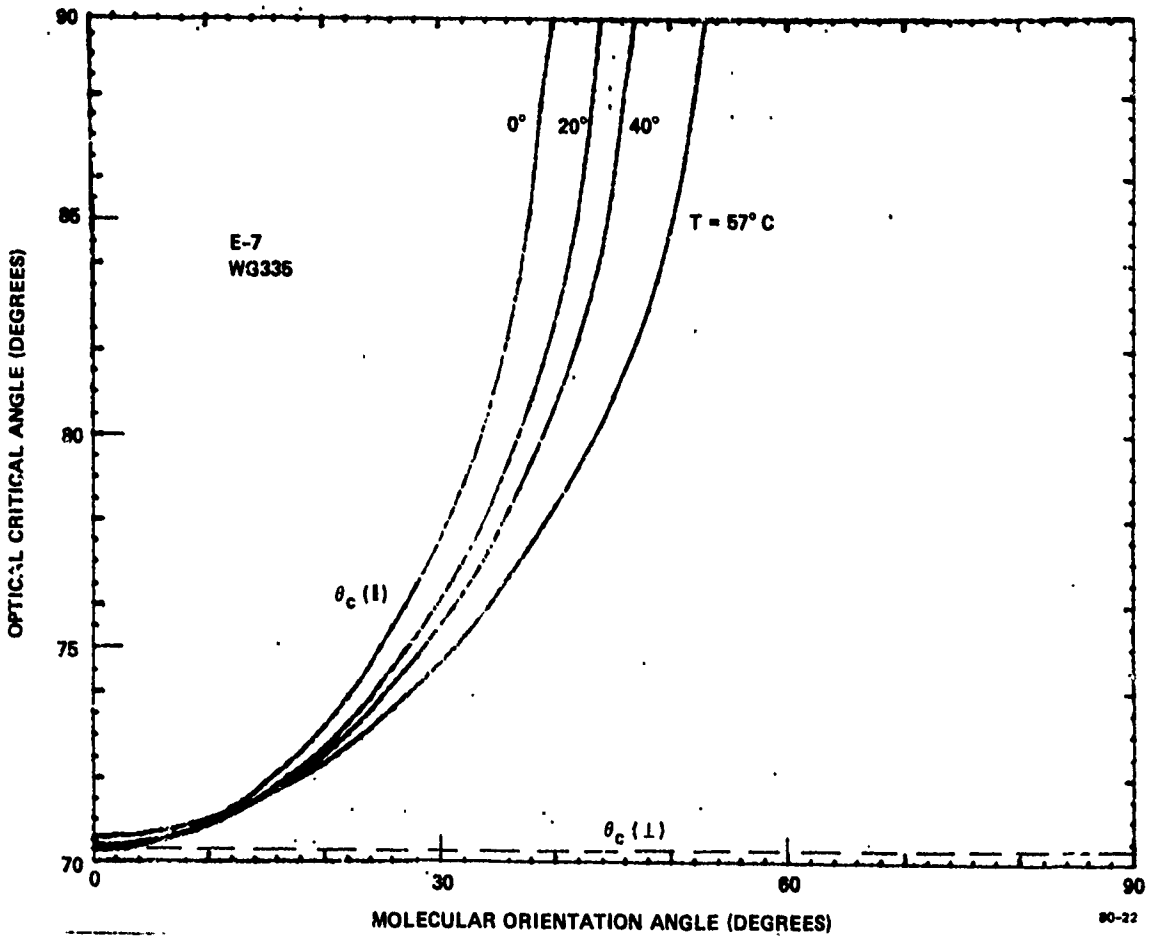

FIG. A22 Critical angle vs. α for glass-335/LC-E7.

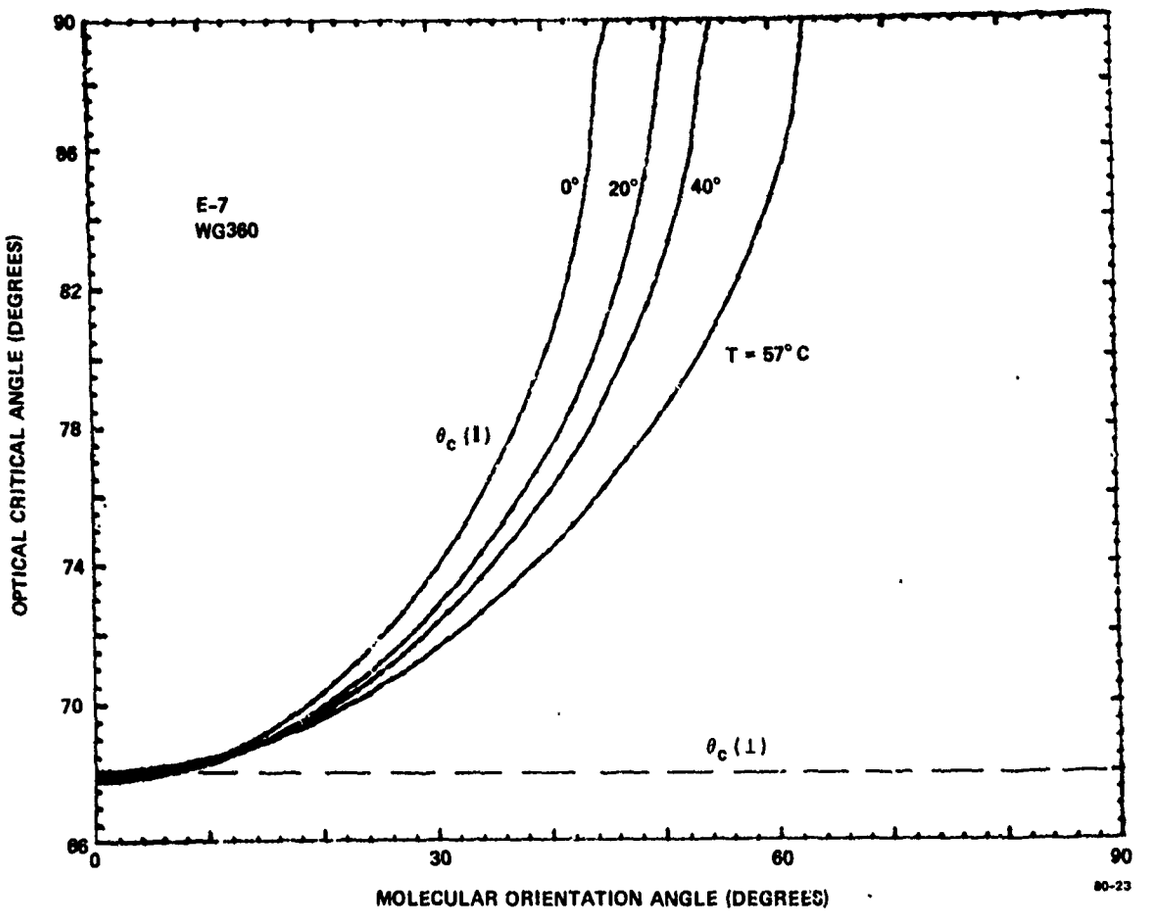

FIG. A23 Critical angle vs. α for glass-360/LC-E7.

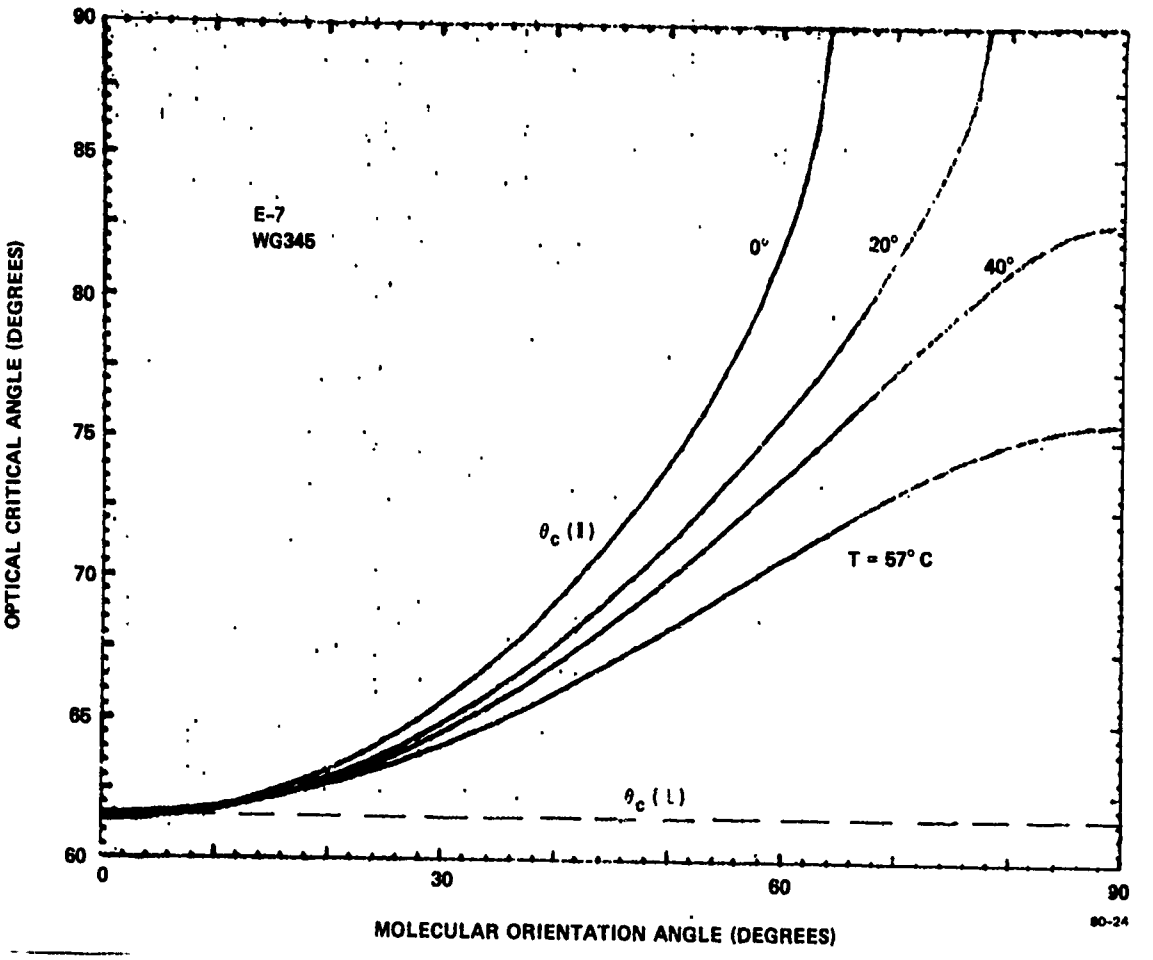

FIG. A24 Critical angle vs. α for glass-345/LC-E7.

MISSION
of
Rome Air Development Center

RADC plans and executes research, development, test and selected acquisition programs in support of Command, Control Communications and Intelligence (C^3I) activities. Technical and engineering support within areas of technical competence is provided to ESD Program Offices (POs) and other ESD elements. The principal technical mission areas are communications, electromagnetic guidance and control, surveillance of ground and aerospace objects, intelligence data collection and handling, information system technology, ionospheric propagation, solid state sciences, microwave physics and electronic reliability, maintainability and compatibility.

Printed by
United States Air Force
Hanscom AFB, Mass. 01731